THE ROLE AND REGULATION OF PYRUVATE DEHYDROGENASE IN SKELETAL MUSCLE BIOENERGETICS AND TYPE 2 DIABETES

By

Jonathan D. Kasper

A DISSERTATION

Submitted to
Michigan State University
in partial fulfilment of the requirements
for the degree of

Physiology – Doctor of Philosophy

2018

ABSTRACT

THE ROLE AND REGULATION OF PYRUVATE DEHYDROGENASE IN SKELETAL MUSCLE BIOENERGETICS AND TYPE 2 DIABETES

By

Jonathan D. Kasper

As of 2015 over 30 million people had type 2 diabetes with another 84.1 million with prediabetes comprising ~35% of the adult US population. The hallmark of this disease is characterized by impaired glycemic control exhibiting elevations in blood glucose in the post-absorptive and absorptive states. Skeletal muscle comprises ~40% of total body mass and is an early site of insulin resistance. Skeletal muscle contributes to whole body glycemic control through mitochondrial glucose oxidation which is catalyzed and regulated by pyruvate dehydrogenase (PDH). Early type 1 diabetic rodent studies implicated reduced muscle PDH activity in the etiology of hyperglycemia but current human studies indicate either normal or elevated post-absorptive glucose oxidation in resting or contracting skeletal muscle. There is a surprising lack of studies and detailed understanding of the regulation of PDH activity *in vivo*, especially regarding type 2 diabetes. This dissertation will determine the mechanisms that regulate skeletal muscle PDH activation *in vivo*, the effects of altered PDH activation on muscle function and finally will quantify PDH activity in a rodent model of type 2 diabetes.

First, *in vivo* regulation of PDH activation was quantified in muscle during contraction and steady state energetics measured by magnetic resonance. Both muscle energetics and Ca^{2+} are thought to regulate PDH activation, with depressed energetics and increased Ca^{2+} stimulating PDH activation with increasing workloads. Mitochondrial density was reduced chemically to delineate the effects of energetics and Ca2+ on the regulation of PDH during muscle contraction. The primary finding was that PDH regulation is mostly achieved by the adenylate energy charge with little to no effects by cytosolic Ca^{2+}.

Next, skeletal muscle PDH activation and energetics were investigated by altering PDH activation during active workloads with the same compliment of mitochondria. Rats were treated with dichloroacetate (DCA), a potent pharmacological activator of PDH prior to muscle contraction and the bioenergetic response was quantified *in vivo*. PDH activation resulted in a significant increases in steady state energetics collectively described by the free energy of ATP hydrolysis (ΔG_{ATP}). Increased ΔG_{ATP} was apparent at rest and during muscle stimulation at submaximal contractile intensities but this effect was diminished approaching the expected aerobic maximum. This effect was attributed to an increase in the thermodynamic set point of the muscle and not kinetic alterations in the ATP synthesis machinery (F_1F_O ATPase, adenine nucleotide translocator).

Finally, the regulation of PDH activity was determined in the hyperglycemic, insulin resistant, type 2 diabetic Goto Kakizaki (GK) rat. PDH activity was significantly increased in muscle at rest and when stimulated at submaximal intensities. This effect was attributed to hyperglycemia in the GK rat and the slight reduction in mitochondrial density observed. These data do not support earlier rodent studies that implicate decreased PDH activity in the etiology of diabetes but suggest increased PDH activation in response to hyperglycemia and are completely consistent with glucose oxidation measurements described in type 2 diabetic skeletal muscle in humans.

Collectively, these data suggest that muscle glucose oxidation is regulated by the metabolic demand of the muscle in relation to mitochondrial density. Furthermore, shifting muscle substrate selection to glucose at submaximal intensities by increases in PDH activity also increases the steady state ΔG_{ATP} that is maintained and supports PDH as a regulator of muscle bioenergetics. Finally, PDH activity is not reduced in type 2 diabetic skeletal muscle and is not likely a primary contributor to the hyperglycemia seen with the disease.

ACKNOWLEDGEMENTS

I would like to thank my mentor, Robert Wiseman, for his guidance and support in completing this work. I will always appreciate his enthusiasm for science and his patience when troubleshooting some of the technical aspects of this dissertation. I would also like to thank the other members of the lab, Matthew Lewis and Anne Tonson, not only for their help in the work that contributed to this thesis but also for their friendship when things were tough. Finally, I would to thank my family. Throughout the course of my PhD they have been a constant source of support and have always been there for me when I needed them.

TABLE OF CONTENTS

LIST OF TABLES

LIST OF FIGURES

KEY TO ABBREVIATIONS

$\Delta\psi$ – Proton electrical potential

ΔE_h – Redox potential

ΔG_{ATP} – Free energy of ATP hydrolysis

Δp – Proton motive force

ΔPCr – Change in PCr from initial value

ΔpH – Proton chemical potential

ΔPi – Change in Pi from initial value

^{31}P NMR – Phosphorus nuclear magnetic resonance spectroscopy

A-CoA – Acetyl coenzyme A

ADP – Adenosine diphosphate

ANT – Adenine dinucleotide translocase

ATP – Adenosine triphosphate

AUC – Area under the curve

BW – Body weight

CAT – Carnitine acetyltransferase

CK – Creatine kinase

CoA – Coenzyme A

DCA - Dichloroacetate

EC - Extracellular

ETC – Electron transport chain

FFA – Free fatty acid

FID – Free induction decay

GK – Goto Kakizaki

GPT – Glutamate pyruvate transaminase

gWW – Gram muscle wet weight

HOMA-IR – Homeostasis model assessment of insulin resistance

IC - Intracellular

J_{ATPase} – cytosolic ATP hydrolysis rate

J_{GLY} – Glycolytic ATP synthesis rate

J_{MITO} – Mitochondrial ATP synthesis rate

Keq – Equilibrium constant

Ki – Inhibitor constant

LCW – Liter cell water

LETO – Long-Evans Tokushima Otsuka rat

MMI - Methimazole

MW – Muscle weight

NAD^+ - Oxidized nicotinamide adenine dinucleotide

NADH – Reduced nicotinamide adenine dinucleotide

OGTT – Oral glucose tolerance test

OLETF – Otsuka Long-Evans Tokushima fatty rat

PCr - Phosphocreatine

PDH – Pyruvate dehydrogenase

PDH_a – Active pyruvate dehydrogenase

PDH_t – Total pyruvate dehydrogenase

PDK – Pyruvate dehydrogenase kinase

PDP – Pyruvate dehydrogenase phosphatase

pHi – Intracellular pH

Pi – Inorganic phosphate

PME - Phosphomonoester

PMF – Proton motive force

QH_2 - Ubiquinol

RER – Respiratory exchange ratio

RT – Room temperature

RQ – Respiratory quotient

SERCA – Sarco/endoplasmic reticulum Ca^{2+} ATPase

TCA – Tricarboxylic acid cycle

TR – Repetition time

TTI – Total tension time integral

VO_2 – Oxygen consumption rate

VO_{2MAX} – Maximal oxygen consumption rate

ZDF – Zucker diabetic fatty rat

Chapter 1. Introduction

1.1 Regulation of Pyruvate Dehydrogenase Phosphorylation

1.1.1 Pyruvate Dehydrogenase Enzyme Complex

The mitochondrial pyruvate dehydrogenase complex (PDH) catalyzes the irreversible decarboxylation of pyruvate, with the reduction of NAD+ to form acetyl-coa (A-CoA) in support of oxidative ATP synthesis. The PDH reaction involves three catalytic subunits: pyruvate dehydrogenase (E1), dihydrolipoamide acetyltransferase (E2), and dihydrolipoamide dehydrogenase (E3). Together, these three subunits and the overall reaction will be collectively referred as PDH or the PDH reaction. Overall reaction rate is regulated by phosphorylation of three serine residues on the α-subunits of E1, with phosphorylation causing inactivation and dephosphorylation causing activation of the enzyme complex (1,2). The three serine residues are designated as site 1 (serine-264), site 2 (serine-271), and site 3 (serine-203) with phosphorylation at any site rendering PDH inactive (3,4). The ATP dependent phosphorylation of the enzyme complex is catalyzed by pyruvate dehydrogenase kinase (PDK), that is linked with the PDH complex via lipoyl binding domains on the E2 catalytic subunit (5). There are four known isoforms of PDK in mammalian tissues (PDK1-4) with PDK2 and PDK4 predominantly expressed in skeletal muscle of both human and rat species (5,6). Dephosphorylation and PDH activation is catalyzed by pyruvate dehydrogenase phosphatase (PDP), which is not as tightly associated with the PDH complex as PDK but still requires binding to the lipoyl domains on the E2 catalytic subunit for maximal activity (7,8). The phosphorylation state of PDH and therefore the fractional activity of the enzyme is then determined by the relative activities of PDK versus PDP, that each

display their own allosteric modulators, affecting their activities and thus steady state PDH phosphorylation (Fig. 1).

1.1.2 Allosteric Regulation of PDK Activity

Since PDK2 and PDK4 are the predominant isoforms expressed in skeletal muscle, discussion of allosteric regulation of PDK activity will focus on these enzymes. Furthermore, translational regulation leading to increases in PDK2 or PDK4 expression will not be discussed here but will be addressed where appropriate for discussion of altered PDH with dietary intervention or diabetes. PDK activity is allosterically inhibited with increased pyruvate concentration as well as increased ADP/ATP, NAD+/NADH, and CoA/A-CoA ratios with activity stimulated by the inverse of these effects (Fig. 1) (9–12). Pyruvate is thought to be the overriding signal inhibiting PDK activity, preventing allosteric stimulation by ATP and working synergistically with increased ADP (9,13). However, increased NADH and A-CoA work to stimulate enzyme activity through modification of the lipoyl domains of E2 through reduction and acetylation, enhancing PDK activity 60-80% and up to 3-fold respectively (14). Therefore, it is the relative energetic status of the muscle fiber that dictates PDK activity at any given metabolic state. In the resting state, PDK is expected to be stimulated through low glycolytic flux and pyruvate concentration as well as low intramitochondrial ratios of ADP/ATP, NAD+/NADH, and CoA/A-CoA. This corresponds with the relatively low PDH activity (~10-20% of total) (15–17) and rates of glucose oxidation in resting skeletal muscle (18–21). However, when the metabolic demand is increased through muscle contractile activity, increased pyruvate and ADP/ATP, NAD+/NADH, and CoA/A-CoA ratios

allosterically inhibit PDK activity resulting in PDH dephosphorylation and stimulation of glucose oxidation (Fig. 1) (22–24).

Inhibition of PDK activity can also be achieved without alteration in muscle contractile status by treatment with dichloroacetate (DCA), a pharmacological compound with a structure analogous to pyruvate that also works synergistically with ADP (13,25). Treatment with DCA *in vivo* results in complete dephosphorylation of PDH in resting skeletal muscle of both rat (25,26) and humans (16,27,28). This results in increased rates of glucose oxidation in rat skeletal muscle both at rest (26,29,30) and during muscle contraction (31). This effect is also observed with DCA treatment in humans with rates of whole-body glucose oxidation increased with DCA treatment both in the rested, fasting state (32) and during submaximal aerobic exercise (33). Although both PDK2 and PDK4 are inhibited by DCA, PDK2 exhibits higher sensitivity to the compound (Ki = 0.2mM) when compared to PDK4 (Ki = 0.5mM) (6). As will be described later in this thesis, the presented research also used DCA to inhibit PDK activity and activate PDH. The dose utilized here corresponded to a whole body DCA concentration in the rat of ~1.4 mM, and assuming whole body water content of 72% of body weight (34) and was nearly triple the Ki of the least sensitive PDK to DCA inhibition.

1.1.3 Allosteric Regulation of PDP Activity

Compared to PDKs, regulation of PDP activity is relatively simple yet understudied. There are two isoforms of PDP expressed in mammalian tissues (PDP1, PDP2) however, only PDP1 is expressed in skeletal muscle and will be the focus of this section (35). PDP1 activity requires Mg^{2+} and is allosterically stimulated by Ca^{2+} (Fig. 1)

(35–37). Similar to PDK, PDP1 activity is enhanced by binding to the lipoyl domain of E2, an effect mediated by increasing mitochondrial matrix Ca^{2+} concentration (8,37). Unlike PDK, there is currently no available inhibitor of PDP1 activity that can be utilized *in vivo*. However, the most widely used inhibitor for *in vitro* inhibition of PDP1 activity is NaF (36). NaF is toxic for use *in vivo* but is useful in blocking dephosphorylation of PDH for assay of PDH activity in muscle homogenates *in vitro*. Whereas PDK activity is inhibited during muscle contraction, it is thought that PDP1 activity is stimulated by increases in muscle Ca^{2+} and helps to mediate PDH dephosphorylation and activation during increased metabolic demand. However, it has not been determined how the relative activities of PDK vs PDP may regulate PDH activation *in vivo* and is the subject of study discussed in Chapter 2 of this thesis.

Figure 1. Regulation of PDH activity schematic.

Schematic representation of the regulation of pyruvate dehydrogenase phosphorylation and the allosteric regulation of PDK2, PDK4, and PDP1 activities.

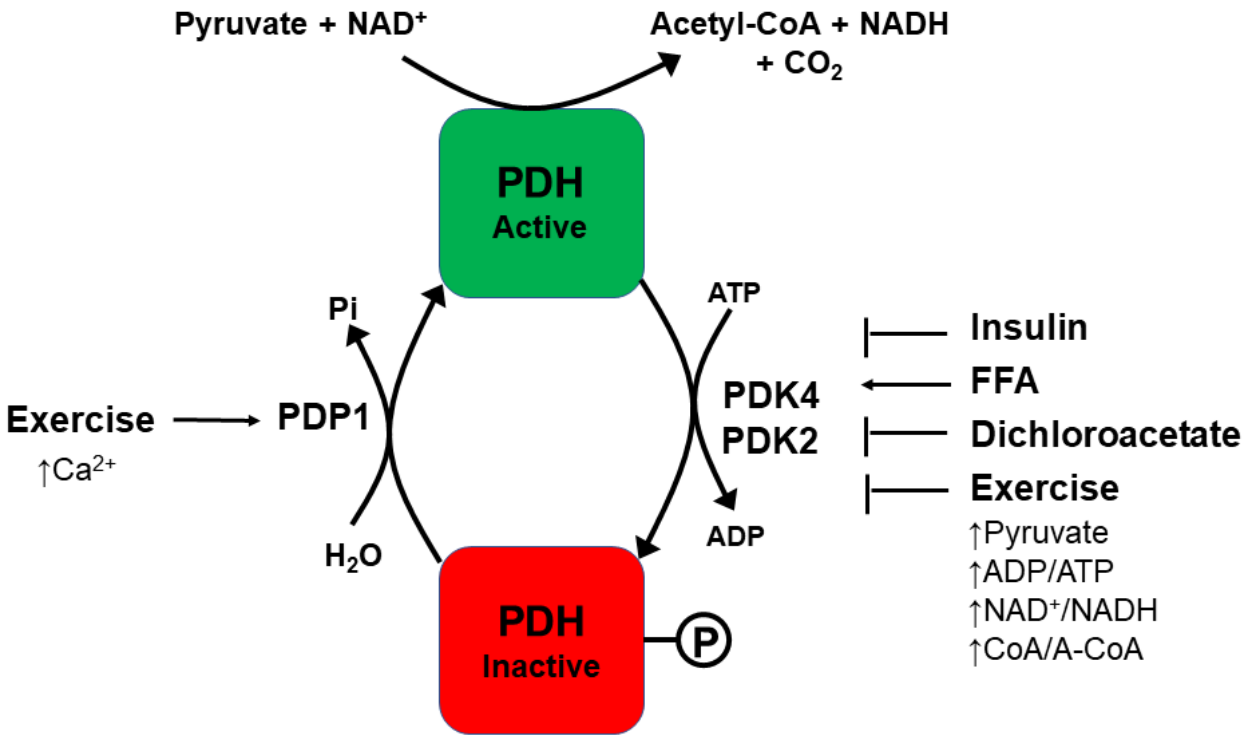

1.2 PDH Activity Determines Skeletal Muscle Substrate Oxidation

1.2.1 PDH Regulation of Resting Substrate Utilization

Skeletal muscle comprises approximately 40% of the total body mass and represents an important sink for substrate disposal. At rest, whole body oxygen consumption (VO_2) is approximately 10% of maximal oxygen uptake (VO_{2MAX}) with skeletal muscle accounting for ~20-25% of the basal oxygen consumption or basal metabolic rate. For a typical non-obese individual at rest after overnight fast, whole body respiratory exchange ratio (RER = VCO_2/VO_2), an indicator of substrate oxidation, is ~0.82 corresponding to 62% and 48% of energy expenditure (kcal/lO_2) from free fatty acid and glucose oxidation respectively (21,38). Clearly this is not solely representative of skeletal muscle as a majority (>75%) of the substrate oxidized at rest is due to other metabolically active tissues (heart, brain, liver, etc). Using the arterial-venous difference in VCO_2 and VO_2 across the resting human forearm muscles, a respiratory quotient (RQ, local RER) of 0.763 was found corresponding to 81% and 19% fat and carbohydrate utilization respectively (18–21). This is similar to that found for the human leg (0.74-0.77) (39,40) and for rates of whole-body substrate utilization in the resting, fasted rat (41). Together these data indicate a preferential utilization of fatty acids in resting, fasted skeletal muscle and agree with the relatively low PDH activity.

In rat skeletal muscle, PDH activity is ~18% of total activity in the rested, fasted state (42–44) which is similar to that for human skeletal muscle (17%-25%) (15–17). Alteration in PDH activation in resting muscle results in reciprocal changes in muscle glucose utilization, with increased activity resulting in increased rates of glucose oxidation and vice versa. Increases in blood glucose or insulin independently stimulate

PDH activity resulting in increased glucose oxidation (45–49). This effect is most likely mediated by mass action effects of glucose uptake on PDH activation via pyruvate inhibition of PDK however, some studies have suggested increased PDP activity through posttranslational modification but has not been fully verified (50). Increasing PDH activity and glucose oxidation can also be achieved through reducing blood free fatty acid levels. Pretreatment with nicotinic acid (NA), an antilipolytic drug, reduces fasting blood free fatty acids from ~0.5 mM to <0.2 mM and increases PDH activity and glucose oxidation in humans (51). This effect is likely due to substrate limitation at the level of the TCA cycle, shifting the activation state of PDH to support basal metabolic demand.

Enhanced glucose oxidation with PDH activation is also observed with dichloroacetate (DCA) treatment. DCA is a potent inhibitor of PDK2 and PDK4 activity and results in complete activation of PDH in the resting state (16,25–28). This results in increased glucose oxidation in rat skeletal muscle (26,29,30) and increases whole body glucose oxidation in humans (32). The opposite effect has also been observed where decreased PDH activity reduces glucose utilization. However, without an effective inhibitor of PDH activity *in vivo*, studies rely on either long-term high fat diet or glycogen depletion to alter PDH activation state and result in stable upregulation of PDK expression and increases in PDK activity.

In humans, consumption of a high fat diet for 3-6 days results in reduced PDH activity in resting, fasted skeletal muscle concomitant with reduced glucose oxidation (52–54). This effect was also observed after high fat diet for only 56 hours and after high fat diet for 24 hours following glycogen depletion (55,56). Blood glucose is the

primary source of glucose for oxidation in resting skeletal muscle and was not reduced with high fat diet (22,53–55). Therefore, changes in glucose availability cannot explain reduced PDH activation or glucose utilization rates. However, high fat diet for as little as 1 day results in increased skeletal muscle PDK activity which further increases after 3 days of diet intervention (57). This is attributable to increases in skeletal muscle PDK4 expression as no alteration in PDK2 protein was found (57). The effect of high fat diet on PDP1 expression or activity has not been evaluated however expression levels were not affected by fasting, refeeding after fast, or insulin treatment and are not expected to be altered with high fat feeding (58,59).

Together, these data support PDH as a critical point of regulation in substrate selection of resting skeletal muscle. This is also apparent in skeletal muscle during exercise and has broad implications in disease states (type 2 diabetes) where dysregulation in skeletal muscle and whole-body fuel oxidation have been observed.

1.2.2 PDH Regulation of Skeletal Muscle Substrate Oxidation during Exercise

During exercise within the aerobic range, intensities where muscle or whole body $VO_2 < VO_{2MAX}$, absolute (Fig. 2) and relative (Fig. 3) substrate disposal rates markedly change as a function of the workload (W) relative to VO_{2MAX} (22,23). From rest to exercise at VO_{2MAX}, relative amounts of fatty acid and glucose oxidation exhibit an inverse relationship with a switch from predominantly fatty acid utilization in favor of glucose at 55-65% of VO_{2MAX} (Fig. 3) (22,23). Accordingly, absolute rates of fatty acid oxidation reach a maximum at ~65% of VO_{2MAX} (60) whereas the absolute rate of glucose oxidation rises continually from rest to VO_{2MAX} (Fig. 2) (22,23). Above 65% of VO_{2MAX}, the absolute rate of fatty acid utilization declines and reaches a minimum as

VO_{2MAX} is reached (22,23). At this point, skeletal muscle heavily relies on glycogen stores to sustain mitochondrial oxidative phosphorylation and ATP production.

This switch in substrate utilization from predominantly fatty acids at rest to glucose during muscle contraction is attributable to activation of PDH. Generally, it is agreed that carbohydrate oxidation regulates fatty acid oxidation and therefore when PDH is activated, the relative amount of glucose oxidation increases while fatty acid oxidation decreases. PDH activation during muscle contraction is a function of the metabolic demand exhibiting a linear relation with exercise intensity up to VO_{2MAX} (24,61,62) and can reach maximal activation within 15 seconds of exercise initiation (63). This is thought to occur as a result of coordinated inhibition of PDK activity and stimulation of PDP activity due to depressed energetics (↑ pyruvate, ADP/ATP, NAD+/NADH, and CoA/A-CoA) and increased Ca^{2+} respectively that occurs during muscle contraction (Fig. 1). The net response is dephosphorylation and activation of PDH, stimulating increases in oxidative glucose disposal that is matched to the metabolic demand.

Figure 4 shows the relationship between steady state PDH activity and exercise intensity relative to individual VO_{2MAX}. Distinct relationships are found between the three studies plotted in Fig. 4 that are likely attributable to difference in methodology in measuring PDH activity as subjects across the three studies displayed similar VO_{2MAX} (3.7-3.9 l/min) (24,61,62). Therefore, changes in total PDH activity or mitochondrial density would not be expected to account for this result. However, when normalizing to total PDH activity, therefore accounting for altered mitochondrial density or methodologies, a linear relation is found between percent PDH active the relative

exercise intensity (%VO_{2MAX}) even where total PDH activity varied between 1.96 and 3.74 U/gWW between studies (Fig. 5) (62–65). Although the relationship between percent PDH active relative to %VO_{2MAX} appears to be conserved, PDH activity can be altered by changes in glucose availability or through pharmacological activation that have reciprocal effects on muscle glucose utilization.

The most common perturbation to effect changes in PDH activity during muscle contraction is to alter the levels of muscle glycogen content prior to exercise. Eating a low fat, high carbohydrate diet increases muscle glycogen content and results in increased PDH activity at rest and during aerobic exercise concomitant with increased rates of glucose oxidation and reduced rates of fatty acid utilization (53,56,66). Conversely, glycogen depletion followed by a low carbohydrate diet results in increased fat oxidation during exercise at 65% VO_{2MAX} and is attributed to a 41% reduction in PDH activity as a result of a 2.6-fold reduction in muscle glycogen content (197±21 vs 504±25 mmol/kg dry weight) (56). PDH activity can also be modulated by changes in blood glucose with hyperglycemia resulting in increased glucose oxidation both at rest and during aerobic exercise in human and canine skeletal muscle (67–69). However, the effect of hypoglycemia on PDH activation during exercise has not been quantified as even during a low carbohydrate diet, blood glucose levels are similar to controls (66).

PDH activity can also be modified through treatment with dichloroacetate (DCA), an inhibitor of PDK activity that results in complete activation of skeletal muscle PDH both in rat (25,26) and humans (16,27,28). PDH activation with DCA treatment results in significant increases in glucose oxidation both in isolated rodent muscle (26,29–31) as well as whole body glucose oxidation in humans at rest (32) and during aerobic exercise

(33). Together, these studies support PDH as the primary regulator of substrate selection in skeletal muscle during aerobic exercise. PDH activity is linearly related to metabolic demand with alteration in PDH activity associated with reciprocal changes in glucose utilization. Regulation of PDH activity and the outcome of altered PDH activity on muscle bioenergetics are the focus of experiments presented in chapters 2 and 3 of this thesis.

Figure 2. **Substrate utilization during voluntary exercise.**

Absolute rates of glucose and fatty acid oxidation during voluntary exercise relative to maximal oxygen uptake (%VO_{2MAX}) in man. Data are adapted from van Loon LJC et al. 2001 (22).

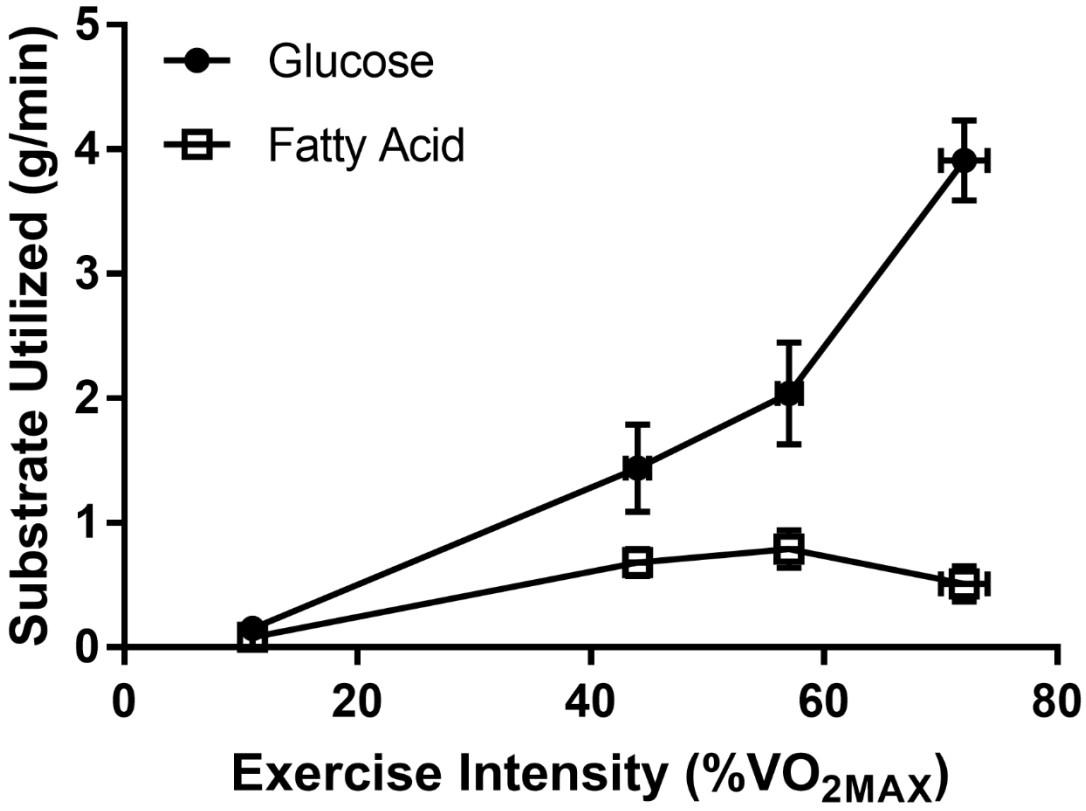

Figure 3. Relative substrate oxidation as a percent of total energy expenditure during voluntary exercise in man.

Data are adapted from van Loon LJC et al. 2001 (22).

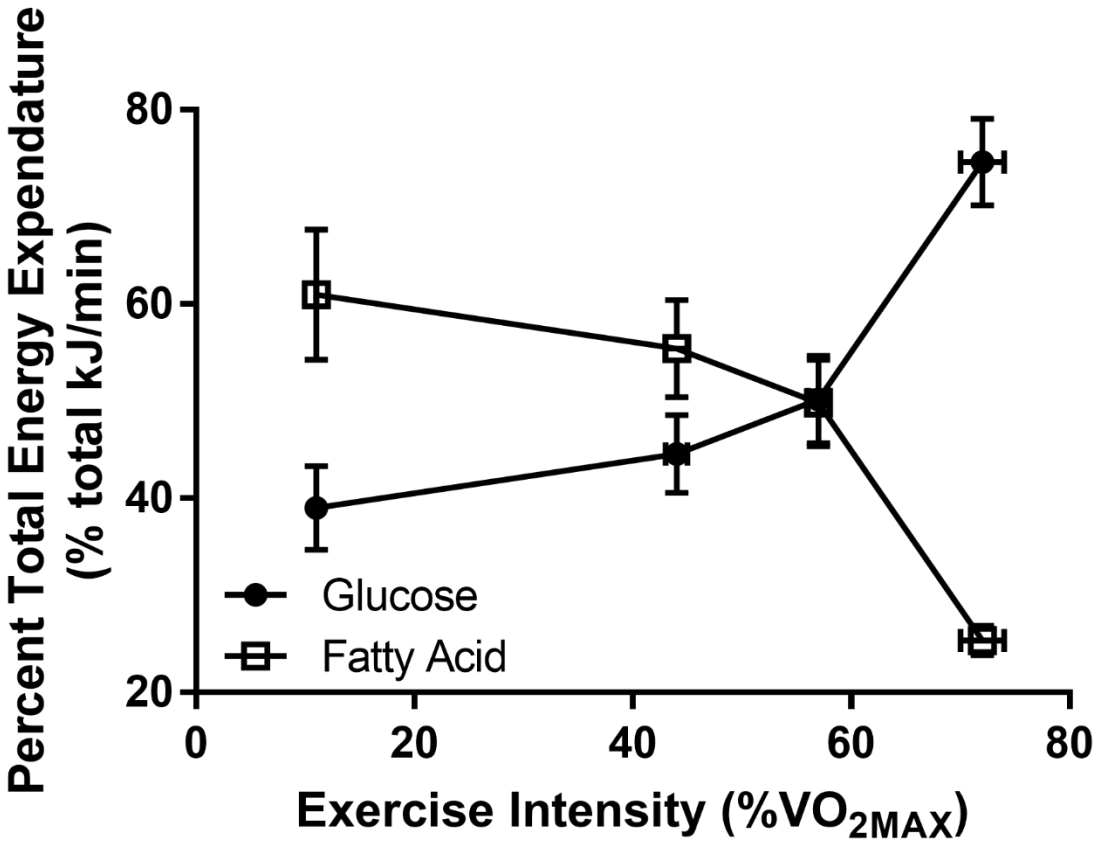

Figure 4. PDH activation is linearly related to exercise intensity.

Active fraction of pyruvate dehydrogenase (PDHa) during voluntary exercise relative to maximal oxygen uptake (%VO_{2MAX}) in man. Data are adapted from Constantin-Teodosiu D et al. 1991 (61), Putman CT et al. 1995 (62), and Howlett RA et al. 1998 (24).

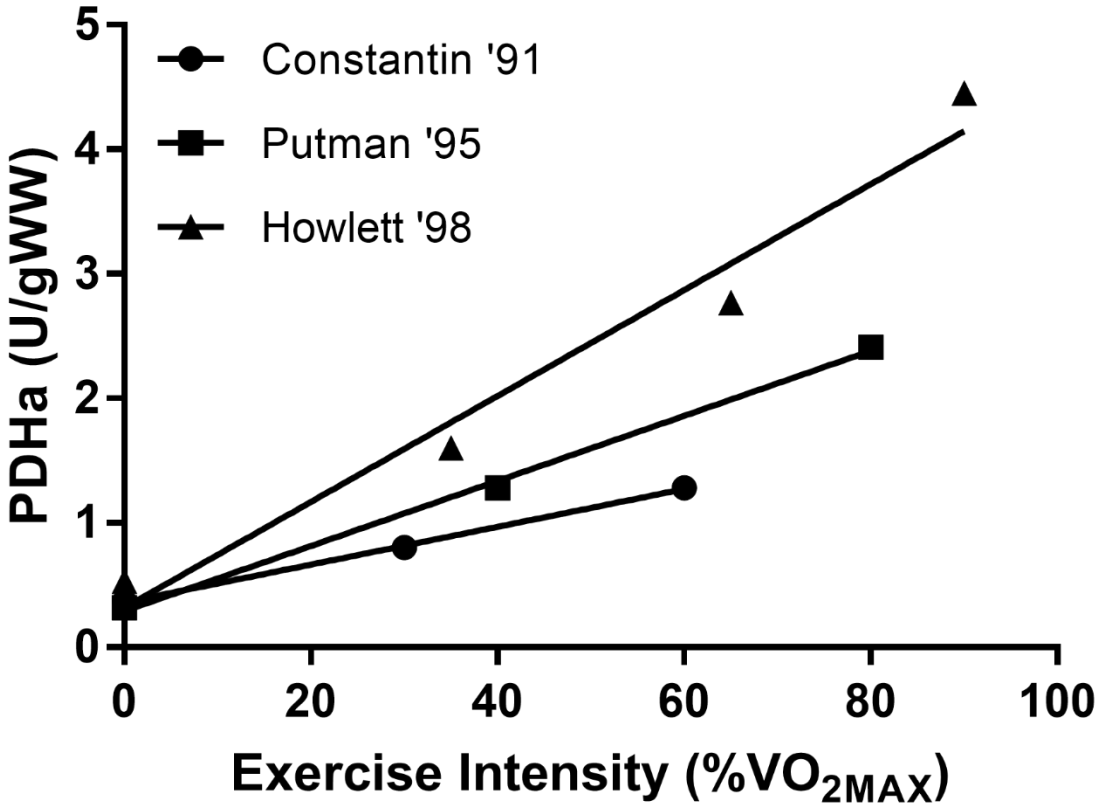

Figure 5. Conserved relationship between percent PDH activity and relative exercise intensity.

Fractional pyruvate dehydrogenase activity relative to total activity (%PDH) during voluntary exercise expressed as a percent of maximal oxygen uptake (%VO_{2MAX}) in man. Data are adapted from Constantin-Teodosiu D et al. 1992 (64), Putman CT et al. 1995 (65), Putman CT et al. 1995 (62), and Parolin ML et al. 1999 (63).

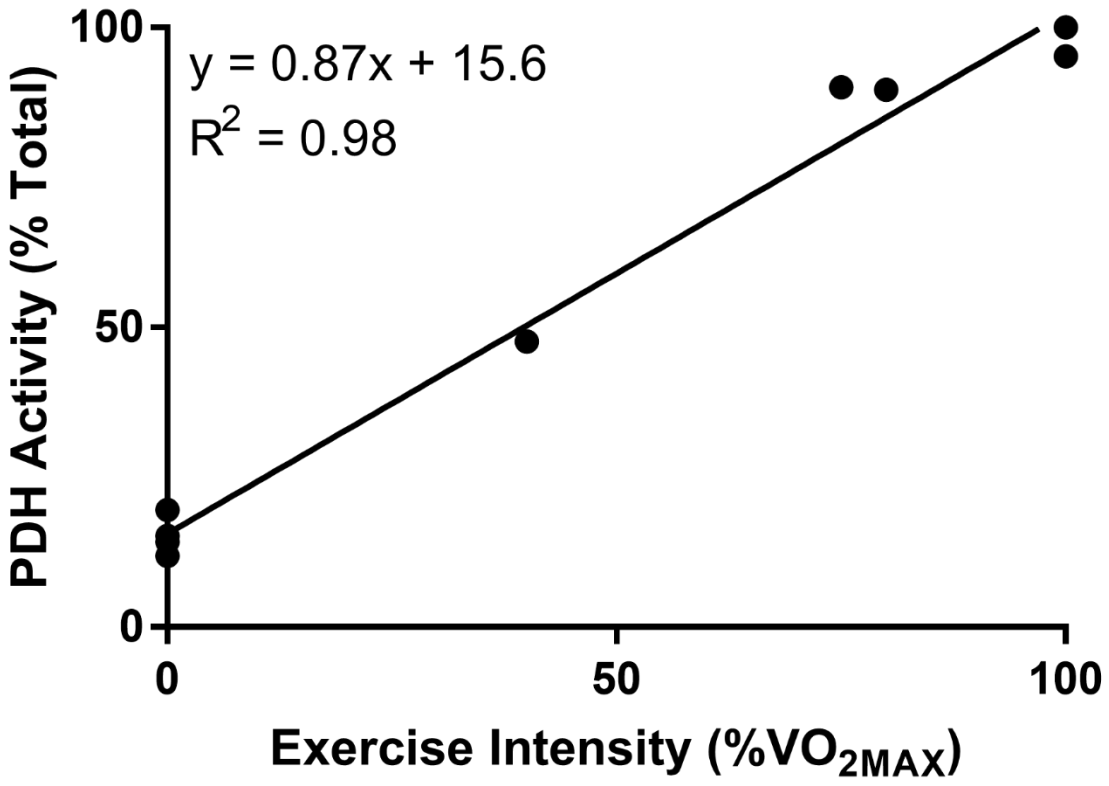

1.2.3 Influence of Fatty Acid Availability on PDH Activity and Substrate Disposal in Skeletal Muscle

Although it is the opinion of this thesis that PDH activity sets the relative utilization of substrate oxidation by skeletal muscle, some studies have argued for a shared role of PDH and fatty acids in the regulation of substrate selection by skeletal muscle mitochondria. In this context, a brief review of fatty acid oxidation and its effects on PDH activity and regulation of substrate selection will be given. Unlike glucose where absolute rates of oxidation increase relative to exercise intensity, absolute rates of fatty acid oxidation reach a peak at ~65% VO_{2MAX} and subsequently is reduced at higher intensities (Fig. 2) (22,23,60). Whether fatty acid availability limits oxidation during exercise in the aerobic domain or whether it can displace glucose through inhibition of PDH activity has been the subject of numerous studies. Fatty acid availability during exercise depends on two main factors: nutritional status and exercise intensity. At rest and up to moderate intensity exercise (<65% VO_{2MAX}) plasma fatty acids represent the majority of fatty acids utilized by skeletal muscle (22,23). Although intracellular triglyceride stores are increasingly utilized as exercise intensity increases, it is recognized that plasma fatty acid availability sets a limit to fatty acid utilization and oxidation during exercise (70).

After an overnight fast, blood fatty acid levels are typically between 0.5-1.0 mM (22,51,71,72). In the post-absorptive state, glucose drives an increase in insulin secretion which subsequently reduces endogenous adipose and tissue lipolysis reducing blood fatty acid levels to <0.3 mM (70,73–77). During moderate exercise (<65% VO_{2MAX}) in either state, fatty acids levels remain unchanged during shorter

duration bouts (<1 hour) (22,71,73) however can increase over time more than 4-fold during long duration exercise (>2 hours) (23,72). At high intensity exercise (>65% VO_{2MAX}), a marked reduction in blood fatty acid levels is seen in some (23,70,74,78) but not all (22,71) studies during voluntary exercise. Although the absolute rate of blood fatty acid oxidation exhibits a linear relationship with exercise up to moderate intensity, rates of fatty acid oxidation during high intensity exercise are reduced compared to peak rates seen at ~65% VO_{2MAX} (22,23,60). Whether the reduction in fatty acid oxidation at high intensity exercise is due to limited plasma availability or indeed whether plasma availability limits oxidation even at moderate intensity exercise has been investigated by modulating blood free fatty acid concentrations.

At moderate intensity exercise (~40-68% VO_{2MAX}), some (73,76,79) but not all (72,80) studies have shown that increasing plasma free fatty acid availability resulted in significant increases in fatty acid oxidation and glycogen sparing. The contradictory results appear to be due to differences in plasma fatty acid and insulin concentrations and its effect PDH activity prior to elevation of plasma fatty acids levels via high fat meal (80), heparin (73) or lipid-heparin infusion (72,76,79). In Odland et al. 1998 (76), Odland et al. 2000 (79) and Costill et al. 1977 (73) blood fatty acid levels were kept artificially low (0.2-0.3 mM) through prior carbohydrate feeding where subjects were given a carbohydrate meal 2hrs (76,79) and 6hrs (73) before the exercise bout and lipid intervention. Conversely in Ravussin et al. 1986 (72) and Decombaz et al. 1983 (80), subjects were merely fasted overnight resulting in blood fatty acid concentrations of 0.5mM and 0.9mM respectively. When blood lipid concentrations were increased, significant effects on whole body substrate utilization during moderate intensity exercise

were only found in those studies where the control subjects' plasma fatty acid levels were reduced (<0.5 mM) compared to normal fasting concentrations (0.5-1.0 mM).

Furthermore, although insulin levels were not measured in Odland et al. 1998 (76) or Odland et al. 2000 (79), carbohydrate feeding is well known to result in an insulin spike at ~0.5-2.5 hours post ingestion concomitant with reduced blood free fatty acid levels (75,77). Insulin is known to increase PDH activity (45,81). Consistent with this notion, significantly elevated PDH activity was found during exercise in both studies where carbohydrates were given 2 hours prior to exercise (76,79). Unlike Odland et al. 1998 (76) and Odland et al. 2000 (79), Costill et al. 1977 (73) waited 6 hours post carbohydrate meal before exercise or lipid intervention. As a result, plasma insulin levels had normalized prior to exercise yet plasma fatty acids remained reduced (~0.2 mM). Although PDH activity was not measured in that study, merely reducing blood fatty acid levels to <0.2 mM results in increased PDH activity during moderate intensity exercise (51). Therefore, it is likely the case that in each study that utilized carbohydrate feeding prior to exercise, a combination of limited fatty acid availability as well as increased PDH activity biased results towards higher carbohydrate utilization in the control group. Thus, the subsequent increases in fatty acid oxidation and glycogen sparing with lipid intervention may merely indicate a return to normal substrate utilization where fatty acid availability is not limiting. In reality, in the fasted state where plasma fatty acids are 0.5-1.0 mM and where PDH activity is not increased by carbohydrate induced insulin release, no effect of increased fatty acid availability was seen on substrate selection at moderate intensity exercise (72,80). This further supports

that at moderate intensity exercise, PDH sets the relative rates of substrate oxidation where substrate availability is not limiting.

At high intensity exercise (>70% VO_{2MAX}), there is more evidence for a physiological role of limited plasma fatty acid availability on substrate selection (23,70,74,78). Not only do some studies show reduced plasma fatty acid availability at these exercise intensities (23,70,74,78), but absolute rates of fatty acid oxidation are also reduced (22,23). However, as is the case for moderate intensity exercise, some (70,74) but not all (71) studies have shown an effect of intravenous administration of heparin-lipid infusion to increase fatty acid oxidation and glycogen sparing. The discrepancy between studies is again likely due to the nutritional status of the subjects prior to the exercise bout as well as the sampling for substrate oxidation. In Romijn et al. 1995 (70) and Dyck et al. 1993 (74), blood fatty acid levels were reduced (<0.2 mM) prior to lipid infusion via ingestion of a glucose load 2-6 hours prior to exercise. This resulted in significant glycogen sparing (15-44%) (70,74) and increased fatty acid oxidation by 27% (70) assessed via whole body RER. Conversely, Hargreaves et al. 1991 (71) found no difference in leg arterial-venous RQ with heparin-lipid infusion however did find a significant reduction in whole body RER during high intensity exercise. This divergence highlights the potential for differential respiratory sampling and nutritional status to influence the interpretation of high fat supplementation. Unlike Romijn et al. 1995 (70) and Dyck et al. 1993 (74), the subjects of Hargreaves et al. 1991 (71) study were merely fasted overnight resulting in a blood fatty acid concentration of 0.6 mM versus <0.2 mM for the previous studies.

Furthermore, where previously significant effects of lipid infusion were seen on whole body RER, no significant effect on leg RQ was found at the level of the working muscle bed (71). Therefore, the significant drop in RER seen with lipid infusion at high intensity exercise may reflect the non-working skeletal muscle or in fact other metabolically active tissues in the body. Nevertheless, even though lipid infusion did not result in a significant drop in leg RQ, it was lower than control values (0.87±0.02 vs. 0.86±0.03) (71). Furthermore, lipid infusion caused a 33% reduction in leg glucose uptake yet resulted in no difference in glycogen breakdown (71). It is unclear how reduced glucose uptake with similar glycogen utilization could result in similar leg RQ however it may be possible that supplementation only minimally increased fat oxidation yet was outside the sensitivity of detection. In any case it appears that at high intensity exercise in the fasted state, reduction in absolute rates of fatty acid oxidation are only marginally related to changes in blood fatty acid availability and are more likely related to intracellular mechanisms that regulate oxidation such as PDH activation.

Together, these studies support that where fatty acid availability is not limiting, skeletal muscle mitochondria will preferentially utilize glucose over fatty acids as oxidative substrate. Therefore, the magnitude of PDH activation during exercise sets the relative utilization of glucose versus fatty acids during aerobic exercise. This concept highlights the necessity of determining the primary mechanisms regulating PDH activity *in vivo* and is the subject of study in chapter 2 of this thesis. Additionally, the ability of PDH to regulate substrate oxidation will be exploited in chapter 3 where the effect of increasing PDH activity on the bioenergetic response of muscle contraction is quantified.

1.2.4 Influence of Muscle Mitochondrial Density on Substrate Selection and PDH Activity During Exercise

Changes in muscle mitochondrial density have clear effects on absolute rates of glucose and fatty acid utilization with increasing capacity for oxidation with increased mitochondrial density and vice versa (82–84). However, the impact of mitochondrial density on relative rates of substrate oxidation, or the preference for glucose or fatty acids during exercise are less clear. Some studies suggest that increased mitochondrial density with exercise training shifts relative substrate oxidation during exercise towards increased fatty acid utilization and reduced glucose oxidation compared to controls at the same relative exercise intensity (%VO_{2MAX}) (85–87). This effect has also been observed in reverse with reduced mitochondrial density associated with increased utilization of glucose and reduced fatty acid oxidation compared to trained individuals during exercise at similar %VO_{2MAX} (88). However, not all studies have found this result with some suggesting that the relative rates of glucose and fatty acid oxidation are the same during exercise at similar %VO_{2MAX} in muscle with different mitochondrial densities (89–91). This is also true when comparing relative rates of substrate oxidation between various mammalian species that exhibit vastly different aerobic capacities (92). When the fractional rates of glucose or fatty acid oxidation are compared during voluntary exercise at intensities relative to individual VO_{2MAX}, it appears there is a conserved relationship between the rat (41), goat (92), dog (92), and human (22,23) (Fig. 6). This would suggest that rates of glucose or fatty acid utilization are proportional to the absolute contractile workload relative to the muscle mitochondrial density with inferences to the regulation of substrate selection and of PDH activity.

In the preceding sections of this thesis it was described how carbohydrate metabolism regulates fatty acid oxidation with the activation state of PDH setting the relative utilization of substrates at rest and during exercise. If substrate selection or relative rates of substrate oxidation at similar %VO_{2MAX} exercise are different in muscle with altered mitochondrial density, it would suggest differential regulation of PDH activation during contraction. However, if relative substrate selection is the same, it would suggest PDH activation is proportional to the workload relative to mitochondrial density, similar to that shown in Figure 3. Unfortunately, few studies have investigated the direct effect of altered mitochondrial density on the regulation of PDH activity. This forms the basis for the work of chapter 2 of this thesis however, a brief review of the available literature on the regulation of PDH activity with altered mitochondrial density is given.

The influence of altered mitochondrial density on PDK, PDP and PDH protein levels or activities are relatively understudied, yet expression levels of the proteins appear to change in concert with skeletal muscle mitochondrial density. For example, mitochondrial density was increased in human subjects after an 8-week endurance training program that resulted in a 15% increase in whole body VO_{2MAX} and was associated with 21% and 108% increases in muscle citrate synthase and cytochrome c oxidase activities respectively (93). This also resulted in a 1.3-fold increase in PDK2 expression and a 2-fold increase in total PDK activity, although changes in PDK4 expression were not found (93). Total PDH activity was also increased by 31% with training and exhibited a 1.3-fold increase E1 subunit (pyruvate dehydrogenase) expression (93). In a separate study it was also shown that PDK2, PDP1 and E1 protein

expression are positively correlated with muscle citrate synthase activity in human subjects (94). This also was true for total PDK and PDP activities, however total PDH activity was not determined (94). Therefore, it appears that reciprocal changes in PDK2, PDP1, and PDH protein levels occur with increased mitochondrial density but few studies have addressed how this may alter regulation of PDH activity during exercise.

Endurance training in human subjects for 7 weeks increased mitochondrial density by 27% and resulted in reduced PDH activity after 15 minutes of aerobic exercise when compared to sedentary controls (84). Importantly, this effect was observed at the same absolute workload and was attributed to reduced signals driving PDH activation (e.g. lower pyruvate, increased steady state energetics) (84). It has been known for some time that when comparing muscle energetics and substrate oxidation at absolute workloads, muscle with higher mitochondrial density supports increased steady state energetics and has a relatively higher reliance on fatty acids for oxidative ATP synthesis (83,95). Therefore, it is expected that during muscle contraction with increased mitochondrial density, percent PDH activity would be reduced when compared to lower mitochondrial density muscle at the same absolute workloads. It follows that when PDH activity was compared between high and low mitochondrial density muscles at the same relative workloads (%VO_{2MAX}), PDH activity was similar between groups at both 50% and 65% of their respective VO_{2MAX} (96). This would suggest as implied earlier that regulation of substrate selection through PDH activation should scale to the workload imposed on the muscle relative to the muscle mitochondrial density or aerobic capacity (Fig. 5, Fig 6). In other words, it would be expected that at similar relative exercise intensities (%VO_{2MAX}), PDH activity and

relative rates of substrate utilization would not be different between muscles with different mitochondrial density. Unfortunately, there are only two studies that have investigated the effect of changing mitochondrial density on the regulation of PDH activity during muscle contraction and further attempts to quantify this relationship are presented in chapter 2.

Figure 6. Substrate selection is conserved across species relative to exercise intensity.

Percentage of total oxygen consumed ($\%VO_2$) by glucose or fatty acid oxidation during voluntary exercise expressed as a percent of maximal oxygen uptake ($\%VO_{2MAX}$) in the dog, goat, rat, and human. Data adapted from Romijn JA et al. 1993 (23), van Loon LJC et al. 2001 (22), Roberts TJ et al. 1996 (92), and Brooks GA et al. 1983 (41).

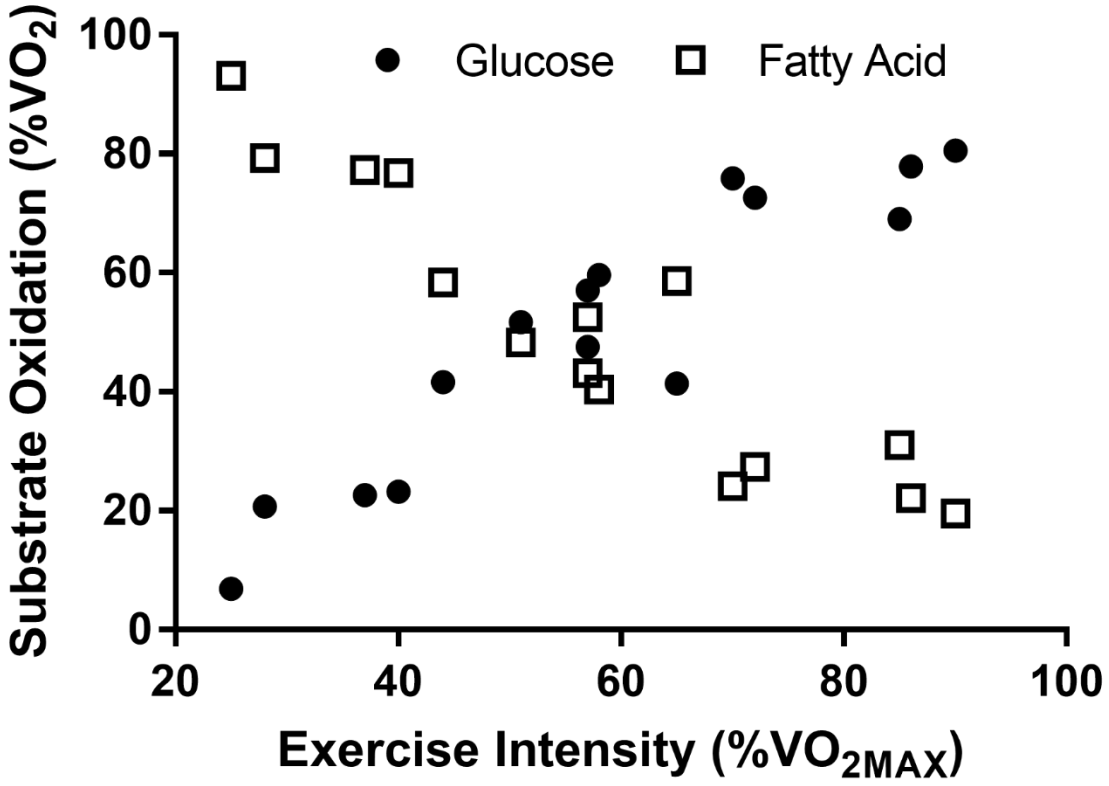

1.2.5 PDH Activity and Skeletal Muscle Substrate Oxidation in Type 2 Diabetes

Type 2 diabetes is hallmarked by overt hyperglycemia and loss of glycemic control as a result of peripheral insulin resistance. Skeletal muscle is an early site of insulin resistance in type 2 diabetes and is thought to play a primary role in the dysregulation of glucose homeostasis (97). Although PDH plays a pivotal role in regulating the magnitude of glucose oxidation in skeletal muscle, surprisingly few studies have investigated or quantified regulation of PDH activity in type 2 diabetes. Early type 1 diabetic rodent models singled out decreased skeletal muscle PDH activity as a potential mechanism of hyperglycemia and loss of glycemic control (43,44,59,81). This effect was attributed to increased phosphorylation of the enzyme complex that resulted in decreased PDH activity in resting, fasted muscle as well as during muscle contraction (43,44). Further study determined that increased PDH phosphorylation was due to increased PDK activity as a result of specific upregulation of PDK4 expression in skeletal muscle (98). PDK4 expression is upregulated with a loss of skeletal muscle insulin signaling as well as with elevated free fatty acids that are found in the type 1 diabetic animal model (98,99) Together, this resulted in reduced rates of skeletal muscle glucose oxidation at rest, after insulin treatment, and during muscle contraction (100,101) This led to a common theme among diabetic literature that suggested decreased PDH activity as a mediator of type 2 diabetes. However, studies to confirm this phenomenon in type 2 diabetic rodents or further, in type 2 diabetic human subjects did not occur until decades later and with contradictory results.

In the two papers that have investigated PDH activity in type 2 diabetic rodent models, both studies confirmed earlier results of the type 1 diabetic rodent studies and

found decreased PDH activity in resting skeletal muscle. In the Otsuka Long-Evans Tokushima Fatty (OLETF) rat, which spontaneously develops type 2 diabetes with age, decreased PDH activity was found in resting skeletal muscle when compared to Long-Evans Tokushima Otsuka (LETO) non-diabetic controls (102). Increased PDK2 and PDK4 mRNA and protein expression was also found in the OLETF rats compared to LETO that resulted in increased total PDK activity in muscle lysates (102). Muscle of the OLETF rat also had reduced PDP1 mRNA and protein expression, and although PDP activity was not determined, it was concluded that increased PDK versus PDP expression was the cause for reduced PDH activity with type 2 diabetes (102). A similar result was also obtained in the more commonly used Zucker Diabetic Fatty (ZDF) rat. This rodent model also spontaneously develops type 2 diabetes with age and like the OLETF rat, ZDF rats displayed reduced PDH activity in skeletal muscle when compare to lean controls (103). This effect was observed both in fed and fasted skeletal muscle that also persisted after oral glucose challenge with lower PDH activity in ZDF rats compared to lean controls (103). Like that of the OLETF rat, ZDF rats also displayed elevated protein expression of PDK4 however expression levels of PDK2 and PDP1 or the total activities of PDK or PDP were not determined (103). Together these data appear to confirm earlier results in type 1 diabetic rodent models and support reduced PDH activity in the etiology of hyperglycemia with the complete loss of insulin in type 1 diabetes or the loss of insulin signaling with insulin resistance in type 2 diabetes.

Interestingly, this does not appear to be the case for type 2 diabetic humans with most studies supporting either similar PDH activity or even increased PDH activity in fasting diabetic skeletal muscle. In separate studies, similar PDH activity was found in

type 2 diabetic vastus lateralis skeletal muscle compared to non-diabetic controls that corresponded to similar rates of whole body (104) and leg (105) glucose oxidation. However, increased PDH activity in type 2 diabetic skeletal muscle has also been observed and resulted in a 1.5-fold increase in leg glucose oxidation compared to non-diabetic controls (106). Furthermore, whole body glucose oxidation is similar to or increased in type 2 diabetics during aerobic exercise and although PDH activity was not measured, these data suggest either similar or increased PDH activity compared to non-diabetic controls (107–112). These results are surprising considering that similar to type 1 and type 2 diabetic rodent models, human type 2 diabetic skeletal muscle also exhibits increased PDK2 and PDK4 mRNA (113) with the mRNA levels positively correlated with the level of insulin resistance (114). However, protein expression or activity of PDK2, PDK4, or PDP1 have not been determined. Therefore, it is difficult to speculate as to why results in human type 2 diabetic skeletal muscle differ from that of rodents. Nevertheless, two singular studies in rodent models of type 2 diabetes is insufficient to determine regulation of PDH activity *in vivo*, and furthermore, no study has quantified the effect of types 2 diabetes on regulation of PDH activity during muscle contraction. The current lack of available data and the contradictory results of PDH regulation in human versus rodent type 2 diabetes has formed the basis for the work presented in chapter 4 of this thesis on PDH regulation in the type 2 diabetic Goto Kakizaki rat.

1.3 Skeletal Muscle Bioenergetics

1.3.1 Mitochondrial Oxidative Phosphorylation

At its core, mitochondrial ATP synthesis involves the coupling of proton (H^+) and electron transfer through an energy conserving membrane to the phosphorylation of ADP to ATP. The mitochondrial electron transport system, or respiratory chain, is comprised of 4 main elements that receive electrons via oxidation of reducing equivalents (e.g. NADH, QH_2) generated through substrate oxidation by mitochondrial matrix dehydrogenases (e.g. PDH, acyl-CoA dehydrogenase, α-ketogluterate dehydrogenase, etc.). The four complexes of the respiratory chain are NADH ubiquinone oxidoreductase (complex I), succinate dehydrogenase (complex II), ubiquinol-cytochrome c oxidoreductase (complex III), and cytochrome c oxidase (complex IV). Electrons are donated at either complex I or II and passed down the chain until complex IV where O_2 is the final electron acceptor, reducing $1/2O_2$ to H_2O. Each complex contains a redox carrier or couple that exists in a reduced or oxidized state and has a characteristic redox potential (ΔE_h), or tendency to donate or accept electrons. A more negative potential (e.g. NADH) indicates the tendency to donate electrons whereas a more positive potential (e.g. O_2) dictates the tendency to accept. The respiratory chain is organized in such a way that the reduction potentials of the redox carriers progressively increase (become more positive) and couple the change in potential energy of the electron during transfer between carriers to proton pumping from the mitochondrial matrix to the intermembrane space. Proton pumping or translocation to the intermembrane space occurs at complex I, II, and III. This creates a proton gradient composed of both an electrical ($\Delta\psi$) and concentration (ΔpH) potential that are

collectively described as the proton motive force (Δp). Therefore, the change in potential energy of the electron as it passes through the respiratory chain is not lost but conserved in the potential energy of the proton electrochemical gradient (Δp). Finally, Δp provides the driving force for ATP synthesis, coupling the energetically favorable backflow of protons through the F_OF_1 ATPase into the matrix with ADP phosphorylation to ATP. Thus, the magnitude of Δp sets the potential energy of ATP which is described as the free energy of ATP hydrolysis (ΔG_{ATP}).

Arranged in this way, the magnitude of ΔG_{ATP} is the result of its steady state relationship between the mitochondrial redox potential (ΔE_h) transduced through the proton motive force (Δp) (115). Therefore, it can be said that ultimately, the magnitude of each potential is limited by the magnitude of ΔG_{ATP}. Put another way, energy transduction through the mitochondria is a pull through mechanism and not a push through mechanism. Forward flux is ultimately determined by the terminal back pressure of ΔG_{ATP}, and therefore it is the cytosolic ATPase activity or ATP demand that drains ΔG_{ATP} and controls forward flux of the system. Therefore, ATPase activity is the primary regulator of oxidative ATP synthesis and provides the pull that stimulates substrate oxidation, oxygen consumption, and ATP synthesis by the mitochondria. However, since these potentials are coupled, first through the respiratory chain and finally the F_OF_1 ATP synthase, modification of any one potential will stimulate flux through the entire system until a new steady state is reached albeit at different magnitudes. Therefore, increasing the matrix redox potential (ΔE_h) could stimulate ATP synthesis flux for a given cytosolic ATPase demand by increasing Δp and therefore ΔG_{ATP} through its steady state relation at the F_OF_1 ATPase. Stimulation of ATP

synthesis in this way would be expected to proceed until ΔG_{ATP} and therefore Δp reached such a magnitude that the “back pressure” of these potentials reached a new steady state with ΔE_h. At this point, forward flux would again be dictated by changes in cytosolic ATP demand however the magnitudes of steady state ΔE_h, Δp, and ΔG_{ATP} would be increased. This concept forms the basis for the hypothesis of how PDH activity could modulate muscle energetics *in vivo* and is presented in its final form in chapter 3 of this thesis.

1.3.2 Bioenergetics of Muscle Contraction

During muscle contraction within the aerobic domain, contractile ATPase activity (myosin, SERCA) reaches a steady state with mitochondrial ATP synthesis. This relation occurs over a wide range of metabolic states exhibiting 10-fold increases in mitochondrial oxygen consumption, and ATP production, during sustainable contractile workloads (116). Throughout the aerobic domain, skeletal muscle ATP content remains stable as ATP is buffered by phosphocreatine (PCr) through its equilibrium relationship at creatine kinase (CK). During muscle contractile activity, ATP is hydrolyzed to ADP and Pi which stimulates the instantaneous hydrolysis of PCr and rephosphorylation of ADP to ATP. This results in reciprocal stoichiometric changes in PCr and Pi with net hydrolysis of PCr and production of Pi that reach steady state levels during submaximal contractile intensities (117). The extent of PCr hydrolysis, and Pi formation, and the time course of PCr recovery after muscle stimulation are linear functions of the ATPase rate, or muscle workload, relative to the mitochondrial density and the total creatine content of the muscle fiber (95,118–120).

Through PCr buffering and mitochondrial ATP synthesis the free energy of ATP hydrolysis (ΔG_{ATP}), which defines the maximal available work per mole of ATP hydrolyzed, is relatively constrained to a narrow range within fast twitch skeletal muscle of ~10 kJ/mol (approx. -65 to -55 kJ/mol) (121,122). ΔG_{ATP} increases (becomes more positive) as a function of muscle contraction due to the increases in ADP and Pi relative to ATP content in the muscle fiber and reaches steady state levels dependent on the contractile intensity and ATPase rate. However, the magnitude of steady state ΔG_{ATP} at a given workload can vary depending on the mitochondrial density of the muscle fiber (95,121). This is due to a change in the sensitivity or "gain" of the system which results in higher or lower feedback signals required to stimulate oxidative phosphorylation with decreased or increased mitochondrial density respectively. Therefore, with reduced mitochondrial density, ΔG_{ATP}, ADP, and Pi must increase to a greater extent to stimulate the same rate of oxidative ATP synthesis. This results in a reduced energetic steady state and limits the maximal sustainable workloads the muscle can maintain before failure/fatigue. Conversely, muscle with higher mitochondrial density exhibits a higher "gain" and therefore responds with greater rates of oxidative ATP synthesis for a given increase in ΔG_{ATP}, ADP, and Pi. Along with the greater capacity to oxidize glucose and fatty acids, this increases the range of sustainable workloads the muscle can maintain and underscores the benefit of increasing mitochondrial density through endurance training. Taken together these observations clearly show that in skeletal muscle energy metabolism is a dynamic pull system where oxidation of substrates in specific chemical form and quantity depend upon the nature of the metabolic demands imposed both in the intensity and the rate of contraction. This concept of a pull system to oxidize

substrates can be readily generalized to other organ systems and is an often overlooked aspect in studies of metabolic regulation.

1.4 Summary

Given the critical importance of PDH in the regulation of glucose oxidation in skeletal muscle, the mechanisms regulating PDH activation *in vivo* and the consequence of dysregulation of PDH activity on muscle function is inadequately understood. Delineating the mechanisms of PDH activation and further, the impact of altered substrate selection on muscle function has clear implications to diseases that exhibit metabolic syndrome with impaired glycemic control where dysregulation of PDH has been suggested (obesity, diabetes, etc.). In order to further understand the role PDH plays in muscle function in health and disease, this dissertation will investigate PDH in three central frameworks:

1. Mechanisms Regulating PDH Activation: PDH activation will be quantified in relation to the primary regulators of its activation status (energetics vs. Ca^{2+}), rather than solely by exercise intensity as has previously been established.
2. Effect of Altered PDH Activity on Muscle Bioenergetics: Given its central position in both mitochondrial substrate selection and reducing equivalent generation, dysregulation of PDH activity could play a significant role in muscle function during exercise. Here the effects of increased PDH activity on muscle function and bioenergetics *in vivo* will be quantified.
3. Regulation of PDH Activity in Type 2 Diabetes: Due to the importance of PDH activity in oxidative glucose disposal and the contradictory reports of PDH activity

in type 2 diabetes, PDH activity will be quantified in type 2 diabetic skeletal muscle both at rest and during muscle contraction.

Chapter 2. Steady State Energetics and Pyruvate Dehydrogenase Activity are Normalized to Workload Relative to Mitochondrial Density in Contracting Skeletal Muscle

2.1 Abstract

Glucose oxidation in skeletal muscle is regulated by pyruvate dehydrogenase (PDH) which exhibits low fractional activity in resting muscle but is activated with increased workload. Activation of PDH occurs through dephosphorylation, presumably as a result of inhibition of pyruvate dehydrogenase kinase and stimulation of pyruvate dehydrogenase phosphatase through reduced energetic status and increased Ca^{2+} respectively. This study sought to define the contribution of energetics or Ca^{2+} in the regulation of PDH activation. Phosphorus energetics were quantified *in vivo* with nuclear magnetic resonance spectroscopy (^{31}P NMR) in conjunction with muscle force output and PDH activity during electrical stimulation of rat superficial gastrocnemius muscle. To evaluate the influence of mitochondrial density on PDH regulation, muscle mitochondrial density was reduced through experimental hypothyroidism by four weeks of methimazole (MMI) treatment. MMI treatment resulted in an ~50% reduction in gastrocnemius muscle mitochondrial density determined by significant reduction in whole muscle lysate cytochrome c oxidase and total PDH activity, as well as increased time constant of PCr recovery measured *in vivo* with ^{31}P NMR. At absolute contractile workloads, reduced mitochondrial density with MMI treatment resulted in significant depression of steady state energetics concomitant with increased PDH activation compared to controls. However, when compared at workloads relative to mitochondrial oxidative capacity comprising contractile intensities that were half that of controls for

MMI treated rats, energetics and PDH activation were no different between groups, Therefore, PDH activation is primarily a function of the energetic status of the muscle fiber and not Ca^{2+} concentration during muscle contraction.

2.2 Introduction

Skeletal muscle utilizes both glucose and free fatty acids as substrate for mitochondrial oxidative ATP synthesis (22,23). In fasted skeletal muscle under resting conditions, free fatty acids are the predominant substrate utilized to support basal ATPase activity, comprising ~80% of total carbon substrate utilization (18–20,40,48). In the transition from rest to aerobic contractile workloads, i.e. intensities that can be supported by mitochondrial ATP synthesis, the relative proportion of glucose oxidation increases with reciprocal decreases in fatty acid oxidation until the maximal aerobic capacity is reached (22,23,92). This transition in substrate utilization is attributed to activation of pyruvate dehydrogenase, the mitochondrial matrix enzyme that regulates glucose oxidation by controlling pyruvate decarboxylation to acetyl-CoA. PDH activity is regulated via reversible phosphorylation where phosphorylation reduces the apparent Vmax and dephosphorylation increases the apparent Vmax (5).

In skeletal muscle the phosphorylation state of PDH is regulated by the relative activities of two isoforms of pyruvate dehydrogenase kinase (PDK2, PDK4) and one isoform of pyruvate dehydrogenase phosphatase (PDP1) (6,35). In resting skeletal muscle, PDH activity is suppressed to ~10-20% of total maximal activity through preferential phosphorylation, coinciding with the low rates of glucose oxidation ((15,24,42–44,63,122). Exercise is associated with increases in PDH activity that are

linearly related to muscle contractile activity reaching peak activation at maximal aerobic workloads (24,63,122,123). This occurs as a function of the depressed energetic state of the muscle fiber resulting in reduced ATP/ADP, NADH/NAD^+, and A-CoA/CoA which reduce PDK activity through allosteric inhibition (5). Simultaneously, increased Ca^{2+} results in allosteric activation of PDP, shifting the relative activities of these enzymes resulting in net PDH dephosphorylation and activation thereby permitting elevated glucose oxidation (5).

In skeletal muscle of exercise-trained humans, the increase in mitochondrial density known to occur with training causes a shift in substrate utilization towards fatty acid oxidation at absolute workloads relative to sedentary individuals which coincides with reduced PDH activity (84,85,124). This shift in substrate utilization in the trained subjects is likely related to the increased sensitivity of oxidative phosphorylation to the feedback products of ATP hydrolysis (ADP, Pi), which decreases energetic signals that modulate PDH activity (95,118). However in some studies, increased fatty acid oxidation was also observed in trained individuals relative to sedentary counterparts even at similar relative workloads (% of max), where the energetic status would be expected to be comparable (89,95,118,125). This observation suggests that altered activation of PDH has occurred relative to muscle contractile activity when controlling for increased oxidative capacity but the necessary measurement of steady state energetics was not performed (89,125).

The purpose of this study was to quantify the effect of mitochondrial density on the regulation of PDH activity and mitochondrial energetics during muscle contraction. Phosphorus magnetic resonance studies were performed on control rat muscle and in

those where mitochondrial density was reduced after 4 weeks of methimazole (MMI) treatment. Posterior leg muscles were stimulated with simultaneous measurements of *in vivo* phosphorus energetics and muscle force production. PDH activity was also measured in muscle samples collected at rest and during stimulation for both control and MMI treated rats. The sustainable steady state phosphorus metabolites were significantly reduced in MMI treated rats at absolute stimulation intensities (Hz) with concomitant increases in glycolytic ATP production and fractional PDH activity compared to controls. However, when mitochondrial density is normalized for each group to their sustainable aerobic work there is no apparent difference in glycolytic ATP production or PDH activity status. Together these data support a highly conserved relationship between muscle energetics and PDH activation during muscle contraction when controlling for metabolic demand relative to mitochondrial density.

2.3 Materials and Methods

2.3.1 Animal Care and Feeding

Male Wistar rats were obtained at 8 weeks of age from Charles River Laboratories (Wilmington, MA). Rats were housed three per cage in a temperature (22 °C) and humidity (50%) controlled room on a 12:12 hour light-dark cycle and provided Purina rat chow and tap water ad libitum. Methimazole treated rats were given the drug in their drinking water (0.025% w/v) for four weeks prior to experimentation. Control and MMI treated rats were used for experiments at 12 weeks of age. All procedures were approved by the Michigan State University Institutional Animal Care and Use Committee

and complied with The American Physiological Society's "Guiding Principles in the Care and Use of Animals".

2.3.2 Muscle Stimulation and Sampling

Fasted animals were anesthetized with 1.5-2.5% isoflurane on a carrier gas of 100% oxygen during the surgical procedure and body temperature was monitored via rectal thermocouple (YSI Model 73a) and maintained (36.5-37.5 °C) with a heated pad. For muscle stimulation the sciatic nerve of one hindlimb was exposed as described previously (122). In brief, a 1.5 cm wide incision was made on the lateral aspect of the hip and blunt dissection through the gluteus was performed to expose the sciatic nerve. The nerve was then insulated from surrounding tissues with a strip of Parafilm and a bipolar platinum electrode was positioned adjacent to the nerve and held in place with cyanoacrylate glue which was also used to seal the wound. A test twitch stimulated with rectangular pulse (5 V, 0.2 ms duration, Grass S48 stimulator) was performed to validate external control of the sciatic nerve. The knee was fixed in place to a custom built knee brace using braided nylon ligature. The posterior leg was carefully dissected free of overlying skin to expose the muscle for post-exercise freeze clamp and a length of suture secured to the Achilles tendon and to a strain gauge (Grass FT03C) with the animal in the prone position. Stimulation voltage (2-10 V) and muscle length were adjusted using the length-tension relation to set the muscle resting length. The sciatic nerve was then stimulated at either 0.5 Hz or 1.0 Hz for control rats and 0.25 Hz or 0.5 Hz for MMI treated rats for 5 minutes at which time the superficial gastrocnemius muscle was excised and immediately freeze clamped in liquid N_2 precooled Wollenberger tongs while still contracting. For resting muscle samples, animals were

similarly anesthetized with immediate removal and storage of the superficial gastrocnemius as described earlier. Muscle samples were stored at -80 °C for later biochemical analyses.

2.3.3 Cytochrome C Oxidase Activity Assay

Resting, non-stimulated superficial gastrocnemius muscle samples were used for the quantification of cytochrome c oxidase activity as previously described with minor modification (126). In brief, a 1 mM solution of reduced cytochrome c solution was first produced and stored at -20 °C. 110 mg of ascorbic acid was dissolved in 1 ml of 10 mM potassium phosphate buffer (pH 7.0) and titrated to pH 6.5-6.8 with tris-HCl powder. Next, 250 mg of cytochrome c was dissolved in 1.2 ml 10 mM potassium phosphate buffer (pH 7.0), followed by the addition of 0.3 ml of ascorbic acid solution to make a 13.5 mM cytochrome c solution. The mixture was incubated with stirring at 4 °C for 1 hour resulting in a color shift from brown to pink-orange. The solution was then added to dialysis tubing (3500 kD cutoff) and dialyzed against 500 ml 10 mM KH_2PO_4 for 1 hour at room temperature with gentle stirring. After changing out the dialysis buffer this process was repeated and finally dialyzed a third time overnight at 4 °C. The cytochrome c solution was removed from the dialysis tubing into another vessel and the tubing was rinsed 3 times with 1.5 ml 10 mM KH_2PO_4 and added to cytochrome c solution. The concentration, percent reduction, and auto reduction rate of the cytochrome c solution was verified utilizing spectrophotometric absorbance at 550 nm using the extinction coefficient of 29,500 $M^{-1}cm^{-1}$. Muscle samples were then assayed for determination of whole muscle lysate cytochrome c oxidase activity. Frozen muscle samples were freshly powdered under liquid N_2 using mortar and pestle immediately

prior to the assay. Muscle powder was added to ice cold homogenization buffer (100 mM Tris-HCl, 1% Triton X-100, pH 7.0) at a final dilution of 1:100 and mixed by inversion at 4 °C for 5 minutes before being placed on ice. For a 1 ml cuvette, 60 ul of 1 mM reduced cytochrome c solution was added to 500 ul 100 mM KH_2PO_4 (pH 7.0 at 37 °C) and 400 ul water. Cuvettes were placed into spectrophotometer preheated to 37 °C and absorption rate was recorded for 3 minutes at 550 nm. Reactions were initiated by the addition of 40 ul 1:100 muscle homogenates and rates recorded for 5 minutes. The initial linear reaction rate was used for calculation of cytochrome c oxidase activity using the molar extinction coefficient for cytochrome c of 28,000 $M^{-1}cm^{-1}$ at 550 nm. Muscle homogenates were assayed in triplicate and activities normalized to the muscle wet weight.

2.3.4 Citrate Synthase Activity Assay

Resting, non-stimulated superficial gastrocnemius muscle samples were used for the quantification of citrate synthase activity as previously described with minor modification (127). Outlined briefly, frozen muscle samples were powdered under liquid N_2 using mortar and pestle and muscle powder was added to ice cold homogenization buffer (100 mM Tris-HCl, 1% Triton X-100, pH 8.1) at a final dilution of 1:100 and mixed by inversion at 4 °C for 5 minutes. 50 µl of muscle homogenate was then added to 900 µl assay reaction mixture (100 mM Tris-HCl, 1 mM DTNB, 0.3 mM Acetyl-CoA, pH 8.1), mixed by inversion and allowed to warm up to room temperature for 10 minutes. Background reaction rate was recorded continuously following absorption at 412 nm for 3 to 5 minutes. Reaction was initiated with the addition of 50 µl 10 mM oxaloacetate followed by rapid mixing. Activity was monitored continuously for 5 to 10 minutes and

the initial linear rate was used for calculation of citrate synthase activity after subtracting background rate using the molar extinction coefficient for DTNB of 14,150 $M^{-1}cm^{-1}$ at 412nm. Muscle homogenates were assayed in triplicate and activities normalized to the muscle wet weight.

2.3.5 Assay for Muscle ATP and Total Creatine Content

Resting, non-stimulated superficial gastrocnemius muscle samples were used for the quantification of ATP and total creatine content as previously described with minor modification (128,129). In brief, frozen muscle samples were powdered under liquid N_2 and metabolites were extracted by adding to ice-cold perchloric acid solution (2 N $HClO_4$, 5 mM EDTA) at a final dilution of 1:10 as previously described (129). Extracts were mixed at 4 °C for 20 minutes and subsequently centrifuged at 20,000 G for 20 minutes. The supernatant was neutralized by the addition of an equivalent volume of potassium hydroxide buffer (2 N KOH, 150 mM TES, 300 mM KCl) and a second centrifugation (3,000 G,10 minutes) step removed precipitated perchlorate salts. Neutralized extracts were assayed for ATP content at room temperature (RT) using a coupled spectrophotometric enzyme assay (128). For total creatine content, extracts were first incubated with equal volume of 0.4 N HCl for 9 minutes at 65 °C then neutralized in an equivalent volume of 0.4 N NaOH. This step ensures complete PCr hydrolysis prior to HPLC analysis for total creatine content as described previously (129). Millimole ATP and creatine content were normalized to liter muscle cell water (LCW) assuming 1 g of muscle is 75% water content (34).

2.3.6 [2-14C]-Pyruvate Tracer Solution for PDH Activity Assay

PDH activity and fractional activation studies were performed as previously described (122). A standard solution of 35 mM pyruvate was made in water and its concentration verified. Briefly, 1 µl of 35 mM pyruvate was added to 0.99 ml of 303 mM TEA, 3.03 mM EDTA, and 10 µl of 25 mM NADH, pH 7.5 at RT. Pyruvate concentration was assayed in triplicate utilizing a spectrophotometric lactate dehydrogenase (LDH) assay following consumption of NADH at 340 nm at 25 °C. Baseline absorbance was measured and excess LDH (5-10 U) was added and incubated for 5 minutes or until no absorbance change was present. The pyruvate concentration was then calculated from the change in absorbance from baseline utilizing the extinction coefficient of NADH ($\varepsilon 340 = 6220\ M^{-1}cm^{-1}$) assuming reaction of NADH is 1:1 with pyruvate. 5ml of standardized 35 mM pyruvate solution was then added to 250 µCi [2-^{14}C]-pyruvate sodium salt (specific activity 7.3 mCi/mmol, Perkin Elmer #NEC256) and the final concentration verified using spectrophotometric LDH assay as described above. Specific activity of the [2-^{14}C]-pyruvate tracer solution was then determined via reaction with glutamate with glutamate pyruvate transaminase (GPT) to form [2-^{14}C]-alanine. This step was performed to determine the fraction of the ^{14}C label that is specific to pyruvate in the tracer solution. In brief, 1 µl of [2-^{14}C]-pyruvate tracer solution was added to 500 µl of 50 mM TEA, 0.5 mM EDTA, and 250 mM glutamate, pH 7.5 at RT. Assays were carried out in duplicate with two negative controls. GPT (~2 U) was then added to initiate the reaction but omitted from negative controls. Reactions were carried out at RT and after 1 hour, 400 µl aliquots were removed and loaded into gravity flow columns containing 1 ml settled volume of anion exchange resin (Bio-Rad AG1x8 resin,

200-400 mesh, Acetate form) contained in a 3 ml syringe with luer lock stopcock. This resin traps the negatively charged [2-^{14}C]-pyruvate while the positively charged [2-^{14}C]-alanine passes through. Resin was then washed 3 times with 500 µl water and column eluate was collected into 25 ml glass scintillation vials containing 20 ml Safety Solve scintillant and counted using a Packard Tric-Carb liquid scintillation analyzer. Background counts from negative controls were subtracted from sample values to obtain the specific activity (CPM/µmol) of the [2-^{14}C]-pyruvate tracer solution. 100 µl aliquots of the [2-^{14}C]-pyruvate tracer solution were stored at -80 °C until needed.

2.3.7 Homogenization and Assay Buffers for PDH Activity Assay

Homogenization buffer A, for measurement of endogenous PDH activity (PDH_a): 0.05 M Tris-HCL, 0.005 M EGTA, 0.005 M $MgCl_2$-$6H_2O$, 0.05 M KCl, 0.05 M NaF, 0.005 M DCA, 0.1% Triton X-100 with 0.001 M DTT, pH 7.8 on ice. Homogenization buffer B, for measurement of total PDH activity (PDH_t): 0.05 M Tris-HCL, 0.024 M $CaCl_2$-$2H_2O$, 0.005 M $MgCl_2$-$6H_2O$, 0.05 M KCl, 0.005 M DCA, 0.1% Triton X-100 with 0.01 M glucose, 0.001 M DTT, and 5 U/ml hexokinase added fresh before use, pH 7.8 on ice. Assay buffer: 0.12 M Tris-HCl, 0.577 mM Na_2EDTA, 0.001 M $MgCl_2$-$6H_2O$, 0.001 M DCA with 3.86 mM NAD^+, 5.77 mM CoASH, 0.001 M TPP, 0.012 M L-carnitine-HCl, and 0.8 U/ml carnitine acetyltransferase (CAT) added fresh before use, pH 7.8 at 37 °C. For assay of total PDH activity, 2.88 mM NaF was also added to assay buffer.

2.3.8 PDH Activity Assay

PDH activity was determined in superficial gastrocnemius muscle samples collected at rest in both control and MMI treated groups and in muscle samples collected during stimulation at 0.5 Hz or 1.0 Hz for controls, and 0.25 Hz and 0.5 Hz for

MMI treated rats. PDH activity was quantified by a method developed previously with modifications outlined below (122,130). In brief, PDH activity in muscle homogenates was determined by a coupled enzyme assay, following the conversion of the radiolabeled substrate ([2-^{14}C]-pyruvate) to radiolabeled product ([1-^{14}C]-acetylcarnitine):

$$[\mathbf{2\text{-}^{14}C}]\text{-}pyruvate + NAD^{+} + CoA \xrightarrow{PDH} [\mathbf{1\text{-}^{14}C}]\text{-}acetyl\text{-}CoA + NADH + CO_2$$

$$[\mathbf{1\text{-}^{14}C}]\text{-}acetyl\text{-}CoA + L\text{-}carnitine \xrightarrow{CAT} [\mathbf{1\text{-}^{14}C}]\text{-}acetylcarnitine + CoA$$

Reaction time points were collected and then passaged through columns containing anion exchange resin allowing for the separation of ^{14}C labeled compounds by trapping the unreacted negatively charged substrate, [2-^{14}C]-pyruvate, while allowing the passage of the positively charged product, [1-^{14}C]-acetylcarnitine, to quantify the reaction rate. Overall reaction rate was limited by the amount of PDH activity as CAT and substrates of the reaction were added in excess. Thus the rate of [1-^{14}C]-acetylcarnitine production was assumed to be 1:1 with [1-^{14}C]-acetyl-CoA production and used to quantify PDH activity in muscle samples. Reactions were carried out in homogenates produced from freeze clamped muscle samples of the superficial gastrocnemius. Samples were first powdered under liquid nitrogen using mortar and pestle followed by two separate assays for determination of endogenous PDH activity (PDH_a) and total PDH activity (PDH_t). This allows for quantification of fractional PDH activity (PDH_a/PDH_t = $PDH_{\%}$) within the same sample. Approximately 30-50 mg of muscle powder was added to 250 µl ice cold homogenization buffer A (PDH_a) and immediately mixed with vigorous shaking. Buffer volume was then adjusted by adding buffer to a final 10% homogenate concentration. Homogenates were then sonicated on

ice using Branson sonicator at 20 kc, 3 times for 15 seconds with 15 second breaks in between. Each homogenate was then immediately assayed by adding 15 µl homogenate to 85 µl assay buffer prewarmed to 37 °C and vortexed to mix. Reactions were carried out in triplicate at time points of 0.5, 1, and 1.5 minutes and initiated by the addition of [2-^{14}C]-pyruvate tracer solution to a final concentration of 1mM. [2-^{14}C]-pyruvate tracer was added as a drop on the side of the reaction Eppendorf tube and time points were started by vortexing, mixing the [2-^{14}C]-pyruvate tracer into the assay solution and initiating the reaction. Reaction temperature was maintained at 37 °C for entire duration by means of a heated water bath. Reactions were then quenched at appropriate time points via the addition of 500 µl of ice cold methanol followed by vortexing. Each time point was run separately and quenched samples were stored on ice until the reaction series of that sample was complete. Once the reaction series was completed for PDH_a, the entire process was repeated by producing another muscle homogenate with homogenization buffer B for determination of PDH_t activity. Quenched reaction time points were then loaded into gravity flow columns containing 1ml settled volume of anion exchange resin (Bio-Rad AG1x8 resin, 200-400 mesh, Acetate form) contained in a 3 ml syringe with Luer lock stopcock. Columns were then washed 3 times with 500 µl water with column eluate collected into 25 ml glass scintillation vials containing 20 ml Safety Solve liquid scintillation cocktail. This process traps the unreacted negatively charged [2-^{14}C]-pyruvate allowing for separation of the positively charged [1-^{14}C]-acetylcarnitine. The radioactivity in each vial was then counted using a Packard Tri-Carb liquid scintillation analyzer and using the specific activity of the tracer solution, the reaction rate was determined for quantification of PDH activity.

2.3.9 31P NMR Spectroscopy during Stimulation

In vivo rat muscle preparations were prepared as previously described for anesthesia and sciatic nerve stimulation for benchtop experiments but for these experiments the skin was left intact. Animals were secured in a custom 74 mm diameter phosphorus nuclear magnetic resonance probe with the knee secured via a tungsten pin fixed through the femur and attached to brass supports. The Achilles tendon was tied to a custom built isometric force transducer at the top of the probe. This arrangement positioned the center of the superficial gastrocnemius muscle directly over a 1.7 cm diameter circular surface coil. Isoflurane anesthesia was maintained at 1.5-2.5% for duration of experiment through a nose cone built into the body of the NMR probe and temperature was monitored via rectal thermistor (YSI model 73A) and maintained at 36.5-37.5 °C using thermostated air. In each experiment the muscle length and supramaximal stimulation voltage (5-15 V) were adjusted to yield peak isometric tension development and the probe was inserted into a Bruker Avance 400 MHz spectrometer (9.4 T, 7.4 cm vertical bore magnet). Magnetic field homogeneity was optimized by shimming on the available proton signal. Phosphorus nuclear magnetic resonance (^{31}P NMR) spectra were acquired at 161.8 MHz (4096 complex data, 8012 Hz sweep width). The summed free induction decays (FID) were apodized with a 30 Hz exponential filter prior to the Fourier transform. The pulse width (15 µs) was chosen to yield maximum signal to noise ratio at a repetition time (TR) of 3.0 seconds. The NMR signal was corrected for partial saturation by acquiring 128 FIDs under the experimental conditions and a second at 5*T1 for PCr at 9.4 T (TR=15

seconds). For each stimulation series spectra (TR=3 seconds, 8 scans) were acquired at rest (6 spectra), during stimulation (12 spectra) and recovery after stimulation cessation (16 spectra). Muscles were stimulated at twitch contractile intensities of 0.25, 0.5, 0.75, 1.0, and 2.0 Hz for controls and 0.125, 0.25, 0.375, 0.5, and 1.0 Hz for MMI treated rats. No more than 4 stimulations were used in any single experiment and frequencies were randomized. There was no effect of stimulation order on the resulting PCr transients. After stimulation series were complete, the triceps surae muscle group (gastrocnemius, plantaris, soleus) was then excised and weighed for normalization of force recordings.

2.3.10 ^{31}P NMR Spectral Analysis

The free induction decays of the stimulation series were analyzed using JMRUI software (version 3.0) and relative peak areas were integrated using AMARES (131). Areas of Pi, PCr, γ-ATP, α-ATP, and β-ATP peaks were normalized to the total phosphorus integral of each individual spectrum. PCr and Pi were quantified from their ratio to γ-ATP and adjusted to absolute chemical content using the enzymatically determined ATP content of the rat superficial gastrocnemius muscle determined from perchloric acid extracts described previously (122). Free creatine content was estimated assuming PCr content is 82% of total creatine (132). Intracellular pH (pH_i) was estimated from the chemical shift of Pi relative to PCr (133):

$$pH = 6.75 + \log\left(\frac{3.37 - \Delta PPM}{\Delta PPM - 5.63}\right) \quad (1)$$

The PCr content during steady state contractions was calculated as a percentage of the initial value by using the summed data from the six resting spectra and the final six spectra during the contractile phase. The dynamics of PCr changes were fit to a

monoexponential function by an iterative least squares algorithm to obtain the time constant of PCr resynthesis. Glycolytic ATP synthesis rate (J_{GLY}) was estimated as follows:

$$J_{GLY} = 1.5\ x\ \beta\ x\ (\frac{dpH_i}{dt}) \quad (2)$$

where 1.5 is the stoichiometric coefficient for ATP/H^+, β the buffering capacity (134), and *d*(pH_i)/*dt* is the rate of acidification during contraction (135). Cytosolic ATPase rate (J_{ATPase}) was calculated from the initial rate of PCr hydrolysis at the start of stimulation plus basal the ATPase rate of 0.012 mM/s (135,136). Mitochondrial ATP synthesis rate (J_{MITO}) was calculated by subtracting J_{GLY} from J_{ATPase}, assuming the steady state phosphate potential is maintained via the matching of cytosolic ATPase activity (J_{ATPase}) to mitochondrial ATP synthesis rate (J_{MITO}) after the glycolytic ATP production rate (J_{GLY}) is accounted for (135). Free energy of ATP hydrolysis (ΔG_{ATP}) was estimated from Pi, PCr, and Cr utilizing the creatine kinase equilibrium equation:

$$Keq = \frac{[ATP][Cr]}{[ADP][PCr][H]} \quad (3)$$

and substituting for [ATP]/[ADP] with $Keq_{CK} = 1.66x10^9\ M^{-1}$ (137):

$$\Delta GATP = -32\ kJ/mol + 2.58 \ln(\frac{[Pi][Cr]}{[PCr][H]Keq}) \quad (4)$$

2.3.11 Statistics

All data are reported as means ± SE. Comparisons of group means were by two tailed Students *t*-test at the $p < 0.05$ level of significance. Linear regression analysis was performed by Graphpad Prism 7 statistics software utilizing a method equivalent to analysis of covariance (ANCOVA) at the $p < 0.05$ level of significance.

2.4 Results

Animal biometrics and gastrocnemius muscle mitochondrial density. MMI treated rats had significantly lower body and muscle weights however significantly increased muscle weight to body weight ratios (Table 1). The average peak twitch force was not significantly different between groups however, normalization of average peak twitch force to muscle weights increased specific force in MMI treated rats when compared to controls (Table 1).

Mitochondrial density was determined by measuring cytochrome c oxidase activity, total PDH activity, and citrate synthase activity in whole muscle lysates from non-stimulated, superficial gastrocnemius muscle with activities presented in Table 2. Cytochrome c oxidase activity, total PDH activity, and citrate synthase activity were all significantly reduced by 53%, 47%, and 29% respectively in MMI treated rats compared to controls (Table 2). This decrease in mitochondrial density was responsible for the increase in the time constant (τ) for PCr recovery following muscle contractions as measured by *in vivo* ^{31}P NMR experiments. This has previously been shown to correlate with muscle mitochondrial oxidative capacity in rat gastrocnemius muscle with increased τ associated with reduced mitochondrial density (121). Here, τ was increased 1.8-fold with MMI treatment and is consistent with the ~50% reduction in muscle mitochondrial density determined by cytochrome c oxidase and total PDH activity in whole muscle lysates when compared to controls (Table 2).

Resting gastrocnemius muscle energetics and pH. Resting superficial gastrocnemius muscle metabolite and pH values are presented in Table 3. Quantification of ^{31}P NMR spectra resulted in significant reductions in pH and Pi/ATP

with MMI treatment however the PCr/ATP ratio was similar to controls (Table 3). In perchloric acid extracts of resting muscle samples, ATP content was similar between groups however total creatine was significantly increased with MMI treatment, consistent with previous reports (121).

Metabolic flux, steady state energetics, and PDH activity as a function of absolute and relative contractile workloads. It was previously established that the maximal aerobic twitch contractile intensity of the rat hindlimb was 1.0 Hz intensity of stimulation (116). In this study, 1.0 Hz intensity of stimulation was considered the maximal aerobic contractile intensity for control rats and used for muscle stimulation. With MMI treated rats displaying ~50% reduced mitochondrial density, assessed by cytochrome c oxidase activity, total PDH activity, and increased τ of PCr recovery (Table 2), 0.5 Hz intensity of stimulation was chosen as the approximate maximal aerobic contractile intensity. Absolute stimulation intensities were chosen to be 25%, 50%, 75%, 100%, and 200% of the maximal aerobic contractile intensity of each group corresponding to absolute intensities of 0.25 Hz, 0.5 Hz, 0.75 Hz, 1.0 Hz, and 2.0 Hz for controls and 0.125 Hz, 0.25 Hz, 0.375 Hz, 0.5 Hz, and 1.0 Hz for MMI treated rats.

Figure 7 shows representative stackplot images of ^{31}P NMR spectra serially-acquired during 0.5 Hz stimulation in a control and MMI treated rat. Resting ^{31}P NMR spectra were acquired for the first 2 minutes 24 seconds (spectra 1-6), during the next 4 minutes 48 seconds of 0.5 Hz stimulation (spectra 7-18) and during the subsequent 7 minutes 12 seconds of recovery (spectra 19-36) to quantify the steady state and kinetic response of PCr hydrolysis and resynthesis in control and MMI treated animals. The response of superficial gastrocnemius PCr content at the start of contraction are

displayed in representative PCr transients in Figure 8, showing PCr hydrolysis during stimulation and PCr recovery at stimulation cessation. Figure 8A displays PCr transients from control and MMI treated rats stimulated at the same absolute intensity of 0.5 Hz. A clear reduction in steady state PCr during stimulation is present with reduced mitochondrial density of the MMI treated rat (Fig. 8A). Figure 8B displays PCr transients from control and MMI treated rats stimulated at the same relative intensity of stimulation corresponding to 50% of the expected maximal aerobic intensity, equivalent to 0.5 Hz and 0.25 Hz absolute intensities for control and MMI treated rats respectively. Here the similarity in steady state PCr content during stimulation is clear as well as the increased recovery time of PCr in the MMI treated rat after stimulation cessation.

Quantification of ^{31}P NMR spectra for steady state PCr content during muscle stimulation results in linear relationships between the magnitude of PCr hydrolyzed from rest (ΔPCr) and absolute stimulation intensity (Hz) in control and MMI treated rats (Fig. 9A). Linear regression fits to the data through the assumed maximal aerobic contractile intensity of each group resulted in a significant difference in slope between control and MMI treated rats that was increased 2.0-fold with MMI treatment. Data from 2.0 Hz and 1.0 Hz stimulation in control and MMI treated rats respectively was assumed to be above the maximal aerobic capacity of the muscle and therefore was not included in linear regression fits. This is supported by the nonlinear response of ΔPCr at these contractile intensities. The exact 2.0-fold increase in slope with MMI treated rats and the linear response of ΔPCr during stimulation up to the assumed aerobic maximum of each group further supports the choice of 1.0 Hz and 0.5 Hz as the assumed maximal aerobic contractile intensity for control and MMI treated rats respectively. When ΔPCr was

plotted versus relative stimulation intensity (%) for each group, data were non-distinguishable between groups and the linear regression was fit to data from both groups up to 100% relative stimulation intensity (Fig. 9B). Plots of steady state ΔPCr versus ΔPi during muscle stimulation should yield reciprocal relationships assuming proper quantification of ^{31}P NMR spectra and was confirmed by the 1.06 and 1.04 slopes for the regression lines in control and MMI treated rats (Fig. 10).

The glycolytic contribution (J_{GLY}) to total ATP demand (J_{ATPase}) was estimated from the chemical shift changes in Pi from the ^{31}P NMR spectra in each group. During stimulation glycolytic ATP production (J_{GLY}) was increased in MMI treated rats when compared to controls and resulted in a significant increase in slope at absolute stimulation intensities (Fig. 11A). However, while the absolute values for the pHi changes were different between groups, the fractional glycolytic contribution relative to total ATP demand (J_{GLY}/J_{ATPase}) were similar and not significantly different between groups. Therefore, a linear regression fit was applied to the whole dataset including both groups to estimate J_{GLY} (Fig. 11B). Cytosolic ATP demand or the ATP hydrolysis rate (J_{ATPase}) also exhibited linear relationships to absolute intensities of stimulation that were not different between groups and data from both groups were fit to a single linear regression (Fig. 12A). This corresponded with similarities in average peak force between control and MMI treated groups at 25% (1183±62 vs.1316±73 g, NS), 50% (1221±53 vs. 1287±70 g, NS), 75% (1227±65 vs. 1275±78 g, NS), and100% (1248±68 vs. 1276±82 g, NS) relative intensity of stimulation. At 200% relative intensity, initial peak force from the first ten twitches during stimulation was similar between groups (1120±127 vs. 1389±98 g, NS) however, stimulation at this intensity resulted in muscle

fatigue (77.7±5.2 vs. 79.4±3.8 % initial force, NS) therefore peak force was not averaged across the entire stimulation.

Mitochondrial ATP synthesis rate (J_{MITO}) was calculated by subtracting J_{GLY} from J_{ATPase}, assuming the steady state phosphate potential is maintained via the matching of cytosolic ATPase activity (J_{ATPase}) to mitochondrial ATP synthesis rate (J_{MITO}) after the glycolytic ATP production rate (J_{GLY}) is taken into account (135). Data from both groups exhibited linear relationships between J_{MITO} and absolute stimulation intensity (Hz) that was not different between groups and therefore data were fit to a single linear regression (Fig. 12B). Mitochondrial transfer function, or the plot of steady state ADP versus mitochondrial ATP synthesis rate (J_{MITO}) is shown in Fig. 13A exhibiting increased ADP concentration to illicit similar rates of ATP synthesis in the MMI treated rats. However, when normalized to relative intensity of stimulation, there was no difference between groups (Fig. 13B). The combined effect of reduced mitochondrial density with MMI treatment on the system response to increased metabolic demand is displayed in the steady state free energy of ATP hydrolysis (ΔG_{ATP}). Figure 14A displays the steady state ΔG_{ATP} maintained by mitochondrial ATP synthesis (J_{MITO}) and shows a 1.5-fold increase in the hill coefficient (η_H) with reduced mitochondrial density through MMI treatment. When data were normalized to J_{MITO} relative to maximal rates of ATP synthesis for each group, no difference was found between the control or MMI treated conditions (Fig. 14B).

Steady state fractional PDH activity was quantified in superficial gastrocnemius muscle samples obtained at rest and during muscle stimulation at 0.5 Hz and 1.0 Hz in controls and 0.25 Hz and 0.5 Hz in MMI treated rats (Fig. 15). Resting fractional PDH

activity was not different between groups but was significantly increased at 0.5 Hz intensity of stimulation in MMI treated rats compared to controls ($p<0.01$). In both groups, fractional PDH activity increased during muscle contraction however the rate of activation was significantly increased in MMI treated rats compared to controls at the same absolute intensity of stimulation (Hz). The rate of PDH activation in MMI treated rats had a significant 2.1-fold increase in slope compared to controls (Fig. 15A). There was no difference in fractional activity when plotted against the relative stimulation intensity and all data were fit to a single linear regression (Fig. 15B).

Table 1. *Body weight, muscle weight, and peak twitch force in control and MMI treated groups used for PDH activity.* Muscle weights include the entire compliment of posterior leg muscles (gastrocnemius, plantaris, soleus). Peak twitch force was the average value including 0.5 and 1.0 Hz stimulations for control and 0.25 and 0.5 Hz stimulations for MMI. Values are means ± SE. *Significant difference between control and MMI treated groups ($p<0.05$) by two tailed Students *t*-test. n, number of animals. MW, muscle weight. BW, body weight.

	Control	MMI
n	10	10
Body Weights (kg)	503±15	414±6*
Muscle Weight (g)	3.0±0.08	2.8±0.04*
MW/BW (%)	0.60±0.01	0.67±0.01*
Peak Twitch Force (g)	516±23	539±17
Peak Force/MW	172±7	196±7*

Table 2. *Measures of superficial gastrocnemius mitochondrial density in control and MMI treated groups.* Enzyme activity was determined from non-stimulated resting muscle samples in each group (n=5). Time constant of PCr recovery (τ) after muscle stimulation was calculated by fitting normalized PCr spectral area acquired by ^{31}P NMR to a monoexponential function by an iterative least squares algorithm. Recovery time constants were determined in control (n=8) and MMI treated (n=18) groups after 0.75 Hz and 0.375 Hz stimulation respectively. Values are means ± SE. *Significant difference between control and MMI treated groups ($p<0.05$) by two tailed Students *t*-test. U, unit of enzyme activity (μmol/min). gWW, gram muscle wet weight.

	Control	MMI
Cytochrome C Oxidase (U/gWW)	3.6±0.3	1.7±0.4*
Total PDH (U/gWW)	0.99±0.12	0.52±0.08*
Citrate Synthase (U/gWW)	24.1±1.2	17.1±0.8*
PCr Recovery Time Constant, τ (s)	64.6±5.6	115.3±6.1*

Table 3. *Resting pH and metabolites in control and MMI treated groups.* Resting pH, PCr/ATP, and Pi/ATP were acquired from ^{31}P NMR spectrum of the superficial gastrocnemius muscle in control (n=8) and MMI treated (n=18) groups. ATP and total creatine were quantified from non-stimulated resting superficial gastrocnemius muscle in both groups (n=5). Values are means ± SE. *Significant difference between control and MMI treated groups ($p<0.05$) by two tailed Students *t*-test. PCr, phosphocreatine. Pi, inorganic phosphate. LCW, liter cell water.

	Control	MMI
pH	6.98±0.02	6.87±0.01*
PCr/ATP	3.7±0.1	4.0±0.1
Pi/ATP	0.77±0.06	0.36±0.03*
ATP (mmol/LCW)	9.2±0.07	8.7±0.3
Total Creatine (mmol/LCW)	38.3±0.8	45.3±1.1*

Figure 7. Representative phosphorus spectrum from control and MMI treated rats. Sample ^{31}P NMR spectra acquired in the rat gastrocnemius muscle before (bottom 6 spectra), during (next 12 spectra), and after (last 18 spectra) 0.5 Hz stimulation in control and MMI treated animals (n=1). Spectra peaks from left to right: Pi, PCr, γ-ATP, α-ATP, β-ATP. Acquisition parameters: total of 36 spectra composed of 8 FIDs, 4096 complex points, 8012 Hz sweep, 3 second TR, and 30 Hz exponential filter. Pi, inorganic phosphate. PCr, phosphocreatine.

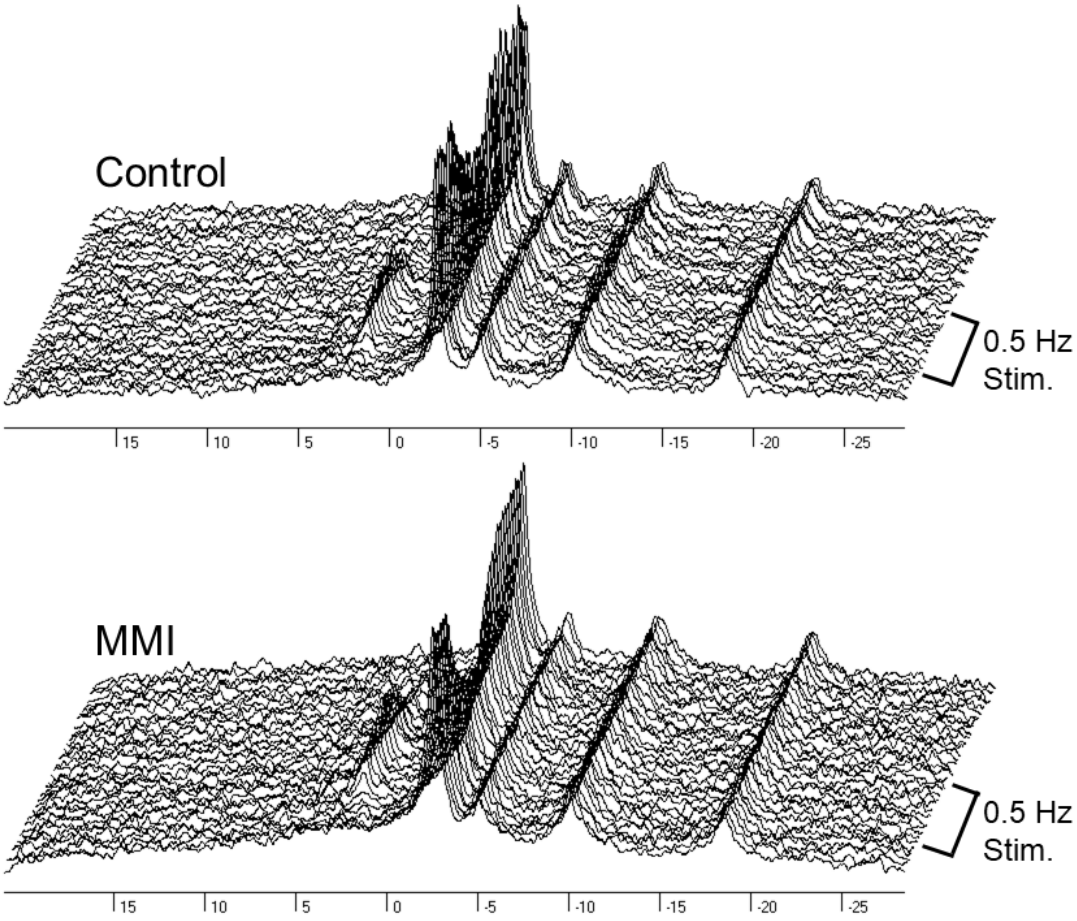

Figure 8. Representative PCr transients quantified from ^{31}P NMR spectra of control and MMI treated rat gastrocnemius muscle in one animal.

A: Control versus MMI PCr transients at the same absolute stimulation intensity of 0.5 Hz. ***B:*** Control versus MMI PCr transients at the same relative stimulation intensity corresponding to 50% of the expected maximum aerobic intensity of 1.0 Hz and 0.5 Hz for control and MMI rats respectively. Actual intensities shown are 0.5 Hz and 0.25 Hz for control and MMI treated rats respectively. PCr presented as percent of initial resting values. PCr, phosphocreatine.

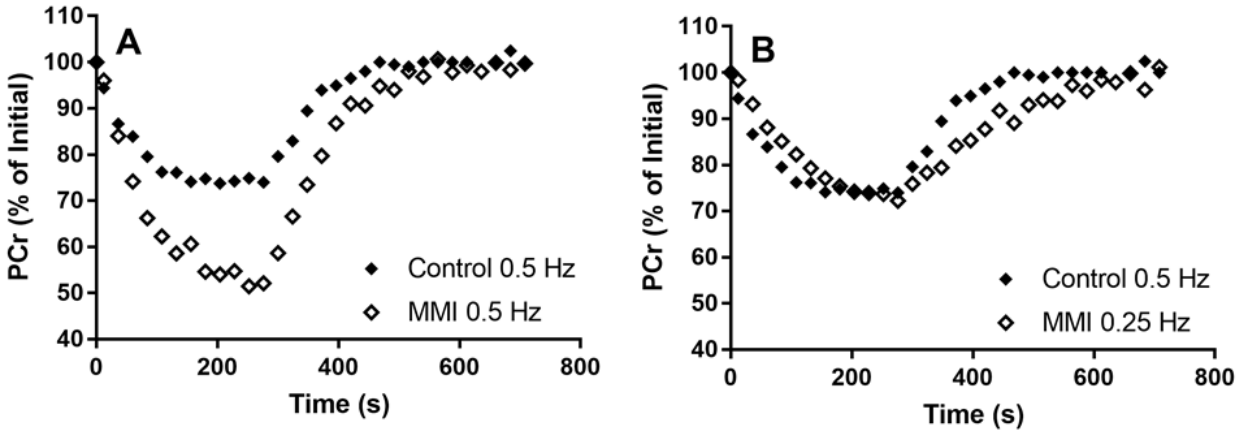

Figure 9. ΔPCr at absolute or relative stimulation intensity in control and MMI treated rats.

A: ΔPCr versus absolute stimulation intensity (Hz) in control (n=8) and MMI treated (n=18) animals. Data were quantified from ^{31}P NMR spectra acquired during 0.25, 0.5, 0.75, 1.0 and 2.0 Hz stimulation for controls and 0.125, 0.25, 0.375, 0.5, and 1.0 Hz stimulation for MMI treated animals. Linear regressions were fit through 0.5 Hz and 1.0 Hz for MMI treated and control groups respectively, which correspond to the expected maximum aerobic stimulation intensity for each group. ***B:*** ΔPCr versus relative stimulation intensity (%) for control (n=8) and MMI treated (n=18) groups. Stimulation intensity was normalized to the maximal absolute intensity which corresponds to the expected aerobic maximum for each group which was 1.0 Hz and 0.5 Hz for control and MMI groups respectively. Linear regression was fit to data from both groups up to 100% relative stimulation intensity. ΔPCr was quantified from the difference in steady state content in resting muscle and steady state content in the last six spectra during muscle stimulation. Values are means ± SE. PCr, phosphocreatine. LCW, liter cell water.

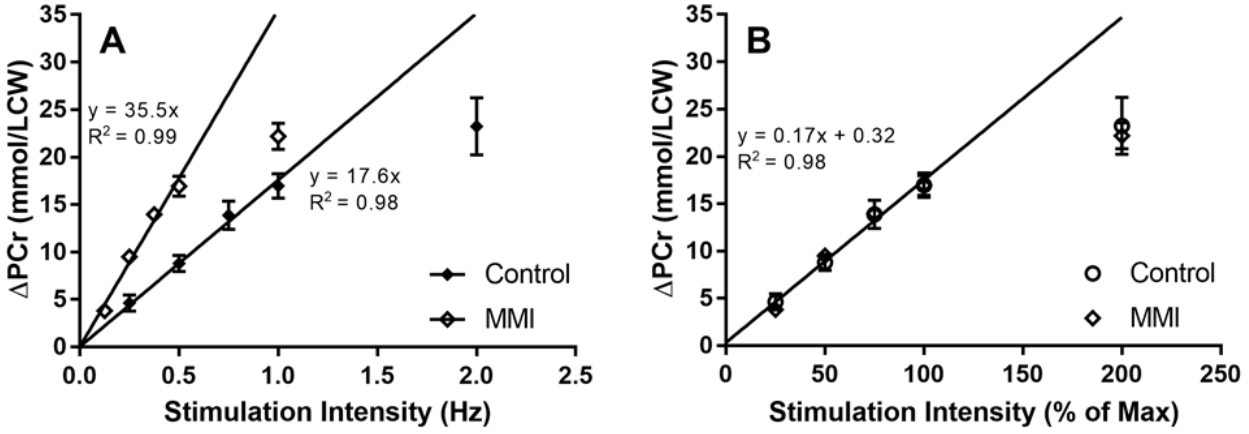

Figure 10. Reciprocal ΔPCr and ΔPi plots for control and MMI treated rats.

Data were quantified from ^{31}P NMR spectra acquired during 0.25, 0.5, 0.75, 1.0 and 2.0 Hz stimulation for controls (***A***, n=8) and 0.125, 0.25, 0.375, 0.5, and 1.0 Hz stimulation for MMI treated (***B***, n=18) animals. ΔPCr and ΔPi values were quantified from the difference in steady state resting content before stimulation, and steady state content during the last six spectra during stimulation. PCr and Pi peak areas were normalized first to the total phosphorus integral of each spectra and quantified using their ratios to ATP peak area and the chemical content of ATP of control and MMI treated rat gastrocnemius muscle. Values are means ± SE. PCr, phosphocreatine. Pi, inorganic phosphate. LCW, liter cell water.

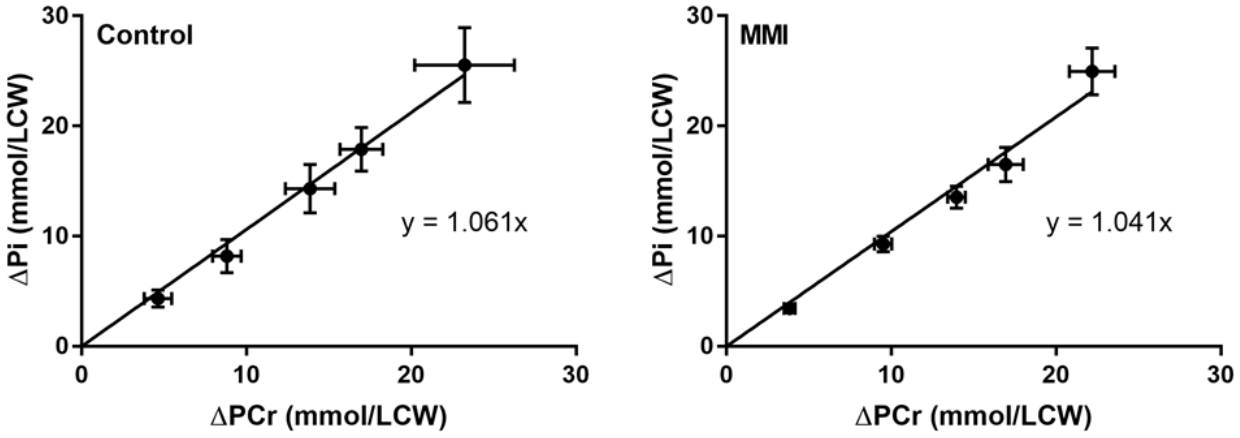

Figure 11. Glycolytic ATP synthesis at absolute and relative stimulation intensities in control and MMI treated rats.

Data were quantified from ^{31}P NMR spectra acquired during 0.5, 0.75, 1.0 and 2.0 Hz stimulation for controls (n=8) and 0.25, 0.375, 0.5, and 1.0 Hz stimulation for MMI treated animals (n=18). ***A:*** J_{GLY} versus absolute stimulation intensity (Hz) in control and MMI treated groups. ***B:*** Percent J_{GLY} contribution to total ATP demand (J_{ATPase}) as a function of relative stimulation intensity (%) in control and MMI treated groups. Stimulation intensity was normalized to the maximal absolute intensity which corresponds to the expected aerobic maximum for each group. For controls, stimulation intensities were normalized relative to 1.0 Hz intensity of stimulation. For MMI treated animals, intensities were normalized relative to 0.5 Hz intensity of stimulation. Linear regression was fit to data from both groups. Data from 0.125 Hz and 0.25 Hz for MMI treated and control animals respectively were omitted from both panels as J_{GLY} was not detectable at such low intensity of stimulation. J_{GLY} was calculated as previously described in the methods. Values are means ± SE. J_{GLY}, glycolytic ATP synthesis rate.

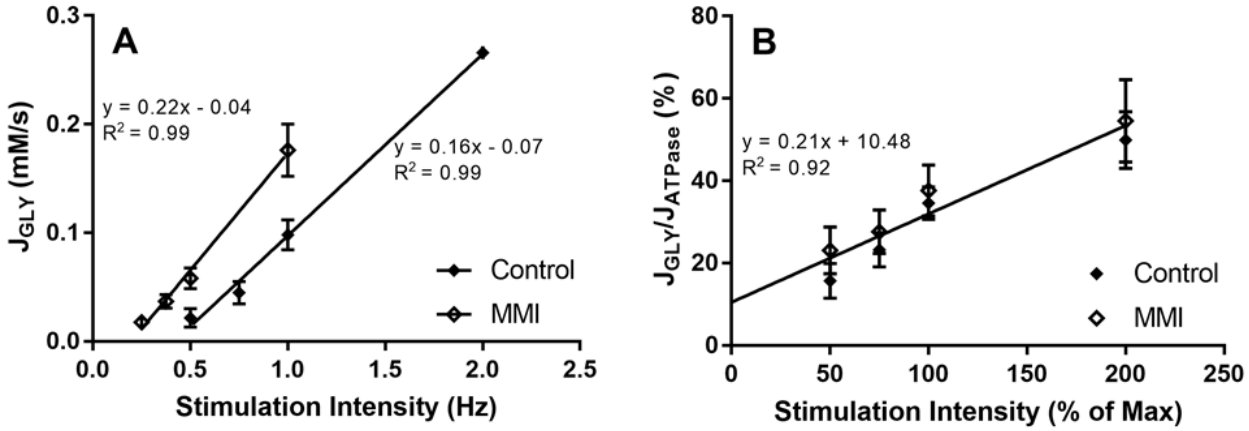

Figure 12. Cytosolic ATPase and mitochondrial ATP synthesis rates in control and MMI treated rats.

Data were quantified from ^{31}P NMR spectra acquired during 0.5, 0.75, 1.0 and 2.0 Hz stimulation for controls (n=8) and 0.25, 0.375, 0.5, and 1.0 Hz stimulation for MMI treated animals (n=18). ***A:*** J_{ATPase} values from gastrocnemius muscle of control and MMI treated animals. J_{ATPase} values were calculated from the initial linear rate of PCr hydrolysis in the first 36 seconds of contraction. Linear regression was fit to data from both groups and no difference in J_{ATPase} rates were found at overlapping stimulation intensities. ***B:*** J_{MITO} versus absolute stimulation intensity in control and MMI treated animals. J_{MITO} was calculated as described previously in methods. Data at 0.25 and 0.125 Hz from control and MMI treated rats had no detectable J_{GLY} and therefore J_{MITO} was taken as equivalent to J_{ATPase}. Data from 2.0 and 1.0 Hz from control and MMI treated rats were omitted as a steady state was not maintainable at these intensities of stimulation. Linear regression was fit to data from both groups and no difference in J_{MITO} rates were found at overlapping stimulation intensities. Values are means ± SE. J_{ATPase}, cytosolic ATP hydrolysis rate. J_{MITO}, mitochondrial ATP synthesis rate. J_{GLY}, glycolytic ATP synthesis rate.

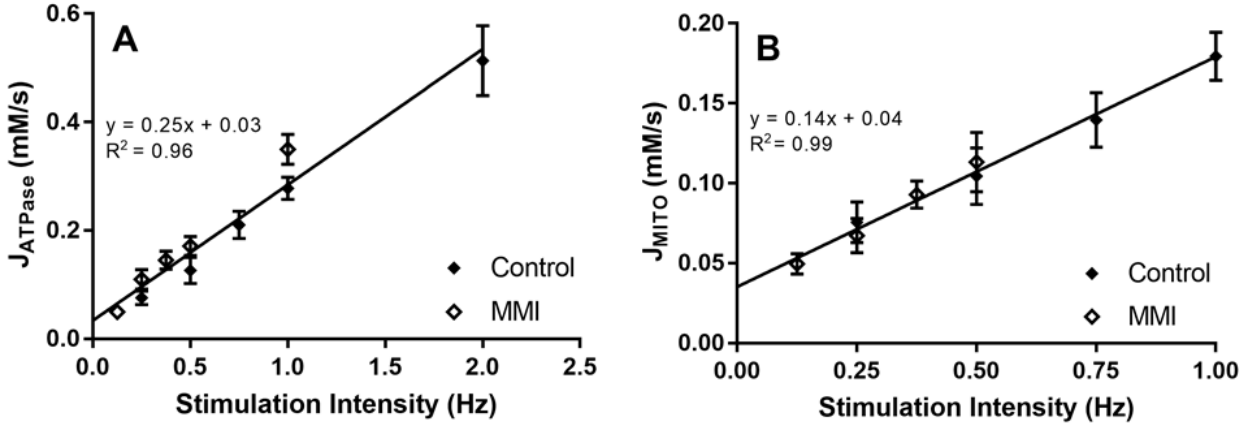

Figure 13. Mitochondrial transfer function in control and MMI treated rats. Relationship between steady state ADP concentration and absolute mitochondrial ATP synthesis rate (J_{MITO}) (***A***) or percent ATP synthesis rate (% JMITO) (***B***) relative to maximal flux at 1.0 Hz for controls (n=8) and 0.5 Hz for MMI (n=18). Data are fit to sigmoidal function with 2.0 Hz and 1.0 Hz data omitted from the graph for control and MMI groups respectively. In ***B***, data from both groups are fit to a single function. ADP was calculated as described in methods. Values are means ± SE. JMITO, mitochondrial ATP synthesis rate. η_H, hill coefficient.

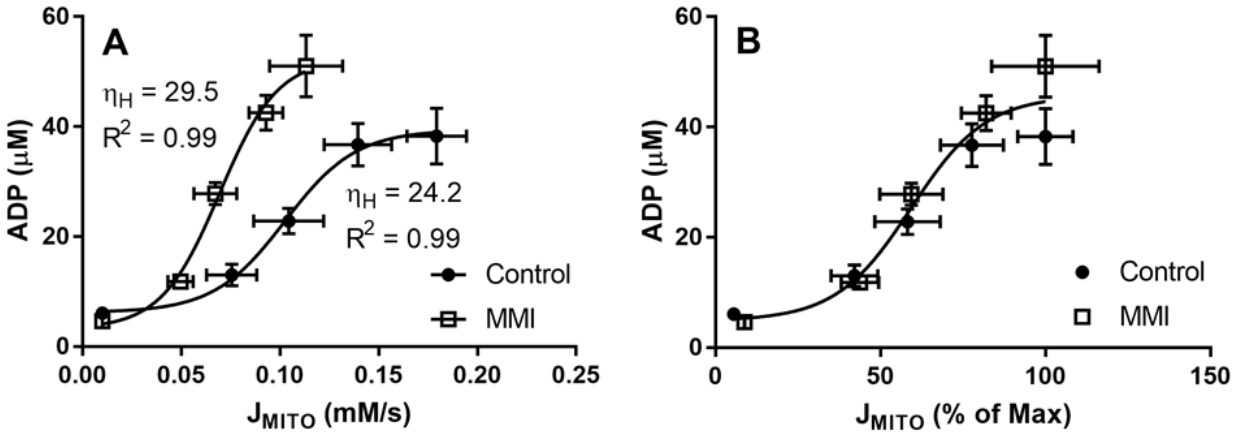

Figure 14. Flow force relationships in control and MMI treated rats.

Relationship between steady state ΔG_{ATP} and absolute J_{MITO} (***A***) or percent J_{MITO} (***B***) relative to maximal flux at 1.0 Hz for controls (n=8) and 0.5 Hz for MMI (n=18). Data are fit to sigmoidal function with 2.0 Hz and 1.0 Hz data omitted from the graph for control and MMI groups respectively. In *B*, data from both groups are fit to a single function. ΔG_{ATP} calculated as described in methods. Values are means ± SE. ΔG_{ATP}, free energy of ATP hydrolysis. JMITO, mitochondrial ATP synthesis rate. η_H, hill coefficient.

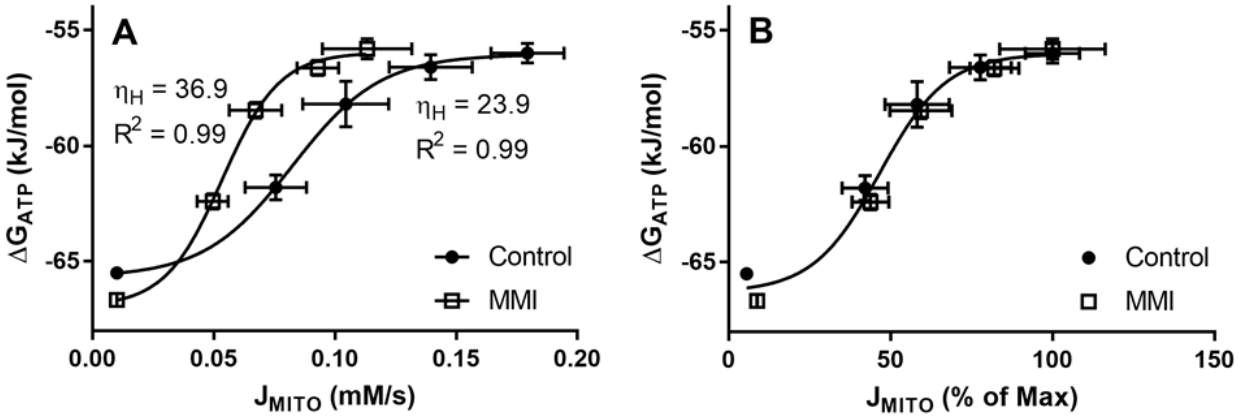

Figure 15. Fractional PDH activity at absolute or relative stimulation intensities in control and MMI treated rats.

A: PDH activity expressed as a percent of total activity versus absolute stimulation intensity (Hz) in control and MMI treated groups. Percent PDH activity was quantified in superficial gastrocnemius muscle samples collected at rest (n=5, both groups) or during 0.5 Hz (n=5) or 1.0 Hz (n=4) stimulation for controls, and 0.25 Hz (n=4) or 0.5 Hz (n=5) stimulation for MMI treated rats. ***B:*** PDH activity expressed as a percent of total activity versus relative stimulation intensity (%) in control and MMI treated groups. Absolute stimulation intensities were normalized to the maximal absolute intensity which corresponds to the expected aerobic maximum for each group which was 1.0 Hz for controls and 0.5 Hz for MMI treated rats. Linear regression was fit to data from both groups. Values are means ± SE.

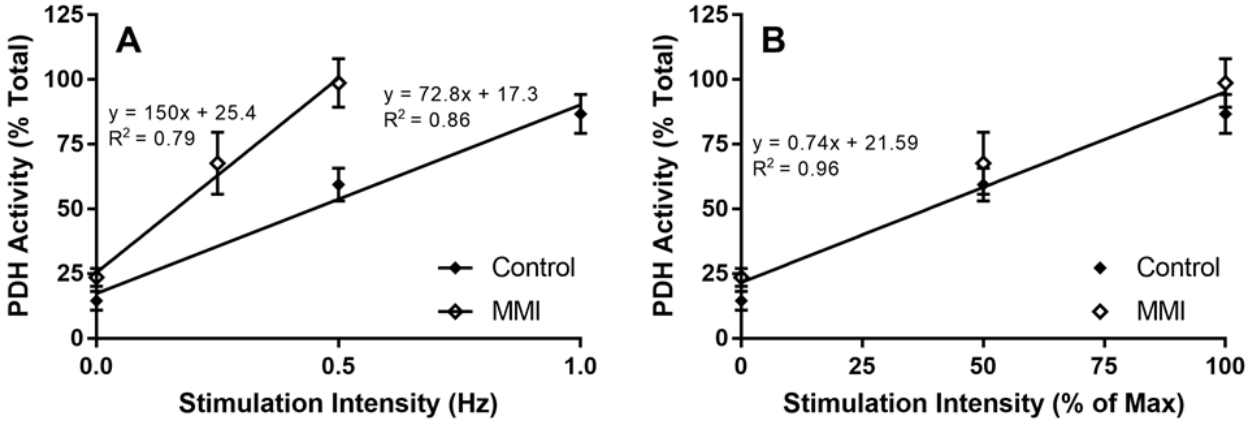

2.5 Discussion

This study quantified the relationship between muscle steady state energetics, metabolic fluxes (J_{GLY}, J_{ATPase}, J_{MITO}) and PDH activation during *in vivo* muscle contraction in relation to mitochondrial density in rat gastrocnemius muscle. Hypothyroidism, induced by MMI treatment, resulted in significant reductions in gastrocnemius mitochondrial density as evidenced by the reduced cytochrome c oxidase activity, total PDH activity, citrate synthase activity, and increased time constant of PCr resynthesis. During muscle twitch stimulation, MMI treated rats exhibited significant reductions in steady state energetics and increased glycolytic ATP production (J_{GLY}) when compared to controls at absolute workloads (Hz). This coincided with increased PDH activity and the rate of PDH activation in MMI rats when compared to controls. These effects are not attributed to changes in the relationship between the ATP cost of contraction (J_{ATPase}) or mitochondrial ATP synthesis (J_{MITO}) relative to absolute workloads (Hz) but is attributed to reduced mitochondrial density and reduced sensitivity to the feedback products of ATP hydrolysis (ADP, Pi). When steady state energetics, metabolic fluxes (J_{GLY}, J_{MITO}) and PDH activity were expressed as a function of stimulation intensity relative to the expected aerobic maximum (%), data were indistinguishable between groups with no significant differences. Together, these data confirm prior study of the relationship between mitochondrial density and muscle energetics at absolute workloads but extends these observations during contraction at intensities relative to the muscle aerobic capacity. In doing so, these data support a conserved relationship between muscle energetics and contractile activity relative to

mitochondrial density that further encompasses regulation of substrate oxidation at the level of PDH activation.

At absolute workloads, MMI rats displayed markedly different steady state energetics with reduced PCr and increased Pi and ADP that resulted in a significant reduction in the magnitude of steady state ΔG_{ATP}. Furthermore, at a given intensity of stimulation, MMI rats exhibited higher rates of glycolytically derived ATP synthesis. This effect is attributable to the depressed energetic status (increased Pi and ADP) of the muscle fiber and not on the stimulatory effects of Ca^{2+} as MMI treated rats exhibited similar force production and ATPase rates at absolute workloads when compared to controls (138). MMI treatment also resulted in significant changes in the rate of change of PCr or ΔG_{ATP} versus workload (Hz) or J_{MITO} exhibiting 2.0 and 1.5-fold increases respectively when compared to controls. Although long term hypothyroid treatment in the rat has resulted in significant changes in muscle fiber type of slow twitch soleus muscle, capillary density or fiber type were unaffected in the gastrocnemius muscle after 7 weeks of hypothyroidism (139). Therefore, we attribute alteration in steady state energetics entirely to a reduction in mitochondrial density with MMI treatment. This is supported by the fact that both the relationship between the ATP hydrolysis rate (J_{ATPase}) and ATP synthesis (J_{MITO}) at absolute workloads was not different between groups and indicates that fiber type changes or limitations to muscle perfusion are not likely occurring with 4 weeks of MMI treatment.

Changes in mitochondrial density alter the sensitivity of respiratory control with reduced mitochondrial density associated with lower energetic states, and therefore higher driving forces to elicit similar rates of mitochondrial ATP synthesis (J_{MITO})

(95,118,140–142). Mitochondrial density of the superficial gastrocnemius muscle was assessed both *in vitro* and *in vivo*. MMI treated rats exhibited significant reductions in markers of mitochondrial density *in vitro* with whole muscle lysates showing 53%, 48%, and 29% reductions in cytochrome c oxidase, total PDH, and citrate synthase activities respectively. MMI rats also exhibited 178% increase in the time constant of PCr resynthesis, an accepted measure of *in vivo* muscle oxidative capacity with increased time to PCr recovery an indication of reduced mitochondrial density (121). The combined effects indicate reduced mitochondrial density that is consistent with other studies utilizing hypothyroid animal models (121,143–145). It is assumed that in the control rat, 1.0 Hz twitch stimulation intensity results in maximal rates of muscle oxygen consumption and by extension, mitochondrial ATP synthesis (116). In the MMI treated rat, stimulation intensities were chosen assuming a ~50% reduction in muscle oxidative capacity from the combined measures of mitochondrial density resulting in 0.5 Hz as the stimulation assumed to elicit maximal rates of oxidative ATP synthesis. Choosing 1.0 Hz and 0.5 Hz as maximal aerobic stimulations seems appropriate as marked deviations in the relationship between steady state PCr and stimulation intensity occur above these stimulation rates (Fig. 9A). Furthermore, when comparing PCr transients (Fig. 8B) or steady state PCr (Fig. 9B) at similar relative intensities of stimulation, data are nearly indistinguishable between groups and delineate from linearity at the expected aerobic maximum for each group. This would be expected if the intensity of stimulation was not sustainable through aerobic ATP synthesis and validates normalization of steady state data to the expected aerobic maximums of 1.0 Hz for controls and 0.5 Hz for MMI treated rats and calling these intensities 100% of the aerobic max.

Normalization of energetic steady states to intensities of stimulation relative to the expected aerobic maximums renders group data indistinguishable from one another. Both steady state PCr and ΔG_{ATP} were not different between groups when intensity of stimulation or mitochondrial ATP synthesis (J_{MITO}) were normalized to maximum values for each group. Although the glycolytic contribution to ATP production was increased in MMI rats at absolute workloads, relative rates were not different from that seen in controls. These data confirm that the primary alteration in muscle after MMI treatment is reduced mitochondrial density and confirm that the aerobic ATP synthesis machinery is functioning similarly between groups relative to maximal capacities. This revelation also extends to regulation of glucose metabolism through activation of PDH at rest and during muscle contraction. At rest, PDH activity was higher in MMI versus controls but was not significantly different. Nevertheless, these data suggest that even at the low metabolic demand of resting skeletal muscle, higher fractional PDH activity is necessary to maintain an energetic steady state. During muscle contraction however, the rate of PDH activation relative to absolute workloads was 2.1-fold higher in MMI treated rats than in control muscle (Fig. 15A) and was remarkably similar to that for the rate of change in steady state PCr (2.0-fold). PDH activation is known to be regulated through the energetic status of the muscle fiber and increases in activity are associated with increased metabolic demand or depressed energetic state (133). Similar to steady state energetics, activation of PDH in relation to relative stimulation intensity normalized data between groups with no differences in the fractional activation of PDH during stimulation at 50% or 100% of the expected aerobic maximums. These data have implications for

regulation of PDH activity *in vivo* but also rates of substrate utilization at absolute and relative workloads.

PDH activity is regulated via reversible phosphorylation with increased activity associated with reduced phosphorylation status (5). Regulation of the phosphorylation state is controlled by the relative activities of PDK's versus PDPs (5). PDK activity is sensitive to the energetic status of the muscle fiber with reduced energetics or increases in the ratios of ADP/ATP, NAD+/NAD, CoA/A-CoA and also pyruvate concentration resulting in allosteric inhibition of PDK activity (9,9–13). Conversely, PDP activity is mainly regulated by changes in Ca^{2+} with increased Ca^{2+} leading to allosteric stimulation of activity (35–37). PDH activation during muscle contraction occurs as a function of muscle contractile activity and is linearly related to increasing exercise intensity during submaximal exercise with maximal activity present during high intensity exercise (24,63). The current paradigm of PDH activation during exercise supposes that a combination of a reduced energetic state and increase Ca^{2+} as a function of muscle contractile activity serve to activate PDH through preferential inhibition of PDK activity and stimulation of PDP activity (5). Our data primarily support a role of muscle energetic status in the regulation of PDH activation as fractional PDH activation was 2.1-fold higher in MMI treated rats compared to controls and was consistent with associated changes in muscle PCr content. Furthermore, normalization of fractional PDH activity to relative stimulation intensities resulted in no difference between groups. Should Ca^{2+} play a central role in the regulation of PDH activity, it would be expected that an offset in fractional PDH activation would be present at relative stimulation intensities between groups. This is due to the fact that at relative intensities, muscle energetics were

indistinguishable between groups however the absolute intensity of stimulation was half of that of controls in the MMI group. Therefore, MMI treated muscle experience one half of the time averaged Ca^{2+} associated with half the absolute stimulation intensity, yet there was no difference in the activation state of PDH between groups. It may also be the case that the increased glycolytic activity in MMI rats served to stimulate PDH activity through pyruvate inhibition of PDKs on top of the allosteric inhibition of the depressed energetics (84,86,140–142,144). However, normalization of glycolytic flux to total ATP demand resulted in no differences between groups indicating the relative stimulatory effects of pyruvate on PDH activity were likely similar between control and MMI treated rats. Therefore, it is likely that PDH activation during muscle contraction is primarily a function of the magnitude of inhibition of PDKs, related to the energetic status of the muscle fiber.

Changes in PDH activation seen in this study raise interesting questions about regulation of muscle substrate utilization *in vivo*. Skeletal muscle primarily oxidizes fatty acids at rest but increases glucose utilization as a function of exercise intensity, with relative utilization surpassing fatty acids at ~65% of the aerobic maximum (VO_{2MAX}) (22,23,60). This effect is attributed to the stimulation of PDH activity, which is linearly related to exercise intensity (24,61,65). By increasing mitochondrial density through exercise training, skeletal muscle utilizes higher absolute and relative rates of fatty acids during similar absolute workloads compared to sedentary or normal mitochondrial density muscle (82,83). This has been associated with reduced PDH activity and is consistent with the results of this study, although here it is the opposite with increased PDH activity at absolute workloads following reduction in mitochondrial density (84).

Whether skeletal muscle of varying mitochondrial densities exhibit similar relative substrate utilization at exercise intensities relative to their aerobic maximums (%VO_{2MAX}) is a point of some controversy. In exercise trained human skeletal muscle it seems that even at similar relative workloads (%VO_{2MAX}), muscle with higher mitochondrial density oxidizes more fatty acids than glucose when compared to sedentary or normal mitochondrial density muscle (89,125). This would suggest an inherent modification to muscle mitochondria that alters substrate selection at relative workloads and may be related to the capacity to oxidize and/or transport fatty acids or may also be related to reduced activation of PDH (82,83,146). However, when comparing multiple mammalian species exhibiting VO_{2MAX} values ranging from 2 l/min to 6 l/min, relative rates of substrate oxidation were similar between species when exercise was normalized to VO_{2MAX} (92). This would suggest that substrate oxidation and selection scales as a function of muscle workload relative to mitochondrial density which has also been observed in human subjects (89–91). The current data support the latter, with PDH activation similar between groups at relative stimulation intensity, however substrate oxidation was not measured in this study so a definitive statement cannot be made without further study.

In summary, reduced mitochondrial density with MMI treatment resulted in marked reduction in steady state energetics when compared to controls at absolute contractile workloads. This effect was not attributed to alteration in the relationship between the ATP cost of contraction (J_{ATPase}) or mitochondrial ATP synthesis (J_{MITO}) at absolute workloads but was attributed to the reduced sensitivity of respiratory control resulting higher APD and Pi content necessary to stimulate similar rates of oxidative

ATP synthesis. When steady state energetics and glycolytic flux was normalized to intensities of stimulation relative to the expected aerobic maximums, no differences were found between groups. This effect was also observed for regulation of PDH activity, with increased rates of PDH activation relative to absolute workloads with MMI treatment that disappears when normalized to intensities of stimulation relative to the aerobic maximum. This suggests PDH activation is primarily regulated by changes in muscle energetics and questions the necessity of PDP stimulation through intracellular Ca^{2+}. Furthermore, these data suggest that at contractile workloads relative to VO_{2MAX}, PDH activation would support similar rates of substrate utilization which is consistent with some (89–92) but not all studies (89,125).

Chapter 3. Effects of Altered Pyruvate Dehydrogenase Activity on Contracting Skeletal Muscle Bioenergetics

3.1 Abstract

During aerobic exercise (>65% of VO2max) the primary source of acetyl-CoA to fuel oxidative ATP synthesis in muscle is the pyruvate dehydrogenase (PDH) reaction. This study investigated how regulation of PDH activity affects muscle energetics by determining whether activation of PDH with dichloroacetate (DCA) alters the dynamics of the phosphate potential of rat gastrocnemius muscle during contraction. Twitch contractions were induced *in vivo* over a broad range of intensities to sample submaximal and maximal aerobic workloads. Muscle phosphorus metabolites were measured *in vivo* before and after DCA treatment using phosphorus nuclear magnetic resonance spectroscopy. At rest, DCA increased PDH activation compared to control (90±12 vs 23±3%, $p<0.05$) with parallel decreases in inorganic phosphate (Pi) of 17% (1.4±0.2 vs 1.7±0.1 mM, $p<0.05$) and an increase in the free energy of ATP hydrolysis (ΔG_{ATP}) (-66.2±0.3 vs -65.6±0.2 kJ/mol, $p<0.05$). During stimulation DCA increased steady state phosphocreatine (PCr) and the magnitude of ΔG_{ATP} with concomitant reduction in Pi and ADP concentrations. These effects were not due to kinetic alterations in PCr hydrolysis, resynthesis, or glycolytic ATP production and altered the flow force relationship between mitochondrial ATP synthesis rate (J_{MITO}) and ΔG_{ATP}. DCA had no significant effect at 1.0-2.0 Hz stimulation because physiological mechanisms at these high stimulation levels cause maximal activation of PDH. These data support a role of PDH activation in the regulation of the energetic steady state by altering the phosphate potential (ΔG_{ATP}) at rest and during contraction.

3.2 Introduction

Skeletal muscle utilizes glucose and fatty acids as substrates for mitochondrial ATP production at rest and during contraction (22,23). The rate of mitochondrial ATP synthesis and magnitude of substrate oxidation is dependent upon the contractile intensity and thus ATP demand of the contractile ATPases (actinomyosin and SERCA ATPase). In the transition from rest to submaximal work, ATP demand from contractile processes reaches a steady state with mitochondrial ATP synthesis. This response to a step change in cytosolic ATP demand results in a new steady state whereby the phosphate potential (*i.e.* free energy of ATP hydrolysis, ΔG_{ATP}) is maintained by the proton motive force (PMF) which is supported through increased rates of substrate oxidation and delivery of reducing equivalents (NADH, QH_2) to the electron transport chain (ETC). At steady state, the rate of mitochondrial ATP synthesis and ETC flux is determined by cytosolic ATPase activity. The magnitudes of the steady state phosphate potential and the PMF are controlled primarily by feedback via the concentrations of the products of ATP hydrolysis, ADP and Pi (147). However, additional regulatory mechanisms have been proposed through which mitochondrial matrix redox status ($NADH/NAD^+$) and consequently the steady state phosphate potential, may be modified independently of feedback regulation by ATP hydrolysis (148–150).

Stimulation of mitochondrial matrix dehydrogenase activity via $[Ca^{2+}]_i$ is one mechanism by which redox regulation of the phosphate potential is proposed to occur, not only through their direct link to matrix redox status via NADH production, but also through regulation of mitochondrial substrate selection and subsequent reducing equivalent generation by tricarboxylic acid (TCA) cycle flux (148,149). Among those

enzymes sensitive to $[Ca^{2+}]_i$, only pyruvate dehydrogenase (PDH) has the capacity to increase acetyl-CoA (A-CoA) delivery to the TCA cycle through regulation of substrate oxidation (151). PDH catalyzes the irreversible decarboxylation of pyruvate to A-CoA for use in the TCA cycle and subsequent production of reducing equivalents (NADH) for maintenance of oxidative ATP synthesis (152,153). Production of A-CoA by PDH represents the entry point for carbohydrates into the TCA cycle, and thus potentially plays a role in governing the cell's preference for oxidation of carbohydrates versus fatty acids (154). PDH activity is regulated via reversible phosphorylation catalyzed by pyruvate dehydrogenase kinase (PDK) and pyruvate dehydrogenase phosphatase (PDP) (152,153). In the phosphorylated state, PDH is inactive and restricts pyruvate flux at times when ATP demand is low, as in resting skeletal muscle. However during muscle contraction, increases in $[Ca^{2+}]_i$ and pyruvate as well as a decrease in the intra-mitochondrial ratios of ATP/ADP, NADH/NAD^+, and A-CoA/CoA activate PDH through coordinated allosteric stimulation of PDP activity and inhibition of PDK activity resulting in net PDH dephosphorylation (152,153). As a result, PDH activation during contraction is proportional to exercise intensity and serves to increase pyruvate flux to provide substrate (A-CoA, NADH) in support oxidative ATP synthesis (24).

Treatment with dichloroacetate (DCA), a potent inhibitor of PDK activity, results in dephosphorylation and complete activation of PDH in resting or contracting skeletal muscle (16,25–28) concomitant with increased rates of glucose oxidation (29–33). PDH activation through DCA treatment is believed to increase the matrix redox status (NADH/NAD+) as evidenced by significant increases in skeletal muscle content of both A-CoA and acetyl-carnitine (15,16,155,156). Acetyl-carnitine formation occurs through

carnitine acetyltransferase (CAT), the mitochondrial matrix enzyme that catalyzes the conversion of A-CoA and carnitine to acetyl-carnitine and free CoA. CAT flux is stimulated when there is excess A-CoA production not matched to TCA cycle utilization (61). PDH production of A-CoA occurs with NADH at a 1:1 ratio and the millimolar increases in acetyl-carnitine of DCA treated skeletal muscle likely results in an increase in the matrix redox state. However, it remains unclear whether alteration in the activation status of skeletal muscle PDH can exert any regulation over mitochondrial oxidative phosphorylation or muscle energetics at rest and/or during exercise.

Therefore, the purpose of this study was to quantify the effect of pharmacological activation of PDH at rest and during contraction on rat gastrocnemius skeletal muscle energetics and function. Here, dichloroacetate (DCA) treatment was used to fully activate PDH irrespective of the gastrocnemius contractile state. PDH activation via DCA treatment resulted in a significant increase in the magnitude of the steady state phosphate potential (ΔG_{ATP}) at rest and during muscle twitch contractile intensities below the reported aerobic threshold (116). This effect occurred without alteration to the contractile metabolic demand, glycolytic ATP contribution, or the kinetics of PCr hydrolysis or resynthesis. At twitch contractile intensities above the expected aerobic threshold (1.0-2.0 Hz), PDH activation with DCA had no significant effect on the net bioenergetic response. Taken together, these data suggest that PDH activity does regulate steady state energetics during muscle contraction below the maximal aerobic capacity and that this effect is likely mediated through alteration in the steady state mitochondrial redox potential.

3.3 Materials and Methods

3.3.1 Animal Care and Feeding

Male Wistar rats (250-350 g; Charles River) were housed three per cage in a temperature (22 °C) and humidity (50%) controlled room on a 12:12 hour light-dark cycle. Rats were provided Purina Rat Chow and tap water ad libitum except when noted below.

3.3.2 Muscle Stimulation and Sampling for PDH Activity

The average body weight of all treatment groups was 240±9 g. Animals were fasted 12 hours overnight before isoflurane anesthesia induction at 5% for 3 minutes. Anesthesia was maintained at 1.5-2.5% during the surgical procedure and body temperature was monitored via rectal thermocouple (Omega HH11) and maintained at 36.5-37.5 °C. For control resting (n=5) and DCA (n=4) treatment groups no stimulation was performed. Control gastrocnemius-plantaris muscle group was excised immediately after anesthesia induction whereas DCA treated muscles were excised one hour after tail vein injection of DCA (150 mg/Kg at 220 mg/ml) dissolved in isotonic saline. Muscles were immediately freeze clamped after excision in liquid N2 precooled Wollenberger tongs and stored at -80 °C for analysis. For 0.5 Hz (n=4) and 1.0 Hz (n=4) stimulation groups the sciatic nerve of one hindlimb was exposed as described previously (133). In brief, a 1.5 cm wide incision was made on the lateral aspect of the hip and blunt dissection was performed through the gluteus adjacent to the sciatic nerve. The nerve was then insulated from surrounding tissues with a small strip of Parafilm and a bipolar platinum electrode was placed in around the nerve and the wound closed with cyanoacrylate glue. A length of suture (20 lb. test braided nylon) was fixed to the

patellar tendon which was fixed in place on a custom Perspex animal holder. The lower limb was dissected free of overlying skin and a length of suture was secured to the Achilles tendon. The calcaneus was cut to remove anterior muscles from interfering with the force recording from the gastrocnemius-plantaris-soleus muscles. The animal was positioned prone in the Perspex animal holder with the knee fixed in place and the Achilles tendon attached to a strain gauge (Grass FT03C). Maximum force output was then achieved by determining the supramaximal stimulation voltage and the optimal resting length using the length-tension relation. After measuring initial maximal tension, muscles were stimulated at either 0.5 Hz or 1.0 Hz for 5 minutes. Immediately following this period, the gastrocnemius-plantaris muscle group was freeze clamped in liquid N_2 precooled Wollenberger tongs while the muscles were still contracting to maintain the phosphorylation status of PDH. Samples were then stored at -80 °C for later biochemical analyses.

3.3.3 [2-14C]-Pyruvate Tracer Solution for PDH Activity Assay

A standard solution of 35 mM pyruvate was made in water and its concentration verified. Briefly, 1 µl of 35 mM pyruvate was added to 0.99 ml of 303 mM TEA, 3.03 mM EDTA, and 10 µl of 25 mM NADH, pH 7.5 at room temperature (RT). Pyruvate concentration was assayed in triplicate utilizing a spectrophotometric lactate dehydrogenase (LDH) assay following consumption of NADH at 340 nm at 25 °C. Baseline absorbance was measured and excess LDH (5-10 U) was added and incubated for 5 minutes or until no absorbance change was present. The pyruvate concentration was then calculated from the change in absorbance from baseline utilizing the extinction coefficient of NADH (ε_{340} = 6220 $M^{-1}cm^{-1}$) assuming reaction of

NADH is 1:1 with pyruvate. 5 ml of standardized 35 mM pyruvate solution was then added to 250 µCi [2-^{14}C]-pyruvate sodium salt (specific activity 7.3 mCi/mmol, Perkin Elmer #NEC256) and the final concentration was verified using spectrophotometric LDH assay as described above. Specific activity of the [2-^{14}C]-pyruvate tracer solution was then determined via reaction with glutamate with glutamate pyruvate transaminase (GPT) to form [2-^{14}C]-alanine. This step was performed to determine the fraction of the ^{14}C label that is specific to pyruvate in the tracer solution. In brief, 1 µl of [2-^{14}C]-pyruvate tracer solution was added to 500 µl of 50 mM TEA, 0.5 mM EDTA, and 250 mM glutamate, pH 7.5 at RT. Assays were carried out in duplicate with two negative controls. GPT (~2 U) was then added to initiate the reaction but omitted from negative controls. Reactions were carried out at RT and after 1 hour, 400 µl aliquots were removed and loaded into gravity flow columns containing 1 ml settled volume of anion exchange resin (Bio-Rad AG1x8 resin, 200-400 mesh, Acetate form) contained in a 3 ml syringe with Luer lock stopcock. This resin traps the negatively charged [2-^{14}C]-pyruvate while the positively charged [2-^{14}C]-alanine passes through. Resin was then washed 3 times with 500 µl water and column eluate was collected into 25 ml glass scintillation vials containing 20 ml Safety Solve scintillant and counted using a Packard Tri-Carb liquid scintillation analyzer. Background counts from negative controls were subtracted from sample values to obtain the specific activity (CPM/µmol) of the [2-^{14}C]-pyruvate tracer solution. 100 µl aliquots of the [2-^{14}C]-pyruvate tracer solution were stored at -80 °C until needed.

3.3.4 Homogenization and Assay Buffers for PDH Activity Assay

Homogenization buffer A, for measurement of PDH active fraction (PDH_a): 0.05 M Tris-HCL, 0.005 M EGTA, 0.005 M $MgCl_2$-$6H_2O$, 0.05 M KCl, 0.05 M NaF, 0.005 M DCA, 0.1% Triton X-100 with 0.001 M DTT, pH 7.8 on ice. Homogenization buffer B, for measurement of total PDH activity (PDH_t): 0.05 M Tris-HCL, 0.024 M $CaCl_2$-$2H_2O$, 0.005 M $MgCl_2$-$6H_2O$, 0.05 M KCl, 0.005 M DCA, 0.1% Triton X-100 with 0.01 M glucose, 0.001 M DTT, and 5 U/ml hexokinase added fresh before use, pH 7.8 on ice. Assay buffer: 0.12 M Tris-HCl, 0.577 mM Na_2EDTA, 0.001 M $MgCl_2$-$6H_2O$, 0.001 M DCA with 3.86 mM NAD^+, 5.77 mM CoA, 0.001 M TPP, 0.012 M L-carnitine-HCl, and 0.8 U/ml carnitine acetyltransferase (CAT) added fresh before use, pH 7.8 at 37 °C. For assay of total PDH activity (PDH_t), 2.88 mM NaF was also added to assay buffer.

3.3.5 PDH Activity Assay

PDH activity was determined by a method developed previously by Sterk *et al*. 2003 with modifications outlined below (130). In brief, PDH activity in muscle homogenates was determined by a coupled enzyme assay, following the conversion of the radiolabeled substrate ([2-^{14}C]-pyruvate) to radiolabeled product ([1-^{14}C]-acetylcarnitine):

$$[\mathbf{2\text{-}^{14}C}]\text{-}pyruvate + NAD^+ + CoA \xrightarrow{PDH} [\mathbf{1\text{-}^{14}C}]\text{-}acetyl\text{-}CoA + NADH + CO_2$$

$$[\mathbf{1\text{-}^{14}C}]\text{-}acetyl\text{-}CoA + L\text{-}carnitine \xrightarrow{CAT} [\mathbf{1\text{-}^{14}C}]\text{-}acetylcarnitine + CoA$$

Reaction time points were collected and then passaged through gravity flow columns containing anion exchange resin allowing for the separation of ^{14}C labeled compounds by trapping the unreacted negatively charged substrate, [2-^{14}C]-pyruvate, while allowing

the passage of the positively charged product, [1-^{14}C]-acetylcarnitine, to quantify the reaction rate. Overall reaction rate was limited by the amount of PDH activity as CAT and substrates of the reaction were added in excess. Thus, the rate of [1-^{14}C]-acetylcarnitine production was assumed to be 1:1 with [1-^{14}C]-acetyl-CoA production and used to quantify PDH activity in muscle samples. Reactions were carried out in homogenates produced from freeze clamped muscle samples of the gastrocnemius-plantaris group. Samples were first powdered under liquid nitrogen using mortar and pestle followed by two separate assays for determination of PDH active fraction (PDH_a) and total PDH activity (PDH_t). Approximately 30-50 mg of muscle powder was added to 250 µl ice cold homogenization buffer A (PDH_a) and immediately mixed with vigorous shaking. Buffer volume was then adjusted by adding buffer to a final 10% homogenate concentration. Homogenates were then sonicated on ice using Branson sonicator at 20 kc, 3 times for 15 seconds with 15 second breaks in between. Each homogenate was then immediately assayed by adding 15 µl homogenate to 85 µl assay buffer prewarmed to 37 °C and vortexed to mix. Reactions were carried out in triplicate at time points of 30 seconds, 1 minute, and 1.5 minutes and initiated by the addition of [2-^{14}C]-pyruvate tracer solution to a final concentration of 1 mM. [2-^{14}C]-pyruvate tracer was added as a drop on the side of the reaction Eppendorf tube and time points were started by vortexing, mixing the [2-^{14}C]-pyruvate tracer into the assay solution and initiating the reaction. Reaction temperature was maintained at 37 °C for entire duration by means of a heated water bath. Reactions were then quenched at appropriate time points via the addition of 500 µl of ice-cold methanol followed by vortexing. Each time point was run separately and quenched samples were stored on ice until the reaction series of that

sample was complete. Once the reaction series was completed for PDH_a, the entire process was repeated by producing another muscle homogenate with homogenization buffer B for determination of PDH_t activity. Quenched reaction time points were then loaded into gravity flow columns containing 1 ml settled volume of anion exchange resin (Bio-Rad AG1x8 resin, 200-400 mesh, Acetate form) contained in a 3 ml syringe with Luer lock stopcock. Columns were then washed 3 times with 500 µl water with column eluate collected into 25 ml glass scintillation vials containing 20 ml Safety Solve liquid scintillation cocktail. The radioactivity in each vial was then counted using a Packard Tri-Carb liquid scintillation analyzer and using the specific activity of the tracer solution, the reaction rate was determined for quantification of PDH activity.

3.3.6 Assay for Muscle ATP Content

Muscle samples were assayed for ATP content by the method of Lowry *et al*. 1972 (128). In brief, the superficial gastrocnemius was sampled under isoflurane anesthesia and immediately freeze clamped. Muscles were powdered under liquid nitrogen and stored at -80 °C until analysis. Metabolites were extracted from powdered muscle samples by adding to ice-cold perchloric acid solution (2 N $HClO_4$, 5 mM EDTA) at a final dilution of 1:10 as previously described (129). Extracts were mixed at 4 °C for 20 minutes and subsequently centrifuged at 20,000 G for 20 minutes. The supernatant was neutralized by the addition of an equivalent volume of potassium hydroxide buffer (2 N KOH, 150 mM TES, 300 mM KCl) and a second centrifugation (3,000 G,10 minutes) step removed precipitated perchlorate salts. Neutralized extracts were assayed for ATP content at RT using a coupled spectrophotometric enzyme assay (128).

3.3.7 NMR Spectroscopy During Stimulation

In vivo rat muscle preparations were prepared as previously described for benchtop experiments but for these experiments the skin and calcaneus process were left intact. An intraperitoneal (IP) catheter (PE 20) was inserted for DCA administration and sealed in place with cyanoacrylate glue. The animal was secured in a custom 74 mm diameter phosphorus nuclear magnetic resonance probe with the knee secured via a tungsten pin fixed through the femur and attached to brass supports. The Achilles was tied to a custom-built isometric force transducer at the top of the probe. This arrangement positioned the center of the superficial gastrocnemius muscle directly over a 1.7 cm diameter circular surface coil. Isoflurane anesthesia was maintained at 1.5-2.5% for duration of experiment through a nose cone built into the body of the NMR probe and temperature was monitored via rectal thermistor (YSI model 73A) and maintained at 36.5-37.5 °C using thermostated air. In each experiment the muscle length and supramaximal stimulation voltage (5-15 V) were adjusted to yield peak isometric tension development and the probe was inserted into a Bruker AM400 spectrometer (9.4 T, 7.4 cm vertical bore magnet). Magnetic field homogeneity was optimized by shimming on the available proton signal. Phosphorus nuclear magnetic resonance (^{31}P NMR) spectra were acquired at 161.8 MHz (4096 complex data, 8012 Hz sweep width). The summed free induction decays (FID) were apodized with a 30 Hz exponential filter prior to the Fourier transform. The pulse width (15 µs) was chosen to yield maximum signal to noise ratio at a repetition time (TR) of 3.0 seconds. The NMR signal was corrected for partial saturation by acquiring 128 FIDs under the experimental

conditions and a second at 5*T1 for PCr at 9.4 T (TR=15 seconds). For each stimulation series spectra (TR=3 seconds, 8 scans) were acquired at rest (6 spectra), during stimulation (12 spectra) and recovery after stimulation cessation (16 spectra). Muscles were stimulated at twitch contractile intensities of 0.35, 0.5, 0.75, 1.0, and 2.0 Hz but no more than 4 stimulations were used in any experiment and frequencies were randomized. There was no effect of stimulation order on the resulting PCr transients. Following the first series of stimulations, DCA was administered IP (150 mg/kg at 220 mg/ml in isotonic saline) followed by a one-hour incubation before an identical stimulation series was performed in the exact order. The triceps surae muscle group was then excised and weighed for normalization of force recordings.

3.3.8 High Resolution NMR Spectroscopy for Resting Metabolites

To obtain quantitative metabolite values in resting muscle, animals were mounted in the NMR probe and a series of spectra (20) were acquired (2400 free induction decays, 4096 complex points, 8012 Hz sweep, 3 second recycle delay, 30 Hz exponential filter) under the control condition. A second series was acquired 1 hour after IP administration of DCA (150 mg/Kg at 220 mg/ml in isotonic saline) with the same acquisition settings.

3.3.9 Spectral Analysis

The free induction decays of the stimulation series were analyzed using JMRUI software (version 3.0) and relative peak areas were integrated using AMARES (131). Areas of Pi, PCr, γ-ATP, α-ATP, and β-ATP peaks were normalized to the total phosphorus integral of each individual spectrum. PCr and Pi were quantified from their ratio to γ-ATP and adjusted to absolute chemical content using the enzymatically

determined ATP content of the rat superficial gastrocnemius muscle determined from perchloric acid extracts described previously (132). Creatine content was estimated assuming PCr content is 82% of total creatine (132). Intracellular pH (pH_i) was estimated from the chemical shift of Pi relative to PCr (157):

$$pH = 6.75 + \log\left(\frac{3.37 - \Delta PPM}{\Delta PPM - 5.63}\right) \quad (1)$$

The PCr content during steady state contractions was calculated as a percentage of the initial value by using the summed data from the six resting spectra and the final six spectra during the contractile phase. The dynamics of PCr changes were fit to a monoexponential function by an iterative least squares algorithm to obtain the time constants of both PCr hydrolysis and resynthesis. Glycolytic ATP synthesis rate (J_{GLY}) was estimated as follows:

$$J_{GLY} = 1.5\ x\ \beta\ x\ \left(\frac{dpH_i}{dt}\right) \quad (2)$$

where 1.5 is the stoichiometric coefficient for ATP/H^+, β the buffering capacity (134), and $d(pH_i)/dt$ is the rate of acidification during contraction (135). Cytosolic ATPase rate (J_{ATPase}) was calculated from the initial rate of PCr hydrolysis at the start of stimulation plus basal the ATPase rate of 0.012 mM/s (135,136). Mitochondrial ATP synthesis rate (J_{MITO}) was calculated by subtracting J_{GLY} from J_{ATPase}, assuming the steady state phosphate potential is maintained via the matching of cytosolic ATPase activity (J_{ATPase}) to mitochondrial ATP synthesis rate (J_{MITO}) after the glycolytic ATP production rate (J_{GLY}) is accounted for (135). Free energy of ATP hydrolysis was estimated from Pi, PCr, and Cr utilizing the creatine kinase equilibrium equation:

$$Keq = \frac{[ATP][Cr]}{[ADP][PCr][H]} \quad (3)$$

and substituting for [ATP]/[ADP] with Keq_{CK} = 1.66x10^9 M^{-1} (137):

$$\Delta GATP = -32\ kJ/mol + 2.58 \ln(\frac{[Pi][Cr]}{[PCr][H]Keq}) \quad (4)$$

Analysis of high resolution, non-stimulation spectra was done using NUTS analysis software ver. 6.1 and manual Lorentzian line fitting. Individual peaks were normalized to the total phosphorus integral and quantified as described previously.

3.3.10 Statistics

All data are reported as means ± SE. Comparisons of group means were by paired two tailed Students *t*-test at the $p < 0.05$ level of significance.

3.4 Results

PDH activity at rest, during contraction, or DCA treatment. The percent active fraction of the total PDH activity (PDH_a/PDH_t) present in rat gastrocnemius-plantaris muscle samples collected at rest, during twitch stimulation or DCA treatment are presented in Figure 16. The active fraction of PDH in resting muscle was 23±3%, consistent with published values in the rat (42–44). Muscle twitch stimulation resulted in significant increases in the active fraction of PDH compared to resting values resulting in 53±7% and 75±13% active fractions for 0.5 Hz and 1.0 Hz respectively (Fig. 16). Treatment of resting muscle with DCA resulted in complete activation of PDH, consistent with previous reports both in rat and human skeletal muscle (16,25–28). PDH activity with DCA treatment was significantly increased compared to control values at rest (90±12% vs 23±3%, $p<0.05$) and during 0.5 Hz stimulation (90±12% vs 53±7%,

$p<0.05$) but was not significantly different than the activity measured during stimulation at 1.0 Hz (90±12% vs 75±13%, NS).

ATP free energy in resting muscle. In vivo metabolite levels measured by ^{31}P NMR spectroscopy in control and DCA treated superficial gastrocnemius muscles are presented in Figure 17. Activation of PDH with DCA resulted in a 17% decrease in resting Pi compared to control values ($p<0.05$) within the same animal (Table 4). However, this was not met with a measurable stoichiometric increase in PCr or any alteration in intracellular pH. This decrease in intracellular Pi concentration through PDH activation with DCA treatment resulted in a measurable increase in the magnitude of ΔG_{ATP} from -65.7±0.22 to -66.4±0.30 kJ/mol ($p<0.05$) in control and DCA-treated animals respectively. (Table 4).

Effect of PDH activation on PCr dynamics during contractile activity. Dynamic changes in PCr and reciprocal stoichiometric changes in Pi occur at the onset and cessation of contractile activity and deviate further from their resting levels as contraction intensity increases. Figure 18 shows a representative stackplot of individual ^{31}P NMR spectra serially-acquired over the time course of one such experiment in control and DCA treated conditions. Resting ^{31}P NMR spectra were acquired for the first 2 minutes 24 seconds (spectra 1-6), during the next 4 minutes 48 seconds of 0.5 Hz stimulation (spectra 7-18) and during the subsequent 7 minutes 12 seconds of recovery (spectra 19-36) to quantify the steady state and kinetic response of PCr hydrolysis and resynthesis in control and DCA treated animals (Fig. 18). Force recordings from the triceps surae group were measured concurrently and muscle force generation was quantified as the total tension time integral (TTI) for each muscle twitch and averaged

between groups. No difference in force production between control and DCA treatment conditions was found at 0.35 Hz (67.1±8.1 vs. 58.2±5.9 g*s, n=6), 0.5 Hz (62.4±13.0 vs. 59.3±13.1 g*s, n=7), 1.0 Hz (45.5±3.0 vs. 39.2±1.9 g*s, n=7), and 2.0 Hz (47.0±4.7 vs. 43.6±5.1, n=6) with the exception of 0.75 Hz (58.0±10.9 vs. 49.4±10.5 g*s, n=6, $p<0.05$).

Representative PCr transients during stimulation and recovery before and after DCA treatment are depicted in Figure 19A and 4B respectively. During PCr consumption at the onset of stimulation, ATP hydrolysis rates (J_{ATPase}) are derived from linear fitting to the initial rate of PCr hydrolysis (135). PCr transients quantified from both control and DCA treated rats showed there was no difference in ATP use irrespective of treatment and that a linear relation exists between increases in ATP use and increased stimulation frequency (Table 6). In addition, PDH activation with DCA treatment did not alter the time constant for PCr resynthesis depicted as the rising monoexponential functions in Figures 4A and 4B and further quantified in Table 5 indicating that ATP production is also unaffected by DCA treatment (Table 5). During steady state contractions, intracellular pH values decreased with increasing stimulation frequency as previously shown in other studies (119). DCA treatment did not result in significant deviation in intracellular pH from control conditions with the exception of 0.35 Hz stimulation intensity (Table 5). A representative summed spectrum from one animal during steady state contraction at 0.5 Hz intensity (spectra 13-18) is shown in Figures 4C and 4D for control and DCA conditions respectively. Figure 19E depicts a difference spectrum computed by subtracting the control spectrum (Fig. 19C) from that of the DCA treated condition (Fig. 19D) showing the differences in phosphorus metabolite peak

areas. This resulted in residual areas for PCr and Pi indicating elevated PCr and reduced Pi with DCA when compared to control stimulation within the same animal at the same intensity.

At intensities below the reported aerobic threshold for rat hindlimb muscles (116) (0.35 Hz, 0.5 Hz, 0.75 Hz) PDH activation with DCA resulted in significantly higher steady state PCr levels relative to the comparable control condition within the same animal (Fig. 20). This effect was lost with stimulation at intensities of 1.0 Hz and 2.0 Hz with no discernable differences in the observed steady state energetics. Increased PCr levels at each stimulation frequency were associated with equivalent decreases in Pi levels as illustrated in panel A from Figure 21. The plot of Pi against PCr shows a linear relationship with a slope of -1.0 Pi/PCr (R^2=0.97) indicating a 1:1 stoichiometric balance between PCr reduction and Pi increase, validating the *in vivo* quantification of these metabolites. Panels B and C of Figure 21 show Pi and calculated free ADP levels against J_{ATPase} showing distinct reductions in Pi and ADP in DCA treated contraction frequencies compared to controls.

Effect of PDH activation on mitochondrial flow force relationship. At stimulation intensities below the reported aerobic threshold (116), PDH activation with DCA resulted in a significant increase in the magnitude of steady state ΔG_{ATP}. At stimulation rates above 1.0 Hz this effect was lost (Table 6). As a result of the changes in concentration of phosphate metabolites associated with DCA treatment, PDH activation resulted in a leftward shift in the flow force relationship between the steady state ΔG_{ATP} maintained for a given rate of mitochondrial ATP synthesis (J_{MITO}) (Fig. 22). The shift in the relationship between J_{MITO} and ΔG_{ATP} stems from the significant elevation in the

magnitude of steady state ΔG_{ATP} at intensities below the aerobic threshold as J_{MITO} was not affected by PDH activation (Table 6). The Figure 22 inset shows the linear relationship between J_{MITO} and ΔG_{ATP} for stimulation intensities below (0.35-0.75 Hz) as well as at (1.0 Hz) the reported aerobic threshold of the rat hindlimb (116). PDH activation with DCA treatment resulted in a leftward shift in the flow force relationship between J_{MITO} and ΔG_{ATP} without significant alteration in slope ($p=0.7$). These data support a shift in the thermodynamic set point between the free energy transduction from substrate oxidation to ΔG_{ATP} and not an alteration in the kinetic response of oxidative phosphorylation to muscle contraction.

Table 4. *Resting metabolite, pH, and ΔG_{ATP} before and after DCA treatment.* Resting values were calculated from high resolution spectra as seen in Fig. 17. Peak areas were quantified with NUTS line fitting algorithm and normalized to total ^{31}P peak area for each spectrum. Spectra were quantified with γ-ATP peak area at ATP concentration of 9.24 mM determined enzymatically in control white gastrocnemius muscle. pH was calculated via chemical shift of Pi relative to PCr as shown in Eq. 1. ΔG_{ATP} was calculated as described previously in Eq. 3. Values are means ± SE, n=6. *Significant difference between control and DCA conditions ($p<0.05$) by two tailed paired Students *t*-test. Pi, Inorganic Phosphate. PCr, Phosphocreatine. ATP, Adenosine Triphosphate. LCW, Liter Cell Water.

	Control (n=6)	DCA (n=6)
Pi (mmol/LCW)	1.61±0.11	1.34±0.16*
PCr (mmol/LCW)	38.0±1.21	37.2±1.63
ATP (mmol/LCW)	9.24±0.7	--
PCr/ATP	4.01±0.13	3.92±0.18
pH	7.01±0.02	6.98±0.01
ΔG_{ATP} (kJ/mol)	-65.7±0.22	-66.4±0.30*

Table 5. *PCr kinetics and end of stimulation pH in control and DCA treatment conditions.* Time constant of PCr hydrolysis and recovery was calculated by fitting normalized PCr spectral area to a monoexponential function by an iterative least squares algorithm. pH at the end of stimulation was calculated using Eq. 1 from the average chemical shift of the Pi peak relative to PCr during the last six spectra during stimulation. Values are means ± SE, n=6-7 per stimulation. *Significant difference between control and DCA conditions ($p<0.05$) by two tailed paired Students *t*-test.

	0.35 Hz (n=6)		0.5 Hz (n=7)		0.75 Hz (n=6)		1.0 Hz (n=7)		2.0 Hz (n=6)	
	Control	DCA	Control	DCA	Control	DCA	Control	DCA	Control	DCA
Time constant of PCr Hydrolysis (s)	75.3 ±12.7	47.1 ±20.7	71.1 ±5.3	72.5 ±7.2	56.8 ±4.8	66.4 ±5.5	45.4 ±7.6	61.1 ±13.9	25.2 ±4.5	33.3 ±9.1
Time constant of PCr Resynthesis (s)	46.7 ±5.8	43.5 ±12.62	61.1 ±6.1	58.6 ±4.6	59.8 ±6.6	47.2 ±6.1	65.0 ±6.2	60.0 ±6.6	72.9 ±5.6	68.1 ±4.2
pH	6.96 ±0.02	6.93 ±0.02*	6.94 ±0.02	6.90 ±0.01	6.79 ±0.09	6.84 ±0.03	6.75 ±0.06	6.78 ±0.04	6.65 ±0.12	6.65 ±0.08

Table 6. *Metabolic flux and steady state ΔG_{ATP} in control and DCA treatment conditions*. J_{GLY}, J_{ATPase}, J_{MITO}, and ΔG_{ATP} were calculated as described previously in methods. Values are means ± SE, n=6-7 per stimulation. *Significant difference between control and DCA ($p<0.05$) by two tailed paired Students *t*-test. J_{GLY}, glycolytic ATP synthesis rate. J_{MITO}, mitochondrial ATP synthesis rate. J_{ATPase}, cytosolic ATP hydrolysis rate.

	0.35 Hz (n=6)		0.5 Hz (n=7)		0.75 Hz (n=6)		1.0 Hz (n=7)		2.0 Hz (n=6)	
	Control	DCA	Control	DCA	Control	DCA	Control	DCA	Control	DCA
J_{ATPase} (mM/s)	0.09 ±0.04	0.19 ±0.05	0.16 ±0.02	0.21 ±0.01	0.23 ±0.01	0.32 ±0.04	0.34 ±0.04	0.40 ±0.05	0.87 ±0.14	0.68 ±0.11*
J_{GLY} (mM/s)	0.01 ±0.00	0.01 ±0.00	0.02 ±0.00	0.02 ±0.01	0.06 ±0.02	0.03 ±0.01	0.10 ±0.02	0.07 ±0.01	0.43 ±0.08	0.40 ±0.07
J_{MITO} (mM/s)	0.09 ±0.03	0.12 ±0.01	0.14 ±0.02	0.18 ±0.02	0.16 0.02	0.27 0.04	0.22 ±0.02	0.32 ±0.05	0.40 ±0.16	0.40 ±0.10
ΔG_{ATP} (kJ/mol)	-58.2 ±0.3	-59.9 ±0.4*	-56.8 ±0.4	-57.7 ±0.6*	-55.6 ±0.3	-56.0 ±0.4*	-55.4 ±0.3	-55.6 ±0.4	-54.6 ±0.6	-54.5 ±0.3

Figure 16. DCA fully activates PDH compared to activities at rest or during contraction.

Endogenous PDH activity expressed as percent of total PDH activity in rat gastrocnemius-plantaris muscle at rest, during 0.5 Hz or 1.0 Hz stimulation, and after DCA treatment at rest. Freeze clamped muscle samples were collected from anesthetized Wistar rats and assayed *in vitro* for PDH activity via radioisotopic assay described in methods. Values are means ± SE for resting (n=5), 0.5 Hz (n=4), 1.0 Hz (n=4), and DCA (n=4) treatment groups. *Significantly different from resting ($p<0.05$); †Significantly different from 0.5 Hz ($p<0.05$). Significance determined by two tailed Students *t*-test.

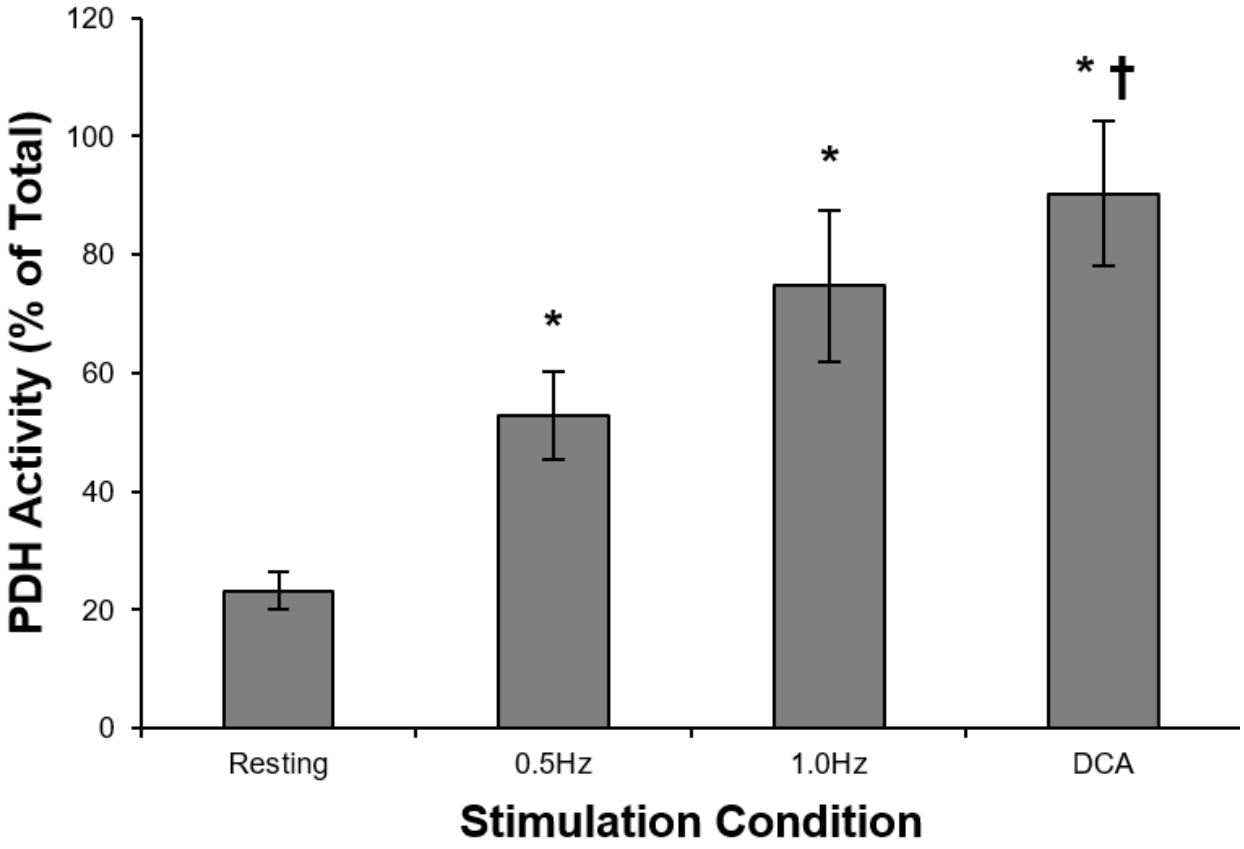

Figure 17. High resolution phosphorus spectra in control and DCA treated rats. Representative high resolution ^{31}P NMR spectrum of control (A) and DCA treated (B) resting rat gastrocnemius muscle within the same animal. Acquisition parameters: 2400 FIDs, 4096 complex points, 8012 Hz sweep, 3 second TR, and 30 Hz exponential filter. EC, Extracellular. IC, Intracellular. PME, Phosphomonoester.

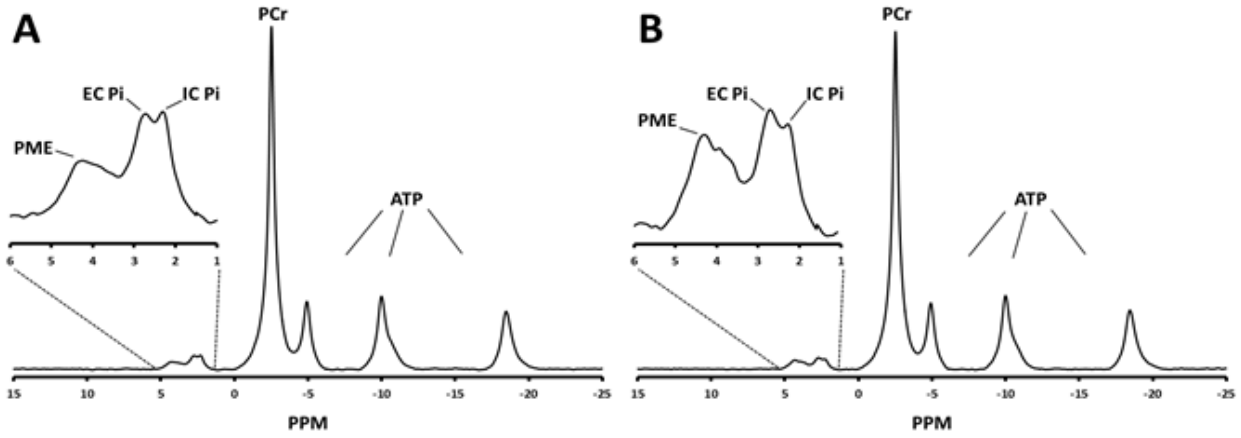

Figure 18. Phosphorus spectra during muscle contraction in control and DCA treated rats.

Sample ^{31}P NMR spectra acquired in the rat gastrocnemius muscle before (bottom 6 spectra), during (next 12 spectra), and after (last 18 spectra) 0.5 Hz stimulation within one animal in control and DCA treated conditions. Acquisition parameters: total of 36 spectra composed of 8 FIDs, 4096 complex points, 8012 Hz sweep, 3 second TR, and 30 Hz exponential filter.

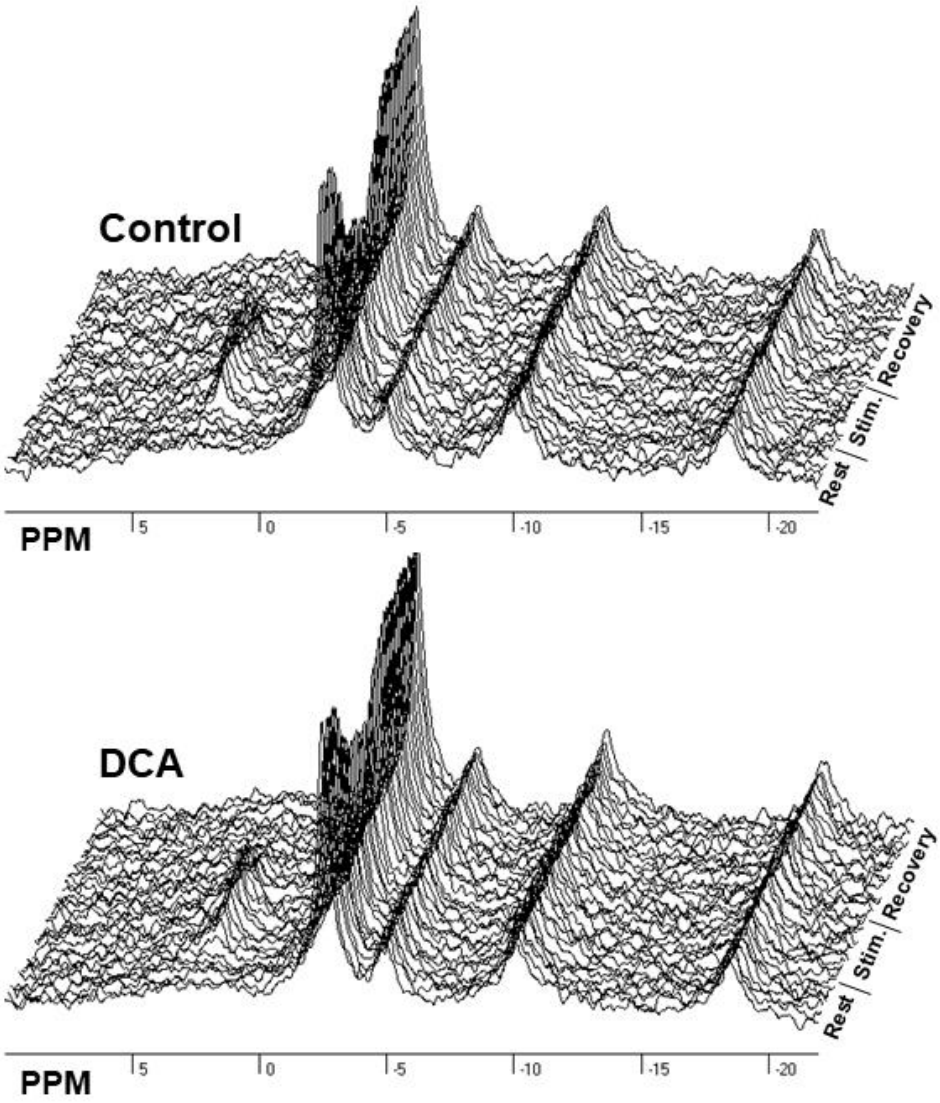

Figure 19. Steady state PCr is increased with DCA treatment but does not affect PCr kinetics.

PCr content expressed as percent of initial resting values and steady state ^{31}P NMR spectrum during 0.5 Hz stimulation before and after DCA treatment in one animal.

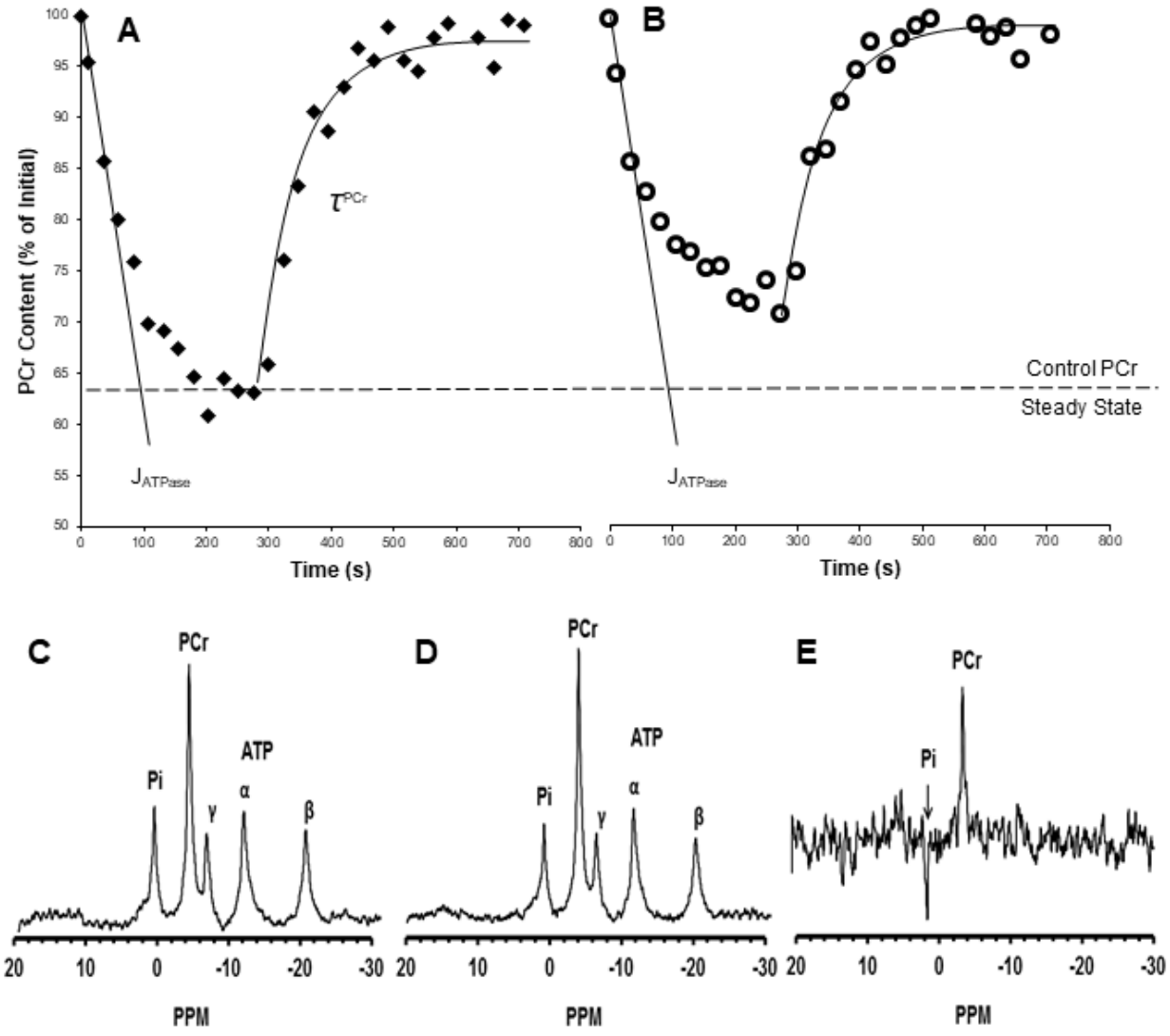

A: Control PCr content during 0.5 Hz stimulation and recovery. *B:* PCr content during 0.5 Hz stimulation and recovery after DCA administration. Dashed line indicates control steady state PCr content at the end of the stimulation, taken as the average PCr content in the last six spectra during stimulation. Linear regression fits of the initial rate of PCr

Figure 19 (cont'd). hydrolysis were used to determine the ATP hydrolysis rate during muscle stimulation. Time constant of PCr recovery was calculated by fitting normalized PCr spectral area to a monoexponential function by an iterative least squares algorithm. *C:* Summed steady state ^{31}P-NMR spectrum of the last 6 spectra acquired during 0.5 Hz stimulation in the control condition. *D:* Summed steady state ^{31}P NMR spectrum of the last 6 spectra acquired during 0.5 Hz stimulation after DCA treatment. *E:* Difference spectrum: DCA – control spectrum. Intensity adjusted to 4 times that of *C* and *D*.

Figure 20. Steady state PCr is increased with DCA treatment below the aerobic capacity.

Steady state PCr expressed as percent of initial resting values before and after DCA treatment. PCr peak area of the last six spectra during gastrocnemius muscle stimulation were averaged and normalized to the average PCr peak area of the first six spectra acquired in the gastrocnemius muscle at rest. Values are means ± SE. *Significantly different than control ($p<0.05$) of the same stimulation intensity by two tailed paired Students *t*-test.

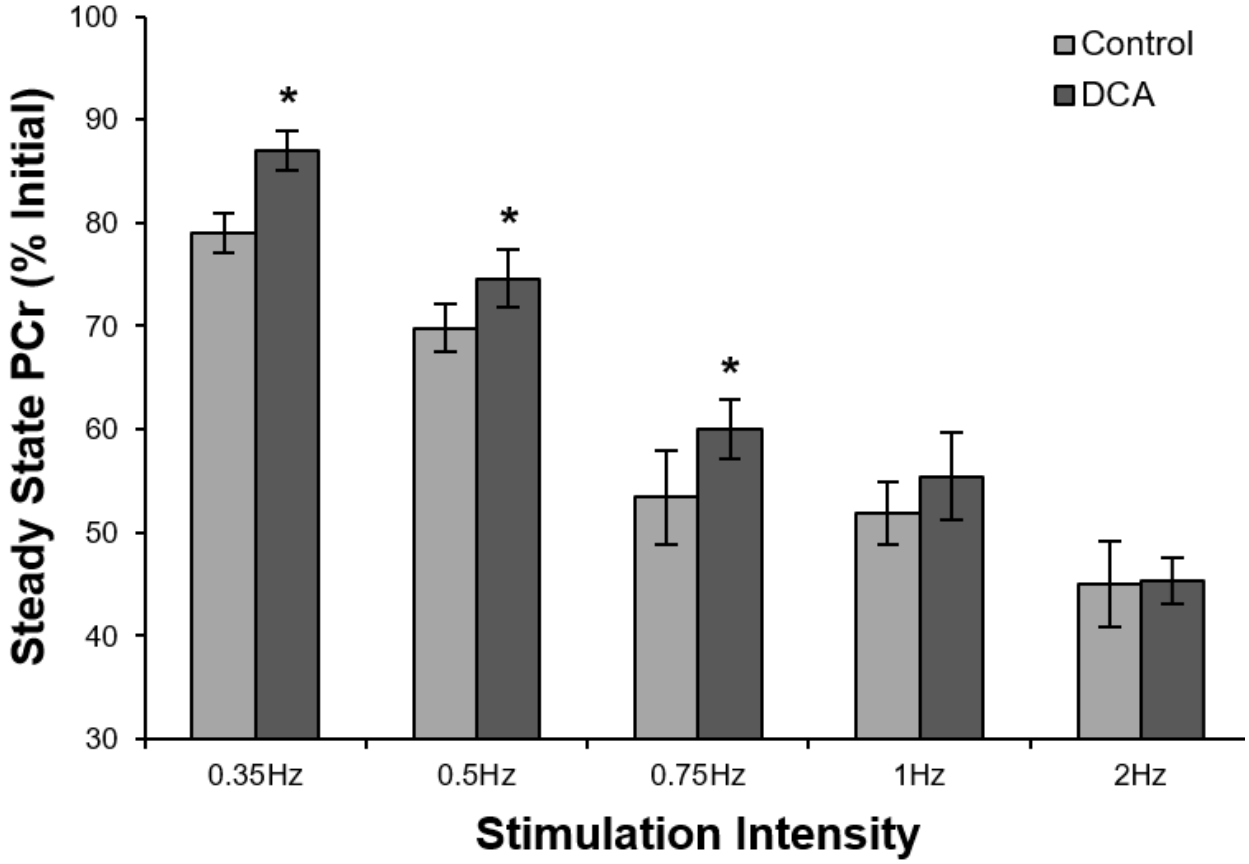

Figure 21. Phosphorus metabolites before and after DCA treatment.

Steady state phosphorus metabolites during contraction at 0.35 Hz, 0.5 Hz, 0.75 Hz, and 1.0 Hz before and after DCA treatment. *A:* Reciprocal relationship between steady state Pi and PCr during contraction. Linear regression was fit to group data as there is no significant difference in slope between conditions. *B:* Steady state Pi content as a function of J_{ATPase}. *C:* Steady state ADP content calculated from the creatine kinase equilibrium reaction as a function of J_{ATPase}. Linear regressions fit to initial linear portion of the data that include the first three points from 0.35 Hz, 0.5 Hz, and 0.75 Hz data. J-ATPase, cytosolic ATP hydrolysis rate.

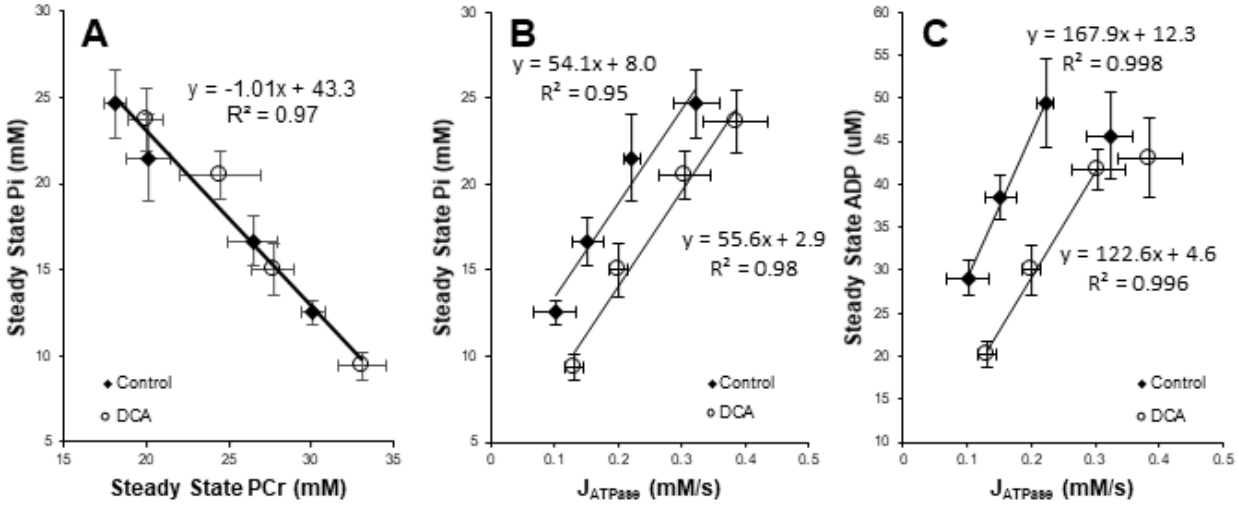

Figure 22. DCA treatment shifts flow force relation during muscle contraction. Steady state ΔG_{ATP} as a function of steady state J_{MITO} at rest and during contraction at 0.35 Hz, 0.5 Hz, 0.75 Hz, 1.0 Hz, and 2.0 Hz in the rat gastrocnemius muscle before (control) and after DCA treatment. *Inset:* Steady state ΔG_{ATP} versus J_{MITO} during contraction at 0.35 Hz, 0.5 Hz, 0.75 Hz, and 1.0 Hz. Data were fit to linear regression with no significant difference in slope between control and DCA treatment. J_{MITO}, mitochondrial ATP synthesis rate.

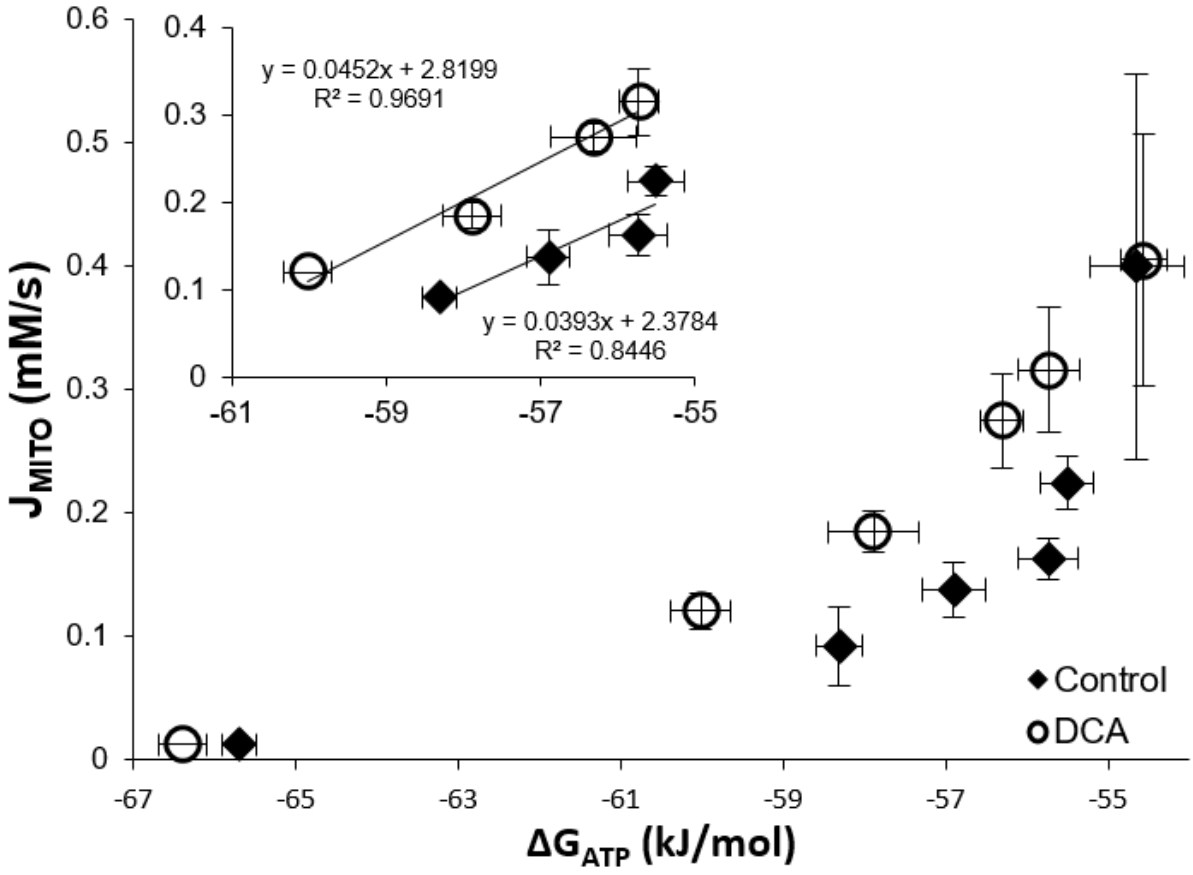

3.5 Discussion

Pharmacological activation of PDH resulted in an increase in the magnitude of steady state ΔG_{ATP} in rat gastrocnemius muscle at rest and during contraction at intensities below the reported aerobic threshold. At rest, treatment with DCA resulted in complete conversion of PDH into the active state concurrent with a significant decrease in the resting Pi levels of 17% and increase in the magnitude of ΔG_{ATP} (Fig. 16, Table 4). During muscle stimulation at contractile intensities below the reported aerobic threshold of 1.0 Hz (116), PDH activation resulted in significant elevation of steady state PCr (lowered free ADP) with a concomitant reduction in Pi content resulting in an increase in the magnitude of ΔG_{ATP} at any contractile frequency (Figures 5, 6, Table 6). This resulted in a leftward shift in the flow force relationship between mitochondrial ATP synthesis rate (J_{MITO}) and the steady state ΔG_{ATP} that was maintained (Fig. 22). The increase in free energy with PDH activation occurred without alteration of the estimated glycolytic contribution to ATP production (Table 6), changes in muscle force generation (TTI) and the corresponding cytosolic ATPase load (Table 6), or the time constants of PCr hydrolysis and resynthesis (Table 5). At or above the reported aerobic threshold for the rat hindlimb (1.0-2.0 Hz), PDH activation with DCA had no significant effect on steady state energetics. Taken together these data suggest that at exercise intensities below maximum J_{MITO} fluxes, the free energy at which ATP is synthesized to meet ATP hydrolysis demand is affected by PDH activity.

The magnitude of PDH activation in skeletal muscle determines the capacity for oxidative glucose disposal. In the current study, resting rat gastrocnemius-plantaris muscle PDH activity was 23% of the total activity, consistent with previous findings both

in rat (14-25%) (42–44) and human skeletal muscle (17-25%) at rest (15,16,27). This agrees with the relatively low whole body respiratory exchange ratio (RER) in the fasted rat of 0.77 corresponding to 23.9% and 76.1% energy expenditure (kcal/lO_2) from glucose and free fatty acid oxidation respectively (21,41) and is consistent with respiratory quotients (RQ) from human leg and forearm skeletal muscle arterial-venous differences (RQ = 0.74-0.77) (18–20,40,48). Low fractional PDH activity in the resting fasted state restricts skeletal muscle glucose oxidation at times when glucose availability is limited and contractile ATP demand is low. This occurs via preferential covalent phosphorylation and inhibition of the enzyme complex through allosteric stimulation of PDK activity (98,158). DCA is a potent inhibitor of PDK resulting in PDH complex dephosphorylation via endogenous PDP activity even where the energetic demand (0.01 mMATP*second^{-1}) (136) and Ca^{2+} concentration (~40-50 nM) (159–161) are low. DCA treatment at rest caused a significant increase in PDH activity towards maximum activation of the enzyme complex (90±12%) similar to that found in both rat (25,26) and human (16,27,28) skeletal muscle. Furthermore, PDH activation with DCA treatment at rest resulted in a significant increase in the magnitude of steady state ΔG_{ATP} (Table 4). This effect was due to a significant reduction in intracellular Pi of 17% as quantified through ^{31}P NMR before and after DCA treatment within the same animal. This reduction in cytosolic Pi content would result in a stoichiometric increase in PCr, however the 0.3 mM reduction in Pi found represents a 0.8% change in PCr content which was below detection limits of the ^{31}P NMR method used due to signal to noise considerations.

Since ATP consumption is balanced by oxidative ATP synthesis under steady-state conditions, the increase in the magnitude of ΔG_{ATP} associated with DCA administration is necessarily associated with increases in the free energy at which ATP is synthesized and transported out of the mitochondrial matrix to the cytosol. This increase is likely explained by a shift in mitochondrial matrix redox potential ($NADH/NAD^+$) to a more reduced steady state, in turn resulting in an increase in mitochondrial PMF that drives the ATP synthesis machinery (the F_1F_O ATPase and the adenine nucleotide translocase (ANT)) to achieve a new steady state relation with ΔG_{ATP}. This has been shown in isolated liver mitochondria *in vitro* where markedly different redox states can be obtained under identical ATPase loads by switching the carbon fuel source utilized to support oxidative phosphorylation (150). Furthermore, the magnitude of the extra-mitochondrial ΔG_{ATP} was substrate dependent and highest with substrates that resulted in a more reduced matrix for a given ATPase stimulation (150). DCA treatment results in significant increases in skeletal muscle glucose utilization, shifting mitochondrial substrate oxidation from primarily fatty acid to glucose in the resting state. In fasting rat epitrochlearis muscle *in vitro*, DCA treatment resulted in a 3-fold increase in glucose oxidation (29). This effect was also observed in the isolated fasted rat soleus muscle, where DCA treatment increased glucose oxidation by 45% with concomitant reduction in oleate oxidation (26). Furthermore, in isolated rat diaphragm, treatment with DCA resulted in 32% and 54% increases in glucose oxidation (30,31). To our knowledge, the effect of DCA solely on human skeletal muscle substrate oxidation has not been determined, however DCA treatment in humans resulted in 14% and 34% increases in whole body glucose oxidation as well (32,33). This effect is

attributed to a significant increase in oxidative pyruvate flux as blood concentrations of both lactate and alanine are significantly reduced with DCA treatment, shifting anaplerotic pyruvate utilization towards oxidation via PDH activation (26,29,162).

If enhancing pyruvate oxidation yields an increase in steady state redox potential, it would be expected that shifting substrate utilization toward glucose or pyruvate would increase the cytosolic phosphate potential (ΔG_{ATP}). In fact, this effect has been demonstrated in both skeletal muscle and cardiac tissue preparations. The addition of 20 mM pyruvate to isolated mouse soleus muscles resulted in a 17% reduction and 8% increase in resting Pi and PCr respectively compared to 11mM glucose alone when measured by ^{31}P NMR spectroscopy (163). Furthermore removal of pyruvate in the superfusate reversed this effect within 30 minutes (163). The effect of increased pyruvate oxidation on tissue bioenergetics, particularly Pi and PCr, was also observed in both the working isolated guinea pig heart *ex vivo* and canine heart *in vivo*. Incubation of the isolated guinea pig heart with 5 mM pyruvate, glucose and lactate nearly doubled both the PCr/Pi ratio (4.93±0.18 vs. 2.63±0.16) and cytosolic phosphate potential [ATP]/([ADP]+[Pi]) (7.3 vs. 3.5) yet there was no significant alteration in either the rate pressure product or oxygen consumption when compared to glucose and lactate alone (164). In separate experiments using isolated guinea pig heart, switching the perfusate medium containing 16.7 mM glucose to that containing 10 mM pyruvate resulted in a significant increase in the intracellular [PCr] (18.3±0.3 vs. 15.2±0.2 mM) and PCr/Pi (30.4±2.2 vs. 10.3±0.09) (165). This effect was also observed in the paced canine heart *in vivo* where perfusion with 5.26 mM pyruvate resulted in a 23% increase in PCr/ATP and 25% reduction in calculated [ADP] with no change in heart rate, ventricular

pressure, or oxygen consumption when compared to pre-perfusion values with blood alone (166). Together these data suggest that not only does PDH activation via pharmacological treatment with DCA result in increases in pyruvate oxidation but also that this switch in substrate utilization would be expected to increase the phosphate potential at similar rates of oxygen consumption or ETC flux.

Our results indicate that activation of PDH results in an increase in the magnitude of ΔG_{ATP}, not only at rest, but also during sub-maximal exercise conditions with the magnitude of the effect of DCA on ΔG_{ATP} dependent on the stimulation level. When DCA treatment was used at stimulation intensities (0.35-0.75 Hz) below the expected aerobic maximum of 1.0 Hz of the rat hindlimb, a significant increase in the magnitude of steady state ΔG_{ATP} was found relative to the matched control condition (Table 6). This was evidenced by a significant increase in the steady state PCr (Fig. 20) through a reduction in ADP and Pi (Fig. 21) levels. This effect was not attributed to any significant alteration in the kinetics of PCr hydrolysis or resynthesis, estimated glycolytic ATP production, muscle force generation (TTI), or the cytosolic ATPase load (Tables 2, 3). However, the relationship between PDH activation and steady state ΔG_{ATP} is not linear even for stimulations below the aerobic threshold. For example, the magnitude of the difference in ΔG_{ATP} between control and DCA treatment conditions is much more pronounced during stimulation at 0.35 Hz when compared to rest (1.7 kJ/mol vs 0.6 kJ/mol respectively). If an increase in the mitochondrial redox status is the mechanism responsible for the increase in the magnitude of ΔG_{ATP} with PDH activation these data suggest that at rest mitochondria are in a highly reduced state and therefore PDH activation has less ability to alter the redox status than during exercise states. It may

also be the case that any increase in the redox status, and therefore PMF, may not be sufficient to stimulate rephosphorylation of ADP to ATP as the ADP concentration at rest is sufficiently low (~10 μM) and potentially limiting to ATP synthesis. However, during stimulation mitochondria become more oxidized as the concentration of ADP increases (150). This may allow for PDH activation to exert a greater influence over cytosolic ΔG_{ATP} and account for the large differences observed in ΔG_{ATP} between control and DCA conditions at rest and during stimulation. The effect of PDH activation on steady state ΔG_{ATP} was largest at the lowest stimulation intensity tested and progressively became smaller as the stimulation intensity increased to 0.75 Hz. This result could be expected as the activation state of PDH increases proportional to stimulation intensity until complete activation is reached at maximal workloads (24,63). Therefore, compared to the control condition, activation of PDH with DCA would result in the greatest difference in fractional PDH activity at lower stimulation intensity and result in the smallest difference in activity as muscle stimulation approaches the aerobic threshold. It is also possible that as stimulation intensity approaches the reported aerobic capacity, limitations to ETC capacity become more important than substrate selection in modifying the flow-force relationship between ATPase activity and cytosolic ΔG_{ATP}.

Prior studies utilizing DCA have also observed increased steady state PCr in skeletal muscle during contraction however have attributed this effect to relief of an “acetyl-group deficit” that mitigates “metabolic inertia”(156,167,168). These studies proposed that the increased acetylcarnitine present in resting skeletal muscle following DCA treatment relieves this deficit, reducing the amount of PCr hydrolyzed during

muscle contraction. However, muscle acetylcarnitine has been altered prior to contraction without significant changes in PDH activity and had no effect on phosphorus metabolites during moderate intensity exercise (62,169,170). Therefore, the effect of DCA treatment on muscle energetics is not likely due to changes in acetylcarnitine content but rather on the activation state of PDH. Furthermore, the current data do not support the concept that activation of PDH relieves “metabolic inertia” as both the time constants of PCr hydrolysis and resynthesis were unaffected by DCA treatment. This suggests both the “on”-kinetics of oxidative phosphorylation and the mitochondrial oxidative capacity were not affected by PDH activation. Instead, the current data support an increase in matrix redox state driven by PDH activation and increases in glucose oxidation, that are transduced through the PMF and ATP synthesis machinery resulting in increased magnitude of steady state ΔG_{ATP}.

In summary, PDH activation through DCA treatment resulted in a significant increase in the magnitude of steady state ΔG_{ATP} at rest and during stimulation below the reported aerobic threshold of 1.0 Hz. This increase in energetic status was achieved without a significant change in the glycolytic contribution to ATP production during stimulation, muscle force generation (excluding 0.75 Hz), cytosolic ATPase load, or the time constants of PCr hydrolysis or resynthesis. From the present data we proposed that the most likely mechanism for the increase in the magnitude of ΔG_{ATP} with PDH activation is an increase in the mitochondrial redox status ($NADH/NAD^+$) contributing to an increase in mitochondrial PMF and driving the ATP synthesis machinery (F_1F_O ATPase, ANT) to a new steady state supporting the elevated ΔG_{ATP}. Furthermore, at exercise intensities above this threshold, PDH activation had no significant effect on

steady state energetics as PDH activity was similar between conditions and the maximal rate of ATP synthesis was likely limiting. Taken together these data do not support a role of PDH activation in relieving “metabolic inertia” but rather support a shift in the thermodynamic set point which is likely attributable to an increase the steady state redox potential through altering mitochondrial substrate oxidation in favor of pyruvate utilization.

Chapter 4. Pyruvate Dehydrogenase Activity in Contracting Skeletal Muscle from the Goto Kakizaki Rat Model of Type 2 Diabetes

4.1 Abstract

Pyruvate dehydrogenase (PDH) regulates skeletal muscle glucose oxidation at rest and during contraction. Dysregulation of PDH activity has been implicated in type 2 diabetes due to decreased glucose oxidation with loss of muscle insulin signaling. However, the few studies to investigate regulation of PDH activity in type 2 diabetes have found contradictory results with none having investigated regulation of PDH activity during muscle contraction. In the current study, skeletal muscle PDH activity was quantified at rest and during contraction in the type 2 diabetic Goto Kakizaki (GK) rat model. Type 2 diabetes was confirmed in GK rats which exhibited significant elevations in fasting blood glucose (194±23.2 vs. 81.3±5.0 mg/dl, $p<0.05$) and HOMA-IR score (16.1±2.5 vs 9.1±3.1, $p<0.05$) with a 3-fold increase in blood glucose after oral glucose challenge that did not return to baseline after 2 hours compared to non-diabetic Wistar controls. Fractional PDH activity was increased in fasted gastrocnemius muscle at rest (16.0±0.7% vs 10.5±0.7%, $p<0.05$) and during muscle stimulation at 0.5 Hz (76.0±3.3% vs 60.8±3.6%, $p<0.05$) in GK rats but was not different from controls at 1.0 Hz (95.6±10.4 % vs 81.1±9.9%, $p<0.05$). Increased fractional PDH activity is attributed to hyperglycemia or reduced mitochondrial density in the GK rat and not to changes in expression levels of the regulatory enzymes of PDH. GK PDH activity data are inconsistent with that found in diabetic rodent models but are consistent with PDH activity and glucose disposal of diabetic humans and suggest skeletal muscle PDH activity is increased with diabetes.

4.2 Introduction

Skeletal muscle is one of the primary sites of peripheral insulin resistance in type 2 diabetes (97). This results in altered muscle fuel selection and contributes to disruptions in whole body glucose and fatty acid homeostasis (171). In animal models of insulin resistance, dysregulation of skeletal muscle pyruvate dehydrogenase (PDH) activity has been implicated in the etiology of type 2 diabetes and promotion of hyperglycemia (102,103). This is a result of decreased PDH activity causing reductions in glucose oxidation and is a target of current drug development to improve glycemic control (172,173). PDH is the mitochondrial matrix enzyme responsible for regulation of glucose oxidation and is regulated by reversible phosphorylation. This interconversion is catalyzed by pyruvate dehydrogenase kinase (PDK2, PDK4) and phosphatase (PDP1) which are expressed in skeletal muscle (5,6,35). PDKs and PDPs are simultaneously active but changes in their relative activity alters the steady state phosphorylation status of PDH and determines overall activity of the enzyme. Insulin is a primary regulator of skeletal muscle PDK4 and in animal models of type 1 and type 2 diabetes, as well as models of insulin resistance through high fat diet, many studies have found increased PDK4 protein expression and total PDK activity (57,98,102,103,113,174–176). In rodent skeletal muscle at rest this increase in PDK activity results in reduced PDH activity and this is thought to contribute to the hyperglycemia associated with type 2 diabetes (44,59,81,101–103).

PDH also regulates glucose oxidation during muscle contraction and is proportionately activated in response to aerobic exercise intensity, reaching steady state levels of activation that parallel the magnitude of glucose oxidation (22–24).

Exercise is a commonly accepted intervention to treat type 2 diabetes, even outperforming pharmaceutical therapies in the prevention of disease progression in prediabetic subjects (177). It is surprising that so few studies have investigated the regulation of skeletal muscle substrate disposal during exercise in type 2 diabetes and that no study has investigated the regulation of PDH activity during exercise either. The data that is currently available suggests that during aerobic exercise in individuals with type 2 diabetes, whole body glucose oxidation is similar to or even greater than that of non-diabetics (107–112). This suggests PDH activities that are either identical to or higher than that of control subjects and are at odds with expected results considering the reduced PDH activities found in resting muscle of type 2 diabetic rodents (102,103).

In light of the conflicting data in rodent and human muscle and the absence of information from contracting muscle, the present study quantified PDH activity was in resting and contracting gastrocnemius muscle of the hyperglycemic, insulin resistant, type 2 diabetic Goto Kakizaki (GK) rat (178). Muscle samples were obtained after overnight fast and during muscle twitch stimulation at submaximal activity levels to quantify PDH activity compared to non-diabetic Wistar controls. Findings indicate that in skeletal muscle of the type 2 diabetic GK rat, fractional PDH activity is increased at rest and during muscle contraction compared to non-diabetic controls despite elevations in free fatty acid levels which are known to inhibit PDH activity levels (53,57,99). The increased activity was not attributed to altered expression of the regulatory PDK or PDP enzymes but is likely related to the direct stimulatory effects of hyperglycemia on PDH activity and the shift in adenylate signaling from the lower mitochondrial density in the diabetic muscle. Taken together these data do not support a role of reduced skeletal

muscle PDH activity in the hyperglycemia of type 2 diabetes but suggests hyperglycemia may actually stimulate PDH activity in insulin resistance to promote glucose oxidation.

4.3 Materials and Methods

4.3.1 Animal Care and Feeding

Male Wistar and Goto-Kakizaki rats were obtained at 11-12 weeks of age from Charles River Laboratories (Wilmington, MA) and Taconic Farms (Taconic Farm, Germantown, NY) respectively. Rats were housed three per cage in a temperature (22 °C) and humidity (50%) controlled room on a 12:12-hr light-dark cycle and provided NIH-31M rat chow (21% calories from protein, 14% calories from fat, 65% calories from carbohydrate) and tap water ad libitum except when noted below. Rats were used for experimentation at 17 weeks of age corresponding to the reported onset of the type 2 diabetic symptoms in the Goto-Kakizaki rats (178). All procedures were approved by the Michigan State University Institutional Animal Care and Use Committee and complied with The American Physiological Society's "Guiding Principles in the Care and Use of Animals".

4.3.2 Oral Glucose Tolerance Test, Blood Insulin and Free Fatty Acids, and HOMA-IR Score

Rats were fasted overnight (12 hours) prior to glucose tolerance testing. Glucose was administered orally at 2 g per kg body weight at a concentration of 0.25 g/ml in tap water by oral gavage and rats were allowed to freely roam in their cages. Blood glucose was measured by tail vein puncture and quantified using a clinical glucose meter

(TrueTrack, Home Diagnostics Inc.). Samples were withdrawn at time 0 and at 5, 15, 30, 60, 90, and 120 minutes after glucose delivery. Total area under the curve was determined from time 0 to 120 minutes.

Blood insulin and free fatty acid (FFA) levels were quantified in blood plasma samples obtained after overnight fast. Plasma insulin and FFA concentrations were determined colorimetrically via commercial kit (Insulin: Millipore Sigma, EZRMI-13K; FFA: FUJIFILM Wako Diagnostics U.S.A., NEFA-HR(2)). HOMA-IR (179) was calculated from values of fasting blood glucose (mM) and insulin (mU/l, using a value of 44.45 μg/U insulin for unit conversion) according to:

$$HOMA\,IR = \frac{glucose \times insulin}{22.5}$$

4.3.3 Muscle Stimulation and Sampling

Fasted animals were anesthetized with 1.5-2.5% isoflurane on a carrier gas of 100% oxygen during the surgical procedure and body temperature was monitored via rectal thermocouple (YSI Model 73a) and maintained (36.5-37.5 °C) with a heated pad. For muscle stimulation the sciatic nerve of one hindlimb was exposed as described previously (122). In brief, a 1.5 cm wide incision was made on the lateral aspect of the hip and blunt dissection through the gluteus adjacent to the nerve was performed to expose the sciatic nerve. The nerve was then insulated from surrounding tissues with a strip of Parafilm and a bipolar platinum electrode was positioned adjacent to the nerve and held in place with cyanoacrylate glue which was also used to seal the wound. A test twitch stimulated with rectangular pulse (5 V, 0.2 ms duration, Grass S48 stimulator) was performed to validate external control of the sciatic nerve. The knee was fixed in place to a custom built knee brace using braided nylon ligature. The posterior leg was

carefully dissected free of overlying skin to expose the muscle for post-exercise freeze clamp and a length of suture secured to the Achilles tendon and to a strain gauge (Grass FT03C) with the animal in the prone position. Stimulation voltage (2-10V) and muscle length were adjusted using the length-tension relation to set the muscle resting length. The sciatic nerve was then stimulated at either 0.5 Hz or 1.0 Hz for 5 minutes at which time the superficial gastrocnemius muscle was excised and immediately freeze clamped in liquid N_2 precooled Wollenberger tongs while still contracting. Muscle samples were stored at -80 °C for later biochemical analyses. Resting muscle samples were collected from the non-stimulated contralateral leg and used for both resting PDH activity and cytochrome c oxidase activity.

4.3.4 [2-14C]-Pyruvate Tracer Solution for PDH Activity Assay

A standard solution of 35 mM pyruvate was made in water and its concentration verified. Briefly, 1 µl of 35 mM pyruvate was added to 0.99 ml of 303 mM TEA, 3.03 mM EDTA, and 10 µl of 25 mM NADH, pH 7.5 at room temperature (RT). Pyruvate concentration was assayed in triplicate utilizing a spectrophotometric lactate dehydrogenase (LDH) assay following consumption of NADH at 340 nm at 25 °C. Baseline absorbance was measured and excess LDH (5-10 U) was added and incubated for 5 minutes or until no absorbance change was present. The pyruvate concentration was then calculated from the change in absorbance from baseline utilizing the extinction coefficient of NADH ($\varepsilon 340 = 6220\ M^{-1}cm^{-1}$) assuming reaction of NADH is 1:1 with pyruvate. 5ml of standardized 35 mM pyruvate solution was then added to 250 µCi [2-^{14}C]-pyruvate sodium salt (specific activity 7.3 mCi/mmol, Perkin Elmer #NEC256) and the final concentration verified using spectrophotometric LDH

assay as described above. Specific activity of the [2-^{14}C]-pyruvate tracer solution was then determined via reaction with glutamate with glutamate pyruvate transaminase (GPT) to form [2-^{14}C]-alanine. This step was performed to determine the fraction of the ^{14}C label that is specific to pyruvate in the tracer solution. In brief, 1 µl of [2-^{14}C]-pyruvate tracer solution was added to 500 µl of 50 mM TEA, 0.5 mM EDTA, and 250 mM glutamate, pH 7.5 at RT. Assays were carried out in duplicate with two negative controls. GPT (~2 U) was then added to initiate the reaction but omitted from negative controls. Reactions were carried out at RT and after 1 hour, 400 µl aliquots were removed and loaded into gravity flow columns containing 1 ml settled volume of anion exchange resin (Bio-Rad AG1x8 resin, 200-400 mesh, Acetate form) contained in a 3 ml syringe with Luer lock stopcock. This resin traps the negatively charged [2-^{14}C]-pyruvate while the positively charged [2-^{14}C]-alanine passes through. Resin was then washed 3 times with 500 µl water and column eluate was collected into 25 ml glass scintillation vials containing 20 ml Safety Solve scintillant and counted using a Packard Tric-Carb liquid scintillation analyzer. Background counts from negative controls were subtracted from sample values to obtain the specific activity (CPM/µmol) of the [2-^{14}C]-pyruvate tracer solution. 100 µl aliquots of the [2-^{14}C]-pyruvate tracer solution were stored at -80 °C until needed.

4.3.5 Homogenization and Assay Buffers for PDH Activity Assay

Homogenization buffer A, for measurement of endogenous PDH activity (PDH_a): 0.05 M Tris-HCL, 0.005 M EGTA, 0.005 M $MgCl_2$-$6H_2O$, 0.05 M KCl, 0.05 M NaF, 0.005 M DCA, 0.1% Triton X-100 with 0.001 M DTT, pH 7.8 on ice. Homogenization buffer B, for measurement of total PDH activity (PDH_t): 0.05 M Tris-HCL, 0.024 M $CaCl_2$-$2H_2O$,

0.005 M $MgCl_2$-$6H_2O$, 0.05 M KCl, 0.005 M DCA, 0.1% Triton X-100 with 0.01 M glucose, 0.001 M DTT, and 5 U/ml hexokinase added fresh before use, pH 7.8 on ice. Assay buffer: 0.12 M Tris-HCl, 0.577 mM Na_2EDTA, 0.001 M $MgCl_2$-$6H_2O$, 0.001 M DCA with 3.86 mM NAD^+, 5.77 mM CoASH, 0.001 M TPP, 0.012 M L-carnitine-HCl, and 0.8 U/ml carnitine acetyltransferase (CAT) added fresh before use, pH 7.8 at 37 °C. For assay of total PDH activity, 2.88 mM NaF was also added to assay buffer.

4.3.6 PDH Activity Assay

PDH activity was determined by a method developed previously by Sterk et al. 2003 with modifications outlined below (122,130). In brief, PDH activity in muscle homogenates was determined by a coupled enzyme assay, following the conversion of the radiolabeled substrate ([2-^{14}C]-pyruvate) to radiolabeled product ([1-^{14}C]-acetylcarnitine):

$$[\mathbf{2\text{-}^{14}C}]\text{-}pyruvate + NAD^+ + CoA \xrightarrow{PDH} [\mathbf{1\text{-}^{14}C}]\text{-}acetyl\text{-}CoA + NADH + CO_2$$

$$[\mathbf{1\text{-}^{14}C}]\text{-}acetyl\text{-}CoA + L\text{-}carnitine \xrightarrow{CAT} [\mathbf{1\text{-}^{14}C}]\text{-}acetylcarnitine + CoA$$

Reaction time points were collected and then passaged through columns containing anion exchange resin allowing for the separation of ^{14}C labeled compounds by trapping the unreacted negatively charged substrate, [2-^{14}C]-pyruvate, while allowing the passage of the positively charged product, [1-^{14}C]-acetylcarnitine, to quantify the reaction rate. Overall reaction rate was limited by the amount of PDH activity as CAT and substrates of the reaction were added in excess. Thus the rate of [1-^{14}C]-acetylcarnitine production was assumed to be 1:1 with [1-^{14}C]-acetyl-CoA production and used to quantify PDH activity in muscle samples. Reactions were carried out in homogenates produced from freeze clamped muscle samples of the superficial

gastrocnemius. Samples were first powdered under liquid nitrogen using mortar and pestle followed by two separate assays for determination of endogenous PDH activity (PDH_a) and total PDH activity (PDH_t). This allows for quantification of fractional PDH activity ($PDH_a/PDH_t = PDH_{\%}$) within the same sample. Approximately 30-50 mg of muscle powder was added to 250µl ice cold homogenization buffer A (PDH_a) and immediately mixed with vigorous shaking. Buffer volume was then adjusted by adding buffer to a final 10% homogenate concentration. Homogenates were then sonicated on ice using Branson sonicator at 20 kc, 3 times for 15 seconds with 15 second breaks in between. Each homogenate was then immediately assayed by adding 15 µl homogenate to 85 µl assay buffer prewarmed to 37 °C and vortexed to mix. Reactions were carried out in triplicate at time points of 0.5, 1, and 1.5 minutes and initiated by the addition of [2-^{14}C]-pyruvate tracer solution to a final concentration of 1mM. [2-^{14}C]-pyruvate tracer was added as a drop on the side of the reaction Eppendorf tube and time points were started by vortexing, mixing the [2-^{14}C]-pyruvate tracer into the assay solution and initiating the reaction. Reaction temperature was maintained at 37 °C for entire duration by means of a heated water bath. Reactions were then quenched at appropriate time points via the addition of 500 µl of ice cold methanol followed by vortexing. Each time point was run separately and quenched samples were stored on ice until the reaction series of that sample was complete. Once the reaction series was completed for PDH_a, the entire process was repeated by producing another muscle homogenate with homogenization buffer B for determination of PDH_t activity. Quenched reaction time points were then loaded into gravity flow columns containing 1ml settled volume of anion exchange resin (Bio-Rad AG1x8 resin, 200-400 mesh, Acetate form)

contained in a 3 ml syringe with Luer lock stopcock. Columns were then washed 3 times with 500 µl water with column eluate collected into 25 ml glass scintillation vials containing 20 ml Safety Solve liquid scintillation cocktail. This process traps the unreacted negatively charged [2-^{14}C]-pyruvate allowing for separation of the positively charged [1-^{14}C]-acetylcarnitine. The radioactivity in each vial was then counted using a Packard Tri-Carb liquid scintillation analyzer and using the specific activity of the tracer solution, the reaction rate was determined for quantification of PDH activity.

4.3.7 Cytochrome C Oxidase Assay

A 1 mM solution of reduced cytochrome c solution was produced and stored at -20 °C following the method of Spinazzi et. al. 2012 with minor modification (126). In brief, 110 mg of ascorbic acid was dissolved in 1 ml of 10 mM potassium phosphate buffer (pH 7.0) and titrated to pH 6.5-6.8 with tris-HCl powder. Next, 250 mg of cytochrome c was dissolved in 1.2 ml 10 mM potassium phosphate buffer (pH 7.0), followed by the addition of 0.3 ml of ascorbic acid solution to make a 13.5 mM cytochrome c solution. The mixture was incubated with stirring at 4 °C for 1 hour resulting in a color shift from brown to pink-orange. The solution was then added to dialysis tubing (3500 kD cutoff) and dialyzed against 500 ml 10 mM KH_2PO_4 for 1 hour at room temperature with gentle stirring. After changing out the dialysis buffer this process was repeated and finally dialyzed a third time overnight at 4 °C. The cytochrome c solution was removed from the dialysis tubing into another vessel and the tubing was rinsed 3 times with 1.5 ml 10 mM KH_2PO_4 and added to cytochrome c solution. The concentration, percent reduction, and auto reduction rate of the cytochrome c solution was verified utilizing spectrophotometric absorbance at 550 nm

using the extinction coefficient of 29,500 $M^{-1}cm^{-1}$. Muscle samples were assayed for determination cytochrome c oxidase activity following the method of Spinazzi et al. 2012 (126). Muscle samples were freshly powdered under liquid N_2 using mortar and pestle immediately prior to the assay. Muscle powder was added to ice cold homogenization buffer (100 mM Tris-HCl, 1% Triton X-100, pH 7.0) at a final dilution of 1:100 and mixed by inversion at 4 °C for 5 minutes before being placed on ice. For a 1 ml cuvette, 60 ul of 1 mM reduced cytochrome c solution was added to 500 ul 100 mM KH_2PO_4 (pH 7.0 at 37 °C) and 400 ul water. Cuvettes were placed into spectrophotometer preheated to 37 °C and absorption rate was recorded for 3 minutes at 550 nm. Reactions were initiated by the addition of 40 ul 1:100 muscle homogenates and rates recorded for 5 minutes. The initial linear reaction rate was used for calculation of cytochrome c oxidase activity using the molar extinction coefficient for cytochrome c at 550 nm. Muscle homogenates were assayed in triplicate and activities normalized to the muscle wet weight.

4.3.8 Immunoblot Analyses

Muscle samples previously collected and freeze-clamped in liquid N_2 were powdered under liquid nitrogen. Muscle powder was homogenized in 9 volumes of ice cold RIPA buffer (10 mM Tris-HCl, 1 mM EDTA, 0.5 mM EGTA, 1% Triton X-100, 0.1% SDS, 140 mM NaCl, pH 8.0) containing protease inhibitor (SIGMAFAST, Sigma Aldrich) and sonicated on ice 3 times for 15 seconds with 15 second breaks in between. Homogenate protein concentration was determined spectrophotometrically with BCA assay (Sigma Aldrich) and final concentration diluted to 2 ug/ul with RIPA buffer and 4x loading buffer (250 mM Tris-HCl, 0.008% Bromophenol Blue, 40% glycerol, 8% SDS,

20% 2-Mercaptoethanol) diluted to 1x final concentration. 20 ug of protein were loaded to 10% polyacrylamide gels, separated via SDS page at 110 V, and transferred at 4 °C at 110 V for 1 hour 15 minutes to PVDF membrane (Immobilon-P, Millipore). Membranes were washed for 25 minutes in TBS buffer (50 mM Tris-HCl, 150 mM NaCl, pH 7.6) followed by blocking in TBST (TBS plus 0.1% Tween-20) with 5% non-fat milk (w/v) for 1 hour at RT. Primary antibodies for anti PDK2 (mouse monoclonal, sc-100534, Santa Cruz Biotechnology, 46kDa), anti-PDK4 (rabbit polyclonal, ab89295, Abcam, 46kDa), and anti-PDP1 (rabbit monoclonal, 65575S, Cell Signaling Technology, 55kDa) were added individually to blocking buffer at 1:1000 dilution and incubated with PVDF membranes overnight with mixing at 4 °C. Membranes were then washed 3 times for 5 minutes in 25 ml TBST buffer and incubated with goat anti-mouse (1:15,000, 926-32351, Licor) or goat anti-rabbit (1:20,000, 925-68021, Licor) fluorescent secondary antibody diluted in blocking buffer with 0.01% SDS for 1 hour at RT with gentile agitation. Membranes were washed 3 times for 5 minutes in TBST buffer and exposed with Licor Odyssey classic at 700 nm or 800 nm channels. Band molecular weight was verified by co-separation and transfer with protein standard (Precision Plus Dual Color, Biorad) and band intensities were quantified with Odyssey software version 3.0. Band intensities were normalized to total lane protein detected by SWIFT protein stain (G-Biosciences) and quantified by blot scanning and Image-J (180) analysis.

4.3.9 Statistics

All data are reported as means ± SE. Comparisons of group means were by two tailed Student's *t*-test at the $p < 0.05$ level of significance.

4.4 Results

Animal Biometrics, Mitochondrial Density, and OGTT. 17 week old control Wistar (n=8) and type 2 diabetic Goto-Kakizaki (GK) (n=8) rats were used for this study. Animal biometrics at the date of study are presented in Table 7. Fasting blood glucose and plasma FFA were significantly increased in the GK rat when compared to age matched controls however plasma insulin concentration was similar between groups (Table 7). The calculated HOMA-IR score, a measure of insulin resistance (179), was significantly increased in the GK rat compared to Wistar controls and agrees with the significant elevation in blood glucose found after oral glucose tolerance testing (Table 7, Fig. 24). After oral glucose delivery, both Wistar control and GK rats exhibited a peak in blood glucose concentration at 30 minutes. Wistar rats blood glucose values returned to fasting values within 120 minutes however, GK rat values were 2 to 3-fold higher than controls and remained elevated for over 120 minutes and did not return to fasting levels confirming type 2 diabetic condition in these animals (Fig. 24A). The glycemic response between the two groups to oral glucose challenge was quantified as the area under the curve (AUC) of blood glucose concentration versus time. GK rats had a 3-fold increase in AUC relative to Wistar controls confirming type 2 diabetes (Fig. 24B).

GK rats had significantly lower body and muscle weights compared to non-diabetic Wistar controls (Table 7). Normalization of muscle weight to total body weight did not correct for reduced muscle weights in the GK rat which displayed significant reductions in the muscle weight to body weight ratio (Table 7). Mitochondrial density, estimated using cytochrome c oxidase activity in whole muscle lysates, was reduced by 19% in the superficial gastrocnemius muscle of the GK rat relative to controls (Table 7).

Muscle Force Production and Twitch Mechanics. Wistar and GK rats were subjected to either 0.5 Hz (n=4) or 1.0 Hz (n=4) twitch stimulation of the posterior leg muscles (gastrocnemius, plantaris, soleus) prior to sampling of the superficial gastrocnemius for PDH activity. A representative force trace of 1.0 Hz stimulation in the Wistar and GK rat is presented in Figure 25. Group averaged twitch peak force, specific force, and tension time integral (TTI) from the entire 5 minute stimulation is summarized in Table 8. Peak force was significantly greater in Wistar controls and was attributed to the larger muscle mass compared to the GK rats as the specific force, peak force normalized to muscle weight, was similar between groups at 0.5 Hz but slightly greater in GK rats at 1.0 Hz stimulation intensity. The TTI, the measure of total workload performed per twitch, was similar between groups at each stimulation intensity tested.

Muscle PDH Activity. PDH activity was determined in superficial gastrocnemius samples taken at rest (n=4) or during stimulation at either 0.5 Hz (n=4) or 1.0 Hz (n=4) intensities in Wistar and GK rats. PDH activity was measured under two separate buffer conditions that clamped the PDH phosphorylation state giving the active fraction of PDH, PDH active (PDH_a), and the completely dephosphorylated maximally activated enzyme activity, PDH total (PDH_t). Normalization of PDH_a to total PDH activity (PDH_t) yields the fractional, or percent active fraction of PDH (PDH%). PDH activity assay data is shown in Figure 23 for superficial gastrocnemius muscle collected at rest and during stimulation at either 0.5Hz or 1.0Hz intensity in Wistar control (Fig. 23A) and GK (Fig. 23B) rats. Total PDH activity (PDH_t) was similar between groups from muscle sampled during 0.5Hz and 1.0Hz stimulation however was significantly reduced in GK rats in muscle sampled at rest (Fig. 26A). PDH active (PDH_a) was similar between groups

irrespective of sampling condition (Fig. 26B). However the fractional PDH activity ($PDH_{\%}$), PDH_a expressed as a percent of PDH_t, was significantly increased in GK rats both at rest and during 0.5 Hz stimulation however was similar to control Wistar rats at 1.0 Hz stimulation intensity (Fig. 26C).

Western Blot. Immunoblot analysis was performed on resting superficial gastrocnemius muscle samples collected from Wistar control (n=4) and GK (n=4) rats. In whole muscle lysates, the protein expression of PDK2 (Fig. 27A) and PDP1 (Fig. 27C) were significantly reduced in GK rats by 1.7 and 1.3-fold respectively with no significant difference found in PDK4 expression when compared to Wistar controls (Fig. 27B). However, normalizing to the total PDH activity (PDH_t) of each respective sample did alter relative expression levels. PDK2 expression was still significantly reduced in GK rats however the fold change was decreased compared to whole muscle lysate values (1.7 vs 1.2, Fig. 27D). Furthermore, correcting band intensities to PDH_t normalized PDP1 expression between groups (Fig. 27F) but resulted in a significant increase in the relative PDK4 expression in GK rats when compared to Wistar controls (Fig. 27E).

Table 7. *Animal metrics and superficial gastrocnemius muscle mitochondrial density in Wistar control and GK rats.* Blood glucose measured from whole blood samples collected from the tail vein of overnight fasted anesthetized rats. Muscle weight was determined from the entire posterior leg including gastrocnemius, plantaris, and soleus muscles. Cytochrome c oxidase activity was measured in freeze clamped superficial gastrocnemius muscle collected in the resting state from anesthetized rats as described in the methods section. Values are means ± SE. *Significant difference between Wistar control and GK rats ($p<0.05$) by two tailed Students *t*-test. U, µmol cytochrome c oxidized per minute. gWW, gram muscle wet weight.

	Control	GK
n	8	8
Blood Glucose (mg/dl)	81.3±5.0	194±23.2*
Blood Free Fatty Acids (mEq/l)	0.55±0.03	0.74±0.04*
Blood Insulin (mU/l)	41.8±11.9	36.4±7.6
HOMA-IR	9.1±3.1	16.1±2.5*
Body Weight (g)	506±7	347±12*
Muscle Weight (g)	3.6±0.07	2.0±0.06*
MW/BW (%)	0.71±0.02	0.57±0.02*
Cytochrome C Oxidase Activity (U/gWW)	12.9±0.7	10.4±0.4*

Table 8. *Muscle force and twitch mechanics in Wistar control and GK rats.* Muscle twitch contractile intensity was induced and controlled via direct sciatic nerve stimulation resulting in the contraction of the entire posterior compartment of the leg (gastrocnemius, plantaris, soleus) at 0.5Hz or 1.0Hz intensity. Maximal force was produced by ensuring optimal muscle length and stimulation voltage with the knee fixed in place and force transduced to a strain gauge connected to the Achilles tendon by silk suture. Values are means ± SE. *Significant difference between Wistar control and GK rats ($p<0.05$) by two tailed Students *t*-test. TTI, tension time integral. MW, muscle weight.

	0.5Hz		1.0Hz	
	Control (n=4)	GK (n=4)	Control (n=4)	GK (n=4)
Peak Force (g)	711±41	439±11*	680±32	464±30*
Peak Force/MW	204±9	218±6	183±11	246±23*
Tension Time Integral (g*s)	39.4±3.0	48.5±6.9	41.4±3.8	42.6±3.2

Figure 23. Representative radioisotopic PDH activity assay in superficial gastrocnemius muscle samples from control Wistar and GK rats.

Muscle samples from control Wistar (A) and GK (B) rats were collected at rest or during stimulation at 0.5 or 1.0 Hz. Individual samples were assayed in triplicate for active (PDH_a) and total (PDH_t) PDH activity at three time points as outlined in methods, with group averaged time points displayed here for PDH_a. Total PDH (PDH_t) presented here is the average total activity from rest, 0.5 and 1.0 Hz stimulation conditions. The rate of pyruvate oxidation (µ/min) was normalized to muscle wet weight to determine the specific activity (U/gWW) of individual samples. Values are means ± SE for each time point, n=4 for both groups at each condition tested. gWW, gram muscle wet weight.

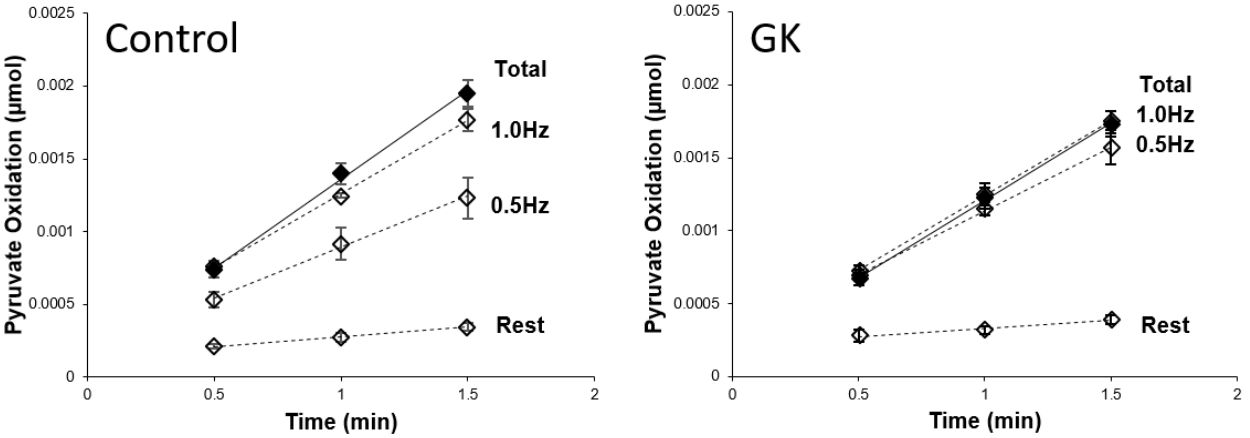

Figure 24. GK rats display impaired glycemic control to oral glucose challenge. Oral glucose tolerance test (OGTT, A) and area under the OGTT curve (AUC, B) for control Wistar (n=3) and GK (n=8) rats. Glucose load was delivered via oral gavage to overnight fasted rats and blood sampled for glucose concentration through tail vein prick as outlined in methods. Values are means ± SE. *Significantly different from control Wistar ($p<0.05$). Significance determined by two tailed Students *t*-test.

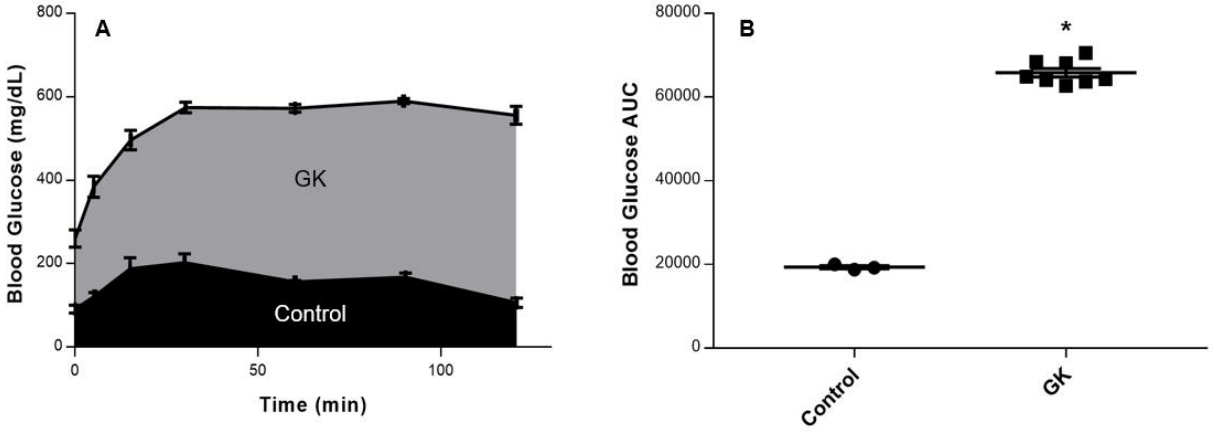

Figure 25. Representative muscle twitch force trace for a control Wistar and GK rat.

Displayed are 10 muscle twitches during 1.0Hz stimulation in a control Wistar (A) and GK (B) rat. Force is expressed as percent of initial twitch force at the start of the contraction series.

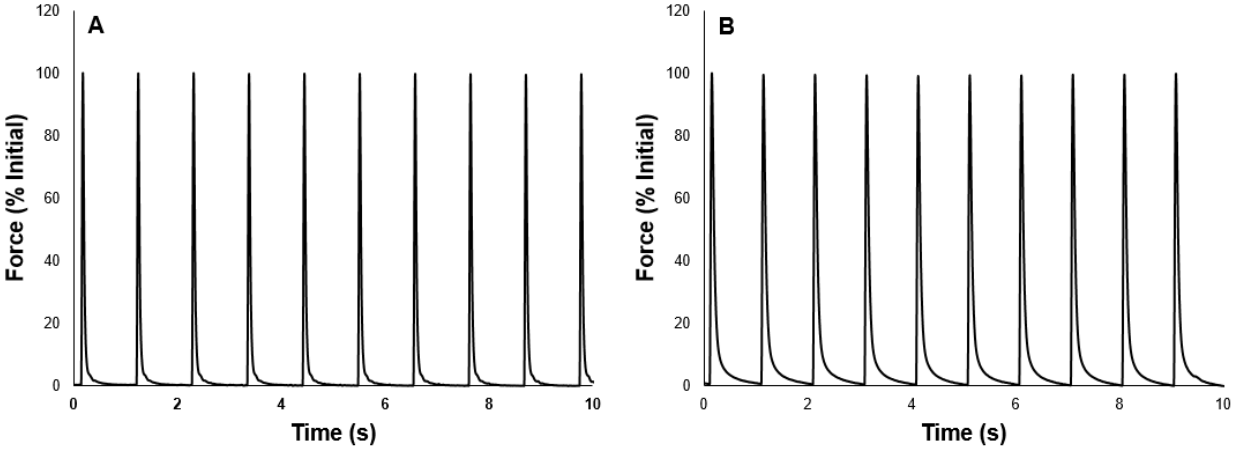

Figure 26. Percent PDH activity is increased in skeletal muscle of the type 2 diabetic GK rat.

PDH activity of the superficial gastrocnemius muscle at rest (n=4) and during stimulation at 0.5Hz (n=4) or 1.0Hz (n=4) intensity in control Wistar and GK rats. *A:* Total PDH activity (PDHt) in muscle samples elicited through tissue homogenization in buffer designed to dephosphorylate and activate PDH complex through selective inhibition of PDK activity and stimulation of PDP activity as outlined in methods. *B:* Active PDH activity (PDH_a) in muscle samples elicited through tissue homogenization in buffer designed to clamp PDH phosphorylation state through inhibition of both PDK and PDP activity. *C:* Fractional PDH activity ($PDH_{\%}$) determined by the ratio of PDH_a/PDH_t. Values are means ± SE. *Significantly different from control Wistar of the same condition ($p<0.05$). Significance determined by two tailed Students *t*-test.

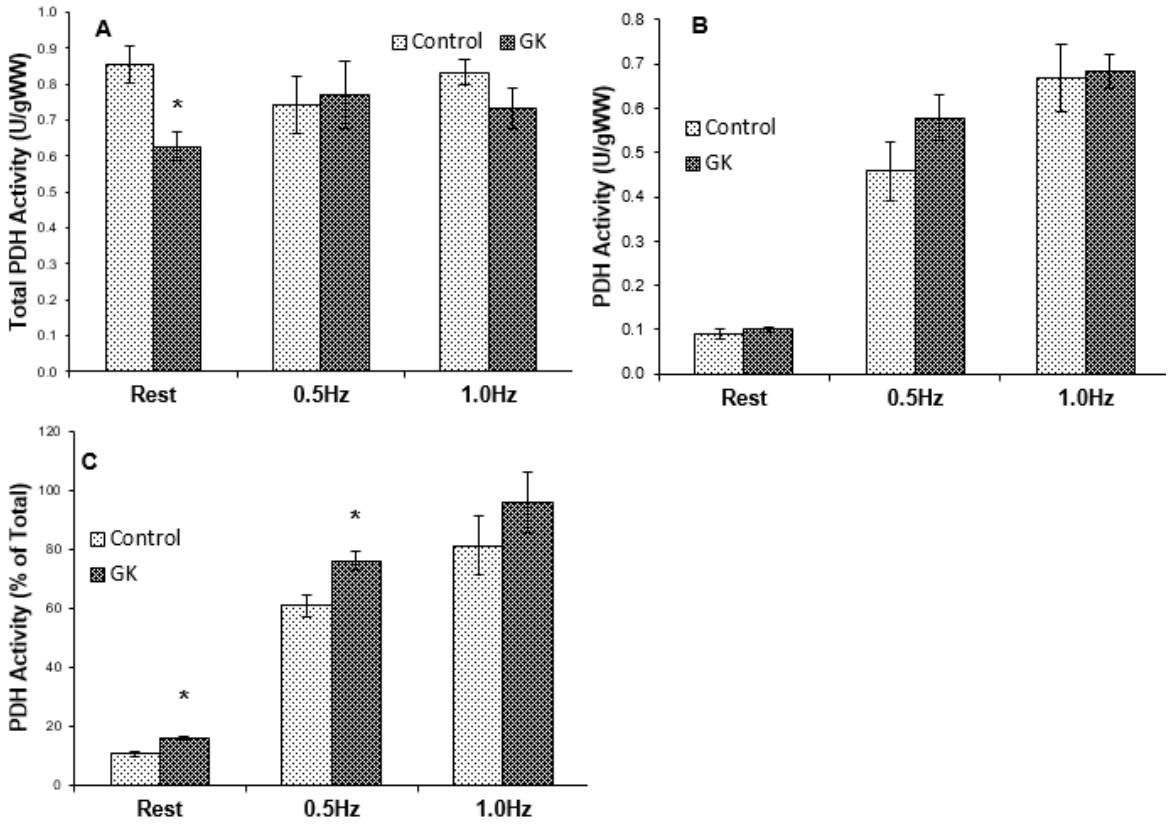

Figure 27. Differential expression of regulatory enzymes of PDH activity in skeletal muscle of the type 2 diabetic GK rat.

Western blot detection of PDK2, PDK4, and PDP1 expression in resting superficial gastrocnemius muscle samples from control Wistar (n=4) and GK (n=4) rats. Equal protein amount was loaded for each sample and band intensities were normalized to total lane protein as described in methods. Images of sample blot detection are displayed over corresponding data panels. Panels *A-C* depict expression data in whole muscle lysates. Panels *D-F* depict whole muscle lysate expression data normalized to total PDH activity (PDH_t) of each respective sample. Bars represent group means ± SE. *Significantly different from control Wistar ($p<0.05$). Significance determined by two tailed Students *t*-test.

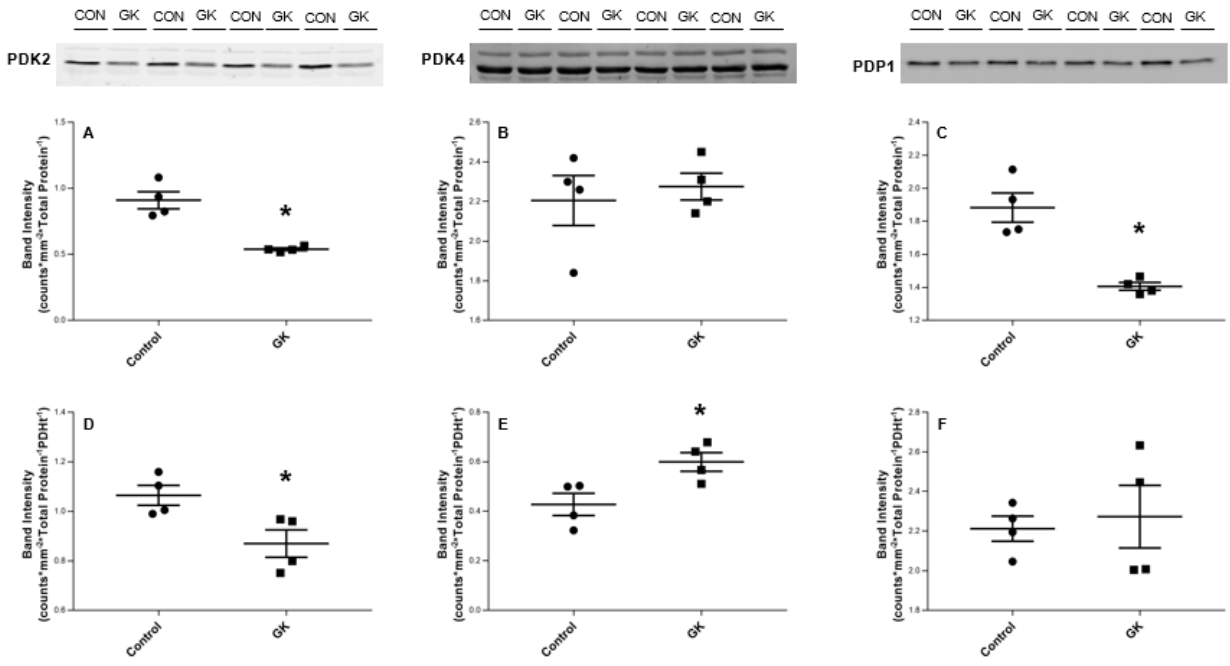

4.5 Discussion

This investigation determined the effect of type 2 diabetes on regulation of rat skeletal muscle PDH activity in both resting and actively contracting muscle. The main outcome of this study was that PDH fractional activity ($PDH_{\%}$) is increased in skeletal muscle of the type 2 diabetic Goto Kakizaki (GK) rat relative to non-diabetic Wistar controls. This increase in activity was apparent in fasted muscle at rest and during active contraction at submaximal intensity. However, at the maximum contractile intensity tested no differences were found in PDH activity between diabetic and control muscle. Protein expression levels of the regulatory enzymes of PDH were altered in skeletal muscle of the GK rat. PDK2 and PDP1 levels were decreased but the level of PDK4 remained unchanged in whole muscle lysates compared to Wistar controls. However, normalization of protein expression levels to total PDH activity in muscle samples resulted in similar PDP1 levels yet increased PDK4 while PDK2 remained depressed in GK rats. Differences in the GK rat are likely attributed to overt diabetes in these animals which displayed significant elevations in fasting blood glucose and plasma FFA but normal plasma insulin levels. The combined effect of fasting hyperglycemia with normal insulin levels was used to calculate the HOMA-IR score (an index of insulin resistance). The score for GK rats was significantly increased relative to controls and together with the 3-fold elevation in blood glucose after an oral glucose challenge reinforce the use of the GK rat as a model of type 2 diabetes. Nevertheless, in the GK rat fractional PDH activities were higher than expected based on reports in the literature in other diabetic rodent models and we propose this is due to mitochondrial density together with the associated hyperglycemia of the GK rat.

The magnitude of PDH activation in skeletal muscle determines the capacity for oxidative glucose disposal (32,33,49,53,56). In the current study, the fractional PDH activity ($PDH_{\%}$) was significantly elevated in type 2 diabetic GK rats relative to their Wistar controls (Fig. 26C). $PDH_{\%}$ values of control resting gastrocnemius muscle are consistent with that found in earlier studies of non-diabetic rat skeletal muscle at rest (44,59,101) but not with that of animal models of type 1 and type 2 diabetes presumably because the relative mitochondrial densities were not determined. Early studies of type 1 diabetic rat models utilizing either high dose streptozotocin or alloxan treatment consistently resulted in decreased resting rat skeletal muscle PDH activity (PDH_a, $PDH_{\%}$) of ~40-70% compared to non-diabetic controls (44,59,81,101). Decreased PDH activity was also seen in rat models of type 2 diabetes where reductions of 30% and 70% were observed in resting skeletal muscle of the Zucker Diabetic Fatty rat (ZDF) and the Otsaku Long Evans Tokushima Fatty rat (OLETF) respectively (102,103). In previous studies this effect has been attributed to selective alteration in the expression levels of PDK versus PDP due to insulin resistance, resulting in a shift in relative activities that increases steady state phosphorylation status and reduces the activity of PDH.

Expression of PDK4 is the most sensitive to alterations in the metabolic or hormonal status of the muscle fiber. PDK4 expression is upregulated in starvation (181,182), high fat diet (57), and with loss of insulin signaling in type 1 or type 2 diabetes (98,102,103,113,176). PDK4 is thought to be the primary reason for reductions in PDH activity seen in diabetic rodent models as PDP1 (58,59) and PDK2 (174,175) expression levels are relatively stable to metabolic perturbation however some changes

in PDK2 with diabetes have also been observed (98,102). In the type 2 diabetic GK rat, PDK2 and PDP1 expression levels were reduced in whole muscle lysates and PDK4 expression was similar to non-diabetic controls. These results are incongruent with previous studies from diabetic rat skeletal muscle. One possible explanation for this may reside in the relative mitochondrial volumes in control and diabetic animals.

In the present study diabetic muscle had a reduced mitochondrial content when assayed by cytochrome c oxidase activity. Previous studies have shown that expression and activity of PDK and PDP isoforms are related to mitochondrial density (93,94). Normalization to cytochrome c oxidase activity (data not shown) or total PDH activity resulted in similar expression of PDP1 and increased PDK4, whereas PDK2 remained reduced compared to Wistar controls. The elevation of PDK4 expression might be attributed to both insulin resistance and a significant elevation of fasting plasma FFA levels (99,174,175). It is unclear why PDK2 levels are reduced in the type 2 diabetic GK rat. It has been shown that expression levels are insensitive to acute alteration of insulin or FFA (174,175). Therefore expression is likely regulated by a different mechanism than PDK4 and may also be strain specific. Furthermore, it is unknown how differential expression of PDK2 versus PDK4 may affect PDH activation *in vivo.* Whole body knockout studies in mice suggests PDK4 plays a larger role in regulation of skeletal muscle PDH activity in the fasted state and PDK2 in regulating activity in the fed state (183). In contrast to the observed fractional activity and based on the changes in expression of the regulatory enzymes relative to total PDH activity, one might expect reduced PDH activity due to the increased PDK4 expression. However, the relationship between altered expression and *in vivo* activities of PDK or PDP have not been

determined so it is impossible to say how changes in expression levels may affect steady state PDH activity. Nevertheless, fractional PDH activity ($PDH_{\%}$) was increased in resting skeletal muscle of the GK rat and may be related to hyperglycemia or reduced mitochondrial density.

Although $PDH_{\%}$ results from this study are incongruent with previous work in type 1 or type 2 diabetic rat skeletal muscle (44,59,81,101–103), the current data is consistent with PDH activity and rates of glucose oxidation reported in post-absorptive human type 2 diabetic skeletal muscle (106,106,184). In resting human type 2 diabetic vastus lateralis muscle, PDH_a was similar to control subjects yet had elevated $PDH_{\%}$ with a 1.5-fold increase in leg glucose oxidation quantified by arterio-venous (A-V) difference (106). Similarly, in a separate work post-absorptive leg glucose oxidation was 2-fold greater in type 2 diabetic humans than controls suggesting elevated basal PDH activity (40). This effect has not been observed in all studies of human type 2 diabetic skeletal muscle with some showing similar rates of glucose oxidation as well as PDH_a and $PDH_{\%}$ when compared to non-diabetic controls (104,184). Nevertheless, PDH activity has not been found to be reduced in type 2 diabetic human skeletal muscle even though they exhibit similar increases in PDK2 and PDK4 mRNA expression as that seen in rodent models of the disease (102,113). This suggests that the regulation of PDK activity is more complex *in vivo* than simply relying on increases in expression levels might indicate with some studies suggesting a role of hyperglycemia in stimulating PDH activity even where PDK expression is upregulated (106).

Hyperglycemia stimulates PDH activity and glucose oxidation independent of insulin signaling in normal skeletal muscle (67) and may be the mechanism for

increased glucose oxidation and PDH activity with hyperglycemia in type 2 diabetes. In normal insulin sensitive humans, hyperglycemic clamp without alteration of blood insulin or FFA levels resulted in a 1.7 fold increase in leg glucose oxidation and a corresponding 1.8 fold increase in PDH_a and 14% increase in $PDH_{\%}$ (49) indicating glucose oxidation is tightly tied to PDH activation status. Furthermore, in type 2 diabetic subjects, normalization of blood glucose from 11.0 to 5.6 mM with overnight low dose insulin treatment (4-12 $mU*m^{-2}*min^{-1}$) significantly reduced PDH_a by 70% in fasted skeletal muscle suggesting hyperglycemia can override the inhibitory effects of PDK activity (106). This is likely due to mass action effects of increased blood glucose resulting in elevated glucose uptake and glycolytic flux, stimulating pyruvate production and inhibiting PDK activity even where expression levels are elevated. This is a possible mechanism that could explain the elevated or normal PDH activity found in this study and others with increased PDK expression in resting post-absorptive type 2 diabetic skeletal muscle and may also explain elevations in PDH activity found during muscle stimulation.

Given the critical importance of regulation of PDH activity in oxidative glucose disposal, it is surprising that so few studies have investigated the effect of exercise on substrate disposal in type 2 diabetes and to our knowledge that none have investigated regulation of skeletal muscle PDH activity in the disease during exercise. In healthy human subjects PDH activity reaches steady state levels within 15s of exercise initiation with the magnitude of activation linearly related to exercise intensity until the muscle aerobic capacity (maximal mitochondrial ATP synthesis flux) is reached (24,63). Glucose oxidation parallels these increases in PDH activity and reaches a maximum

near the aerobic capacity (22,23). In this study, PDH activity in both the GK and Wistar rat increased as a function of exercise intensity with a significant elevation in $PDH_{\%}$ at 0.5 Hz stimulation in the GK rat compared to the non-diabetic Wistar controls. At 1.0 Hz intensity of stimulation, corresponding to the reported mitochondrial capacity for the rat hindlimb (116), no difference in PDH activity was found as $PDH_{\%}$ approached a maximum in both groups. However, the result is quite different in animal models of type 1 diabetes. Chemically-induced type 1 diabetes reduces PDH activity in gastrocnemius muscle relative to non-diabetic controls at 5.0 Hz and 10.0 Hz intensities (44,101) but these stimulations vastly exceed the oxidative capacity of the rat hindlimb and additionally, muscle performance was not measured. In contrast, the current study sought to stimulate the muscle below and up to the reported aerobic maximum where dynamic changes in PDH activation and glucose oxidation are known to occur. Furthermore and unlike previous studies, force production was carefully measured so the metabolic load could be accounted for when interpreting changes in PDH activity.

The increased $PDH_{\%}$ of the GK rat found in this study during muscle stimulation within the aerobic range cannot be attributed to changes in muscle force production and is likely related to hyperglycemia or reduced mitochondrial density. It has previously been shown that hyperglycemia can stimulate glucose oxidation during voluntary aerobic exercise in non-diabetic dogs, where limb glucose oxidation increased linearly as a function of blood glucose concentration with saturating effects occurring above 8.3 mM (69). This occurred without alteration in plasma insulin or limb lactate production and suggests a direct stimulatory effect of hyperglycemia on PDH activity and the increase in glucose oxidation during exercise (69). This effect has also been observed

in humans where increasing blood glucose from 4.2 to 10.8 mM through acute intravenous glucose infusion resulted in a 40% increase in glucose oxidation after 2 hours of aerobic exercise compared to euglycemic controls (68). Fasting blood glucose of the GK rat was double that of Wistar controls and may be responsible for increased PDH activation in the GK rat at 0.5 Hz stimulation intensity.

However, this effect may also be related to the reduced mitochondrial density of the GK rat which displayed a 20% reduction in muscle cytochrome c oxidase activity compared to Wistar controls. At similar absolute workloads, muscle with lower mitochondrial density preferentially oxidizes glucose over fatty acids (124,185). This is attributable to the reduced mitochondrial sensitivity to metabolic demand which results in depressed steady state energetics at absolute workloads (95). This would be expected to increase the signals driving PDK inhibition and result in enhanced PDH activation (84). Regardless of whether PDH activity is stimulated by elevated glucose or increased workload relative to mitochondrial density, these data are consistent with the increased (107,108) or similar (109–112) rates of glucose oxidation in type 2 diabetic skeletal muscle during aerobic exercise and are not consistent with reduced PDH activity found during exercise in animal models of type 1 diabetes (44,101).

In conclusion, PDH activity is upregulated in type 2 diabetic GK rat skeletal muscle at rest and during muscle contraction below the maximal aerobic capacity. This effect is attributed to the stimulatory effects of hyperglycemia on resting skeletal muscle PDH activity and may be due to hyperglycemia or reduced mitochondrial density during muscle contraction. It is unclear how differential regulation of PDK2 and PDK4 protein expression may play a role in PDH activation during exercise but are clearly important in

resting muscle. In any case, upregulation of PDH activity reported in this study is consistent with results from previous studies in human type 2 diabetic skeletal muscle (104,106,184) however, further study during exercise is needed to elucidate the mechanisms of PDH regulation in metabolic disease.

Chapter 5. Summary

This dissertation provides insight into the integrated nature of the regulation of pyruvate dehydrogenase (PDH) and skeletal muscle metabolic demand over a broad range of physiologic function. This body of work provides a useful framework for future studies and clarifies the mechanisms of PDH regulation that may explain changes in substrate oxidation in skeletal muscle with training/detraining and in metabolic diseases such as type 2 diabetes. Below is a summary of the main findings and a description of potential future directions this work has generated.

In chapter 1, regulation of PDH activity was investigated by taking advantage of the known effects of altered mitochondrial density on the relationship between muscle workload and steady state energetics, or the work-cost relation (95). By reducing mitochondrial density in one group of rats, the metabolic effects of muscle contraction on the regulation of PDH activity was separated from the associated Ca^{2+} load during twitch contractions. In doing this, two apparent effects were observed. First, it was evident that steady state energetics and metabolic fluxes scaled as a function of mitochondrial density relative to the cost of contraction. This has been proposed in studies performed by other investigators (95,118,140) but has not been directly demonstrated as presented in this dissertation. In doing so, a conserved relationship is revealed in which the mechanisms and sources of ATP synthesis are similar for a given metabolic demand when the mitochondrial capacity is taken into account quantitatively. Second, this work revealed that the apparent scaling of the work-cost relationship extends to pathways that regulate mitochondrial substrate selection through the activation of PDH. This provides a satisfactory result as the metabolic demand is met to

a similar extent by increases in substrate supply. Furthermore, this suggests that when workload is normalized to mitochondrial ATP synthesis capacity, a predictable pattern of substrate selection between glucose and fatty acids will emerge.

However, this work fell short of quantifying rates of skeletal muscle substrate utilization by direct measure and therefore the inferences derived from the experiments performed with PDH regulation would need to be confirmed in future studies. Furthermore, this work contradicts the observed effect of increased rates of fatty acid oxidation at relative workloads with exercise training (89,125). A potential reason for this may be in the mode of exercise or the type and extent of muscle contraction. Here, we have removed nervous system control of muscle contraction by directly stimulating the motor neuron, eliciting uniform muscle fiber recruitment at controllable rates and duration. In contrast, voluntary exercise is completely reliant on central nervous system control with variable patterns of muscle fiber recruitment and modes of contraction. Thus the ability to scale substrate selection as suggested in this work by electrical stimulation of muscle may not precisely translate to an exercise trained individual undergoing voluntary exercise. However this remains to be experimentally confirmed. It may be that these individuals exhibit fiber recruitment patterns that may be entirely different from their sedentary counterparts which could not be rigorously controlled in this study but could explain changes in substrate oxidation at relative workloads. Currently, fiber recruitment data of this resolution is not available however it would be entirely possible to electrically stimulate the muscle of a trained versus sedentary human and sample substrate oxidation and muscle fibers for PDH activity. If a similar relationship between metabolic demand, mitochondrial density, and PDH regulation

could be determined it would confirm the work of this study and others, and also provide a mechanism for how changes in substrate oxidation occur during voluntary exercise with training/detraining in humans.

In chapter 2, the effect of increased PDH activity on the bioenergetic response to muscle contraction was quantified. This study quantitatively defined the role of PDH activation, which occurs as a function of exercise intensity, in the regulation of muscle energetics during contraction. Enhancing PDH activation at a given workload results in a more favorable energetic status and may even improve or extend muscle functional capacity when pushed to maximal workloads. Conversely, reducing PDH activation would be expected to have the opposite effect, and may even explain exercise intolerance in diseases where reduced PDH activity has been reported. This effect was attributed to the modulation of mitochondrial redox status by increasing pyruvate decarboxylation and the production rate of NADH. However, these effects were not quantified therefore the relationship between mitochondrial redox state and the cytosolic free energy of ATP hydrolysis (ΔG_{ATP}) that it can sustain were not be determined. In future works, the relationship between mitochondrial substrate selection, redox state, and ΔG_{ATP} could be investigated in isolated mitochondria. Koretsky et al. 1987 (150) contributed significant work in this area however did not extend their investigation skeletal muscle. Whether similar results could be found with ketone bodies (β-hydroxybuterate acetoacetate) or fatty acids could be investigated in an isolated system or even *in vivo* as described here. By coupling the ^{31}P NMR spectroscopic method to surface fluorometry, unique relationships between matrix redox state and ΔG_{ATP} could be quantified for various mitochondrial substrates. This has application to exercise

performance during high intensity exercise where maintaining ΔG_{ATP} is critical for prolonging muscle function and may also bear significantly on understanding the metabolic limitations in diabetes and metabolic syndrome.

In chapter 3, the effects of type 2 diabetes on the regulation of skeletal muscle PDH activity at rest and during muscle contraction was quantified in the GK rat. To our knowledge, this is the first report of PDH activity in working type 2 diabetic skeletal muscle and adds valuable insight to an understudied metabolic problem. This work contributes to the mere five studies that have investigated regulation of PDH activity in type 2 diabetes where there are divergent opinions on the role of PDH in diabetes because of these contradictory reports. Here it was determined that in fasting skeletal muscle, PDH activity was increased both at rest and during muscle contraction in type 2 diabetes. This challenges previous work in type 2 diabetic rodents which found reduced PDH activity, yet agrees with reports in type 2 diabetic humans where either increased or normal PDH activity has been found concomitant with reciprocal rates of glucose oxidation. In humans, this has been largely attributed to the stimulatory effects of hyperglycemia on PDH activity. In order to test this hypothesis in the current model, GK rats could be treated with low dose insulin until euglycemic and regulation of PDH activity could be reevaluated. These euglycemic clamp experiments are well beyond the scope of the present body of work but taken together with information about the activation status of PDH they would be invaluable in definitively resolving this controversy. Furthermore, no study has quantified regulation of PDH activity during exercise in type 2 diabetic humans and relatively few have quantified muscle substrate

oxidation. Given the important role of exercise in preventing diabetes and improving glycemic control (177), a comprehensive study is certainly needed.

In total, this dissertation has contributed to the understanding of the central role of PDH between mitochondrial substrate selection and regulation of muscle bioenergetics during contraction. This work has also contributed insight into the integration of PDH activity in muscle function both in health and disease. Nevertheless, many questions remain to be answered and investigations to extend our understanding of PDH and its role in muscle physiology remain an exciting area of future research.

REFERENCES

REFERENCES

1. Linn TC, Pettit FH, Reed LJ. Alpha-keto acid dehydrogenase complexes. X. Regulation of the activity of the pyruvate dehydrogenase complex from beef kidney mitochondria by phosphorylation and dephosphorylation. Proc Natl Acad Sci U S A. 1969 Jan;62(1):234–41.

2. Yeaman SJ, Hutcheson ET, Roche TE, Pettit FH, Brown JR, Reed LJ, et al. Sites of phosphorylation on pyruvate dehydrogenase from bovine kidney and heart. Biochemistry (Mosc). 1978 Jun 13;17(12):2364–70.

3. Teague WM, Pettit FH, Yeaman SJ, Reed LJ. Function of phosphorylation sites on pyruvate dehydrogenase. Biochem Biophys Res Commun. 1979 Mar 15;87(1):244–52.

4. Korotchkina LG, Patel MS. Probing the mechanism of inactivation of human pyruvate dehydrogenase by phosphorylation of three sites. J Biol Chem. 2001 Feb 23;276(8):5731–8.

5. Sugden MC, Holness MJ. Therapeutic potential of the mammalian pyruvate dehydrogenase kinases in the prevention of hyperglycaemia. Curr Drug Targets Immune Endocr Metab Disord. 2002 Jul;2(2):151–65.

6. Bowker-Kinley MM, Davis WI, Wu P, Harris RA, Popov KM. Evidence for existence of tissue-specific regulation of the mammalian pyruvate dehydrogenase complex. Biochem J. 1998 Jan 1;329 (Pt 1):191–6.

7. Teague WM, Pettit FH, Wu TL, Silberman SR, Reed LJ. Purification and properties of pyruvate dehydrogenase phosphatase from bovine heart and kidney. Biochemistry (Mosc). 1982 Oct 26;21(22):5585–92.

8. Yang D, Gong X, Yakhnin A, Roche TE. Requirements for the adaptor protein role of dihydrolipoyl acetyltransferase in the up-regulated function of the pyruvate dehydrogenase kinase and pyruvate dehydrogenase phosphatase. J Biol Chem. 1998 Jun 5;273(23):14130–7.

9. Hucho F, Randall DD, Roche TE, Burgett MW, Pelley JW, Reed LJ. -Keto acid dehydrogenase complexes. XVII. Kinetic and regulatory properties of pyruvate dehydrogenase kinase and pyruvate dehydrogenase phosphatase from bovine kidney and heart. Arch Biochem Biophys. 1972 Jul;151(1):328–40.

10. Roche TE, Reed LJ. Monovalent cation requirement for ADP inhibition of pyruvate dehydrogenase kinase. Biochem Biophys Res Commun. 1974 Aug 19;59(4):1341–8.

11. Pettit FH, Pelley JW, Reed LJ. Regulation of pyruvate dehydrogenase kinase and phosphatase by acetyl-CoA/CoA and NADH/NAD ratios. Biochem Biophys Res Commun. 1975 Jul 22;65(2):575–82.

12. Kerbey AL, Randle PJ, Cooper RH, Whitehouse S, Pask HT, Denton RM. Regulation of pyruvate dehydrogenase in rat heart. Mechanism of regulation of proportions of dephosphorylated and phosphorylated enzyme by oxidation of fatty acids and ketone bodies and of effects of diabetes: role of coenzyme A, acetyl-coenzyme A and reduced and oxidized nicotinamide-adenine dinucleotide. Biochem J. 1976 Feb 15;154(2):327–48.

13. Pratt ML, Roche TE. Mechanism of pyruvate inhibition of kidney pyruvate dehydrogenasea kinase and synergistic inhibition by pyruvate and ADP. J Biol Chem. 1979 Aug 10;254(15):7191–6.

14. Ravindran S, Radke GA, Guest JR, Roche TE. Lipoyl domain-based mechanism for the integrated feedback control of the pyruvate dehydrogenase complex by enhancement of pyruvate dehydrogenase kinase activity. J Biol Chem. 1996 Jan 12;271(2):653–62.

15. Constantin-Teodosiu D, Simpson EJ, Greenhaff PL. The importance of pyruvate availability to PDC activation and anaplerosis in human skeletal muscle. Am J Physiol - Endocrinol Metab. 1999 Mar 1;276(3):E472–8.

16. Howlett RA, Heigenhauser GJF, Hultman E, Hollidge-Horvat MG, Spriet LL. Effects of dichloroacetate infusion on human skeletal muscle metabolism at the onset of exercise. Am J Physiol - Endocrinol Metab. 1999 Jul 1;277(1):E18–25.

17. Parolin ML, Spriet LL, Hultman E, Hollidge-Horvat MG, Jones NL, Heigenhauser GJF. Regulation of glycogen phosphorylase and PDH during exercise in human skeletal muscle during hypoxia. Am J Physiol - Endocrinol Metab. 2000 Mar 1;278(3):E522–34.

18. Andres R, Cader G, Zierler KL. THE QUANTITATIVELY MINOR ROLE OF CARBOHYDRATE IN OXIDATIVE METABOLISM BY SKELETAL MUSCLE IN INTACT MAN IN THE BASAL STATE. MEASUREMENTS OF OXYGEN AND GLUCOSE UPTAKE AND CARBON DIOXIDE AND LACTATE PRODUCTION IN THE FOREARM 12. J Clin Invest. 1956 Jun;35(6):671–82.

19. Baltzan MA, Andres R, Cader G, Zierler KL. Heterogeneity of forearm metabolism with special reference to free fatty acids. J Clin Invest. 1962 Jan;41:116–25.

20. Dagenais GR, Tancredi RG, Zierler KL. Free fatty acid oxidation by forearm muscle at rest, and evidence for an intramuscular lipid pool in the human forearm. J Clin Invest. 1976 Aug;58(2):421–31.

21. Péronnet F, Massicotte D. Table of nonprotein respiratory quotient: an update. Can J Sport Sci J Can Sci Sport. 1991 Mar;16(1):23–9.

22. van Loon LJ, Greenhaff PL, Constantin-Teodosiu D, Saris WH, Wagenmakers AJ. The effects of increasing exercise intensity on muscle fuel utilisation in humans. J Physiol. 2001 Oct 1;536(Pt 1):295–304.

23. Romijn JA, Coyle EF, Sidossis LS, Gastaldelli A, Horowitz JF, Endert E, et al. Regulation of endogenous fat and carbohydrate metabolism in relation to exercise intensity and duration. Am J Physiol. 1993 Sep;265(3 Pt 1):E380-391.

24. Howlett RA, Parolin ML, Dyck DJ, Hultman E, Jones NL, Heigenhauser GJF, et al. Regulation of skeletal muscle glycogen phosphorylase and PDH at varying exercise power outputs. Am J Physiol - Regul Integr Comp Physiol. 1998 Aug 1;275(2):R418–25.

25. Whitehouse S, Cooper RH, Randle PJ. Mechanism of activation of pyruvate dehydrogenase by dichloroacetate and other halogenated carboxylic acids. Biochem J. 1974 Sep;141(3):761–74.

26. Small L, Brandon AE, Quek L-E, Krycer JR, James DE, Turner N, et al. Acute activation of pyruvate dehydrogenase increases glucose oxidation in muscle without changing glucose uptake. Am J Physiol Endocrinol Metab. 2018 Aug 1;315(2):E258–66.

27. Parolin ML, Spriet LL, Hultman E, Matsos MP, Hollidge-Horvat MG, Jones NL, et al. Effects of PDH activation by dichloroacetate in human skeletal muscle during exercise in hypoxia. Am J Physiol - Endocrinol Metab. 2000 Oct 1;279(4):E752–61.

28. Savasi I, Evans MK, Heigenhauser GJF, Spriet LL. Skeletal muscle metabolism is unaffected by DCA infusion and hyperoxia after onset of intense aerobic exercise. Am J Physiol - Endocrinol Metab. 2002 Jul 1;283(1):E108–15.

29. Clark AS, Mitch WE, Goodman MN, Fagan JM, Goheer MA, Curnow RT. Dichloroacetate inhibits glycolysis and augments insulin-stimulated glycogen synthesis in rat muscle. J Clin Invest. 1987 Feb;79(2):588–94.

30. McAllister A, Allison SP, Randle PJ. Effects of dichloroacetate on the metabolism of glucose, pyruvate, acetate, 3-hydroxybutyrate and palmitate in rat diaphragm and heart muscle in vitro and on extraction of glucose, lactate, pyruvate and free fatty acids by dog heart in vivo. Biochem J. 1973 Aug;134(4):1067–81.

31. deBoisblanc BP, Meszaros K, Burns A, Bagby GJ, Nelson S, Summer WR. Effect of dichloroacetate on mechanical performance and metabolism of compromised diaphragm muscle. J Appl Physiol Bethesda Md 1985. 1992 Mar;72(3):1149–55.

32. Brown JA, Gore DC. In vivo metabolic response of glucose to dichloroacetate in humans. J Surg Res. 1996 Mar;61(2):391–4.

33. Carraro F, Klein S, Rosenblatt JI, Wolfe RR. Effect of dichloroacetate on lactate concentration in exercising humans. J Appl Physiol Bethesda Md 1985. 1989 Feb;66(2):591–7.

34. Annegers J. Total body water in rats and in mice. Proc Soc Exp Biol Med Soc Exp Biol Med N Y N. 1954 Nov;87(2):454–6.

35. Huang B, Gudi R, Wu P, Harris RA, Hamilton J, Popov KM. Isoenzymes of pyruvate dehydrogenase phosphatase. DNA-derived amino acid sequences, expression, and regulation. J Biol Chem. 1998 Jul 10;273(28):17680–8.

36. Siess EA, Wieland OH. Purification and characterization of pyruvate-dehydrogenase phosphatase from pig-heart muscle. Eur J Biochem. 1972 Mar 15;26(1):96–105.

37. Karpova T, Danchuk S, Kolobova E, Popov KM. Characterization of the isozymes of pyruvate dehydrogenase phosphatase: implications for the regulation of pyruvate dehydrogenase activity. Biochim Biophys Acta. 2003 Dec 1;1652(2):126–35.

38. Goedecke JH, St Clair Gibson A, Grobler L, Collins M, Noakes TD, Lambert EV. Determinants of the variability in respiratory exchange ratio at rest and during exercise in trained athletes. Am J Physiol Endocrinol Metab. 2000 Dec;279(6):E1325-1334.

39. Kelley DE, Reilly JP, Veneman T, Mandarino LJ. Effects of insulin on skeletal muscle glucose storage, oxidation, and glycolysis in humans. Am J Physiol. 1990 Jun;258(6 Pt 1):E923-929.

40. Kelley DE, Simoneau JA. Impaired free fatty acid utilization by skeletal muscle in non-insulin-dependent diabetes mellitus. J Clin Invest. 1994 Dec;94(6):2349–56.

41. Brooks GA, Donovan CM. Effect of endurance training on glucose kinetics during exercise. Am J Physiol. 1983 May;244(5):E505-512.

42. Caterson ID, Fuller SJ, Randle PJ. Effect of the fatty acid oxidation inhibitor 2-tetradecylglycidic acid on pyruvate dehydrogenase complex activity in starved and alloxan-diabetic rats. Biochem J. 1982 Oct 15;208(1):53–60.

43. Hagg SA, Taylor SI, Ruberman NB. Glucose metabolism in perfused skeletal muscle. Pyruvate dehydrogenase activity in starvation, diabetes and exercise. Biochem J. 1976 Aug 15;158(2):203–10.

44. Hennig G, Löffler G, Wieland OH. Active and inactive forms of pyruvatedehydrogenase in skeletal muscle as related to the metabolic and functional state of the muscle cell. FEBS Lett. 1975 Nov 15;59(2):142–5.

45. Mandarino LJ, Wright KS, Verity LS, Nichols J, Bell JM, Kolterman OG, et al. Effects of insulin infusion on human skeletal muscle pyruvate dehydrogenase, phosphofructokinase, and glycogen synthase. Evidence for their role in oxidative and nonoxidative glucose metabolism. J Clin Invest. 1987 Sep;80(3):655–63.

46. Kilgour E, Vernon RG. Tissue-specific changes in the ability of insulin and noradrenaline to activate pyruvate dehydrogenase in vivo during lactation in the rat. Biochem J. 1987 Apr 1;243(1):69–74.

47. Kruszynska YT, McCormack JG. Effect of nutritional status on insulin sensitivity in vivo and tissue enzyme activities in the rat. Biochem J. 1989 Mar 15;258(3):699–707.

48. Kelley DE, Reilly JP, Veneman T, Mandarino LJ. Effects of insulin on skeletal muscle glucose storage, oxidation, and glycolysis in humans. Am J Physiol. 1990 Jun;258(6 Pt 1):E923-929.

49. Mandarino LJ, Consoli A, Jain A, Kelley DE. Differential regulation of intracellular glucose metabolism by glucose and insulin in human muscle. Am J Physiol. 1993 Dec;265(6 Pt 1):E898-905.

50. Thomas AP, Denton RM. Use of toluene-permeabilized mitochondria to study the regulation of adipose tissue pyruvate dehydrogenase in situ. Further evidence that insulin acts through stimulation of pyruvate dehydrogenase phosphate phosphatase. Biochem J. 1986 Aug 15;238(1):93–101.

51. Stellingwerff T, Watt MJ, Heigenhauser GJF, Spriet LL. Effects of reduced free fatty acid availability on skeletal muscle PDH activation during aerobic exercise. Pyruvate dehydrogenase. Am J Physiol Endocrinol Metab. 2003 Mar;284(3):E589-596.

52. Bigrigg JK, Heigenhauser GJF, Inglis JG, LeBlanc PJ, Peters SJ. Carbohydrate refeeding after a high-fat diet rapidly reverses the adaptive increase in human skeletal muscle PDH kinase activity. Am J Physiol Regul Integr Comp Physiol. 2009 Sep;297(3):R885-891.

53. Putman CT, Spriet LL, Hultman E, Lindinger MI, Lands LC, McKelvie RS, et al. Pyruvate dehydrogenase activity and acetyl group accumulation during exercise after different diets. Am J Physiol - Endocrinol Metab. 1993 Nov 1;265(5):E752–60.

54. St Amand TA, Spriet LL, Jones NL, Heigenhauser GJ. Pyruvate overrides inhibition of PDH during exercise after a low-carbohydrate diet. Am J Physiol Endocrinol Metab. 2000 Aug;279(2):E275-283.

55. Pehleman TL, Peters SJ, Heigenhauser GJF, Spriet LL. Enzymatic regulation of glucose disposal in human skeletal muscle after a high-fat, low-carbohydrate diet. J Appl Physiol Bethesda Md 1985. 2005 Jan;98(1):100–7.

56. Roepstorff C, Halberg N, Hillig T, Saha AK, Ruderman NB, Wojtaszewski JFP, et al. Malonyl-CoA and carnitine in regulation of fat oxidation in human skeletal muscle during exercise. Am J Physiol Endocrinol Metab. 2005 Jan;288(1):E133-142.

57. Peters SJ, Harris RA, Wu P, Pehleman TL, Heigenhauser GJ, Spriet LL. Human skeletal muscle PDH kinase activity and isoform expression during a 3-day high-fat/low-carbohydrate diet. Am J Physiol Endocrinol Metab. 2001 Dec;281(6):E1151-1158.

58. Leblanc PJ, Harris RA, Peters SJ. Skeletal muscle fiber type comparison of pyruvate dehydrogenase phosphatase activity and isoform expression in fed and food-deprived rats. Am J Physiol Endocrinol Metab. 2007 Feb;292(2):E571-576.

59. Fuller SJ, Randle PJ. Reversible phosphorylation of pyruvate dehydrogenase in rat skeletal-muscle mitochondria. Effects of starvation and diabetes. Biochem J. 1984 Apr 15;219(2):635–46.

60. Achten J, Gleeson M, Jeukendrup AE. Determination of the exercise intensity that elicits maximal fat oxidation. Med Sci Sports Exerc. 2002 Jan;34(1):92–7.

61. Constantin-Teodosiu D, Carlin JI, Cederblad G, Harris RC, Hultman E. Acetyl group accumulation and pyruvate dehydrogenase activity in human muscle during incremental exercise. Acta Physiol Scand. 1991 Dec;143(4):367–72.

62. Putman CT, Spriet LL, Hultman E, Dyck DJ, Heigenhauser GJ. Skeletal muscle pyruvate dehydrogenase activity during acetate infusion in humans. Am J Physiol. 1995 May;268(5 Pt 1):E1007-1017.

63. Parolin ML, Chesley A, Matsos MP, Spriet LL, Jones NL, Heigenhauser GJF. Regulation of skeletal muscle glycogen phosphorylase and PDH during maximal intermittent exercise. Am J Physiol - Endocrinol Metab. 1999 Nov 1;277(5):E890–900.

64. Constantin-Teodosiu D, Cederblad G, Hultman E. PDC activity and acetyl group accumulation in skeletal muscle during prolonged exercise. J Appl Physiol. 1992 Dec 1;73(6):2403–7.

65. Putman CT, Jones NL, Lands LC, Bragg TM, Hollidge-Horvat MG, Heigenhauser GJ. Skeletal muscle pyruvate dehydrogenase activity during maximal exercise in humans. Am J Physiol - Endocrinol Metab. 1995 Sep 1;269(3):E458–68.

66. Coyle EF, Jeukendrup AE, Oseto MC, Hodgkinson BJ, Zderic TW. Low-fat diet alters intramuscular substrates and reduces lipolysis and fat oxidation during exercise. Am J Physiol Endocrinol Metab. 2001 Mar;280(3):E391-398.

67. Yki-Järvinen H, Bogardus C, Howard BV. Hyperglycemia stimulates carbohydrate oxidation in humans. Am J Physiol. 1987 Oct;253(4 Pt 1):E376-382.

68. Coyle EF, Hamilton MT, Alonso JG, Montain SJ, Ivy JL. Carbohydrate metabolism during intense exercise when hyperglycemic. J Appl Physiol Bethesda Md 1985. 1991 Feb;70(2):834–40.

69. Zinker BA, Lacy DB, Bracy D, Jacobs J, Wasserman DH. Regulation of glucose uptake and metabolism by working muscle. An in vivo analysis. Diabetes. 1993 Jul;42(7):956–65.

70. Romijn JA, Coyle EF, Sidossis LS, Zhang XJ, Wolfe RR. Relationship between fatty acid delivery and fatty acid oxidation during strenuous exercise. J Appl Physiol Bethesda Md 1985. 1995 Dec;79(6):1939–45.

71. Hargreaves M, Kiens B, Richter EA. Effect of increased plasma free fatty acid concentrations on muscle metabolism in exercising men. J Appl Physiol Bethesda Md 1985. 1991 Jan;70(1):194–201.

72. Ravussin E, Bogardus C, Scheidegger K, LaGrange B, Horton ED, Horton ES. Effect of elevated FFA on carbohydrate and lipid oxidation during prolonged exercise in humans. J Appl Physiol Bethesda Md 1985. 1986 Mar;60(3):893–900.

73. Costill DL, Coyle E, Dalsky G, Evans W, Fink W, Hoopes D. Effects of elevated plasma FFA and insulin on muscle glycogen usage during exercise. J Appl Physiol. 1977 Oct;43(4):695–9.

74. Dyck DJ, Putman CT, Heigenhauser GJ, Hultman E, Spriet LL. Regulation of fat-carbohydrate interaction in skeletal muscle during intense aerobic cycling. Am J Physiol. 1993 Dec;265(6 Pt 1):E852-859.

75. Ravussin E, Pahud P, Thelin-Doerner A, Arnaud MJ, Jequier E. Substrate utilization during prolonged exercise after ingestion of 13C-glucose in obese and control subjects. Int J Obes. 1980;4(3):235–42.

76. Odland LM, Heigenhauser GJ, Wong D, Hollidge-Horvat MG, Spriet LL. Effects of increased fat availability on fat-carbohydrate interaction during prolonged exercise in men. Am J Physiol. 1998 Apr;274(4 Pt 2):R894-902.

77. Horowitz JF, Mora-Rodriguez R, Byerley LO, Coyle EF. Lipolytic suppression following carbohydrate ingestion limits fat oxidation during exercise. Am J Physiol. 1997 Oct;273(4 Pt 1):E768-775.

78. Jones NL, Heigenhauser GJ, Kuksis A, Matsos CG, Sutton JR, Toews CJ. Fat metabolism in heavy exercise. Clin Sci Lond Engl 1979. 1980 Dec;59(6):469–78.

79. Odland LM, Heigenhauser GJ, Spriet LL. Effects of high fat provision on muscle PDH activation and malonyl-CoA content in moderate exercise. J Appl Physiol Bethesda Md 1985. 2000 Dec;89(6):2352–8.

80. Décombaz J, Arnaud MJ, Milon H, Moesch H, Philippossian G, Thélin AL, et al. Energy metabolism of medium-chain triglycerides versus carbohydrates during exercise. Eur J Appl Physiol. 1983;52(1):9–14.

81. Feldhoff PW, Arnold J, Oesterling B, Vary TC. Insulin-induced activation of pyruvate dehydrogenase complex in skeletal muscle of diabetic rats. Metabolism. 1993 May 1;42(5):615–23.

82. Turcotte LP, Richter EA, Kiens B. Increased plasma FFA uptake and oxidation during prolonged exercise in trained vs. untrained humans. Am J Physiol. 1992 Jun;262(6 Pt 1):E791-799.

83. Nordby P, Saltin B, Helge JW. Whole-body fat oxidation determined by graded exercise and indirect calorimetry: a role for muscle oxidative capacity? Scand J Med Sci Sports. 2006 Jun;16(3):209–14.

84. Leblanc PJ, Howarth KR, Gibala MJ, Heigenhauser GJF. Effects of 7 wk of endurance training on human skeletal muscle metabolism during submaximal exercise. J Appl Physiol Bethesda Md 1985. 2004 Dec;97(6):2148–53.

85. Henriksson J. Training induced adaptation of skeletal muscle and metabolism during submaximal exercise. J Physiol. 1977 Sep;270(3):661–75.

86. Hermansen L, Hultman E, Saltin B. Muscle glycogen during prolonged severe exercise. Acta Physiol Scand. 1967 Nov;71(2):129–39.

87. Kjaer M, Bangsbo J, Lortie G, Galbo H. Hormonal response to exercise in humans: influence of hypoxia and physical training. Am J Physiol. 1988 Feb;254(2 Pt 2):R197-203.

88. Coyle EF, Hagberg JM, Hurley BF, Martin WH, Ehsani AA, Holloszy JO. Carbohydrate feeding during prolonged strenuous exercise can delay fatigue. J Appl Physiol. 1983 Jul;55(1 Pt 1):230–5.

89. Jansson E, Kaijser L. Substrate utilization and enzymes in skeletal muscle of extremely endurance-trained men. J Appl Physiol Bethesda Md 1985. 1987 Mar;62(3):999–1005.

90. Hagberg JM, Seals DR, Yerg JE, Gavin J, Gingerich R, Premachandra B, et al. Metabolic responses to exercise in young and older athletes and sedentary men. J Appl Physiol Bethesda Md 1985. 1988 Aug;65(2):900–8.

91. Koivisto V, Hendler R, Nadel E, Felig P. Influence of physical training on the fuel-hormone response to prolonged low intensity exercise. Metabolism. 1982 Feb;31(2):192–7.

92. Roberts TJ, Weber JM, Hoppeler H, Weibel ER, Taylor CR. Design of the oxygen and substrate pathways. II. Defining the upper limits of carbohydrate and fat oxidation. J Exp Biol. 1996 Aug;199(Pt 8):1651–8.

93. LeBlanc PJ, Peters SJ, Tunstall RJ, Cameron-Smith D, Heigenhauser GJF. Effects of aerobic training on pyruvate dehydrogenase and pyruvate dehydrogenase kinase in human skeletal muscle. J Physiol. 2004 Jun 1;557(2):559–70.

94. Love LK, LeBlanc PJ, Inglis JG, Bradley NS, Choptiany J, Heigenhauser GJF, et al. The relationship between human skeletal muscle pyruvate dehydrogenase phosphatase activity and muscle aerobic capacity. J Appl Physiol Bethesda Md 1985. 2011 Aug;111(2):427–34.

95. Dudley GA, Tullson PC, Terjung RL. Influence of mitochondrial content on the sensitivity of respiratory control. J Biol Chem. 1987 Jul 5;262(19):9109–14.

96. Gudiksen A, Bertholdt L, Stankiewicz T, Tybirk J, Plomgaard P, Bangsbo J, et al. Effects of training status on PDH regulation in human skeletal muscle during exercise. Pflugers Arch. 2017 Dec;469(12):1615–30.

97. DeFronzo RA, Tripathy D. Skeletal muscle insulin resistance is the primary defect in type 2 diabetes. Diabetes Care. 2009 Nov;32 Suppl 2:S157-163.

98. Wu P, Inskeep K, Bowker-Kinley MM, Popov KM, Harris RA. Mechanism responsible for inactivation of skeletal muscle pyruvate dehydrogenase complex in starvation and diabetes. Diabetes. 1999 Aug 1;48(8):1593–9.

99. Hoy AJ, Brandon AE, Turner N, Watt MJ, Bruce CR, Cooney GJ, et al. Lipid and insulin infusion-induced skeletal muscle insulin resistance is likely due to metabolic feedback and not changes in IRS-1, Akt, or AS160 phosphorylation. Am J Physiol Endocrinol Metab. 2009 Jul;297(1):E67-75.

100. Goodman MN, Berger M, Ruderman NB. Glucose metabolism in rat skeletal muscle at rest. Effect of starvation, diabetes, ketone bodies and free fatty acids. Diabetes. 1974 Nov;23(11):881–8.

101. Berger M, Hagg SA, Goodman MN, Ruderman NB. Glucose metabolism in perfused skeletal muscle. Effects of starvation, diabetes, fatty acids, acetoacetate, insulin and exercise on glucose uptake and disposition. Biochem J. 1976 Aug 15;158(2):191–202.

102. Bajotto G, Murakami T, Nagasaki M, Tamura T, Tamura N, Harris RA, et al. Downregulation of the skeletal muscle pyruvate dehydrogenase complex in the Otsuka Long-Evans Tokushima Fatty rat both before and after the onset of diabetes mellitus. Life Sci. 2004 Sep 10;75(17):2117–30.

103. Schummer CM, Werner U, Tennagels N, Schmoll D, Haschke G, Juretschke H-P, et al. Dysregulated pyruvate dehydrogenase complex in Zucker diabetic fatty rats. Am J Physiol Endocrinol Metab. 2008 Jan;294(1):E88-96.

104. Mandarino LJ, Consoli A, Kelley DE, Reilly JJ, Nurjhan N. Fasting hyperglycemia normalizes oxidative and nonoxidative pathways of insulin-stimulated glucose metabolism in noninsulin-dependent diabetes mellitus. J Clin Endocrinol Metab. 1990 Dec;71(6):1544–51.

105. Kelley DE, Mintun MA, Watkins SC, Simoneau JA, Jadali F, Fredrickson A, et al. The effect of non-insulin-dependent diabetes mellitus and obesity on glucose transport and phosphorylation in skeletal muscle. J Clin Invest. 1996 Jun 15;97(12):2705–13.

106. Kelley DE, Mandarino LJ. Hyperglycemia normalizes insulin-stimulated skeletal muscle glucose oxidation and storage in noninsulin-dependent diabetes mellitus. J Clin Invest. 1990 Dec;86(6):1999–2007.

107. Martin IK, Katz A, Wahren J. Splanchnic and muscle metabolism during exercise in NIDDM patients. Am J Physiol. 1995 Sep;269(3 Pt 1):E583-590.

108. Ghanassia E, Brun JF, Fedou C, Raynaud E, Mercier J. Substrate oxidation during exercise: type 2 diabetes is associated with a decrease in lipid oxidation and an earlier shift towards carbohydrate utilization. Diabetes Metab. 2006 Dec;32(6):604–10.

109. Kang J, Kelley DE, Robertson RJ, Goss FL, Suminski RR, Utter AC, et al. Substrate utilization and glucose turnover during exercise of varying intensities in individuals with NIDDM. Med Sci Sports Exerc. 1999 Jan;31(1):82–9.

110. Blaak EE, van Aggel-Leijssen DP, Wagenmakers AJ, Saris WH, van Baak MA. Impaired oxidation of plasma-derived fatty acids in type 2 diabetic subjects during moderate-intensity exercise. Diabetes. 2000 Dec;49(12):2102–7.

111. Colberg SR, Hagberg JM, McCole SD, Zmuda JM, Thompson PD, Kelley DE. Utilization of glycogen but not plasma glucose is reduced in individuals with NIDDM during mild-intensity exercise. J Appl Physiol Bethesda Md 1985. 1996 Nov;81(5):2027–33.

112. Borghouts LB, Wagenmakers AJM, Goyens PLL, Keizer HA. Substrate utilization in non-obese Type II diabetic patients at rest and during exercise. Clin Sci Lond Engl 1979. 2002 Dec;103(6):559–66.

113. Kulkarni SS, Salehzadeh F, Fritz T, Zierath JR, Krook A, Osler ME. Mitochondrial regulators of fatty acid metabolism reflect metabolic dysfunction in type 2 diabetes mellitus. Metabolism. 2012 Feb;61(2):175–85.

114. Majer M, Popov KM, Harris RA, Bogardus C, Prochazka M. Insulin downregulates pyruvate dehydrogenase kinase (PDK) mRNA: potential mechanism contributing to increased lipid oxidation in insulin-resistant subjects. Mol Genet Metab. 1998 Oct;65(2):181–6.

115. Meyer RA, Wiseman RW. The metabolic systems: Control of ATP sysnthesis in skeletal muscle. In: ACSM's advanced exercise physiology. Philadelphia, PA: Lippincott Williams & Wilkins; 2006. p. 363–78.

116. Hood DA, Gorski J, Terjung RL. Oxygen cost of twitch and tetanic isometric contractions of rat skeletal muscle. Am J Physiol - Endocrinol Metab. 1986 Apr 1;250(4):E449–56.

117. Kushmerick MJ. Energetics of Muscle Contraction. Handbook of Physiology Section 10: Skeletal Muscle. The Williams and Wilkins Company; 1983.

118. Meyer RA. A linear model of muscle respiration explains monoexponential phosphocreatine changes. Am J Physiol - Cell Physiol. 1988 Apr 1;254(4):C548–53.

119. Meyer RA. Linear dependence of muscle phosphocreatine kinetics on total creatine content. Am J Physiol - Cell Physiol. 1989 Dec 1;257(6):C1149–57.

120. Paganini AT, Foley JM, Meyer RA. Linear dependence of muscle phosphocreatine kinetics on oxidative capacity. Am J Physiol - Cell Physiol. 1997 Feb 1;272(2):C501–10.

121. Paganini AT, Foley JM, Meyer RA. Linear dependence of muscle phosphocreatine kinetics on oxidative capacity. Am J Physiol - Cell Physiol. 1997 Feb 1;272(2):C501–10.

122. Kasper JD, Meyer RA, Beard DA, Wiseman RW. Effects of altered Pyruvate Dehydrogenase Activity on contracting skeletal muscle bioenergetics. Am J Physiol Regul Integr Comp Physiol. 2018 Nov 21;

123. Putman CT, Jones NL, Hultman E, Hollidge-Horvat MG, Bonen A, McConachie DR, et al. Effects of short-term submaximal training in humans on muscle metabolism in exercise. Am J Physiol. 1998 Jul;275(1 Pt 1):E132-139.

124. Kiens B, Essen-Gustavsson B, Christensen NJ, Saltin B. Skeletal muscle substrate utilization during submaximal exercise in man: effect of endurance training. J Physiol. 1993 Sep;469:459–78.

125. Bergman BC, Brooks GA. Respiratory gas-exchange ratios during graded exercise in fed and fasted trained and untrained men. J Appl Physiol Bethesda Md 1985. 1999 Feb;86(2):479–87.

126. Spinazzi M, Casarin A, Pertegato V, Salviati L, Angelini C. Assessment of mitochondrial respiratory chain enzymatic activities on tissues and cultured cells. Nat Protoc. 2012 May 31;7(6):1235–46.

127. Srere PA. [1] Citrate synthase. Methods Enzymol. 1969 Jan 1;13:3–11.

128. Lowry OH, Passonneau JV. A flexible system of enzymatic analysis. Academic Press; 1972. 310 p.

129. Wiseman RW, Moerland TS, Chase PB, Stuppard R, Kushmerick MJ. High-performance liquid chromatographic assays for free and phosphorylated derivatives of the creatine analogues beta-guanidopropionic acid and 1-carboxy-methyl-2-iminoimidazolidine (cyclocreatine). Anal Biochem. 1992 Aug 1;204(2):383–9.

130. Sterk JP, Stanley WC, Hoppel CL, Kerner J. A Radiochemical pyruvate dehydrogenase assay: activity in heart. Anal Biochem. 2003 Feb 1;313(1):179–82.

131. Stefan D, Cesare FD, Andrasescu A, Popa E, Lazariev A, Vescovo E, et al. Quantitation of magnetic resonance spectroscopy signals: the jMRUI software package. Meas Sci Technol. 2009 Oct 1;20(10):104035.

132. Kushmerick MJ, Moerland TS, Wiseman RW. Mammalian skeletal muscle fibers distinguished by contents of phosphocreatine, ATP, and Pi. Proc Natl Acad Sci. 1992 Aug 15;89(16):7521–5.

133. Kushmerick MJ, Meyer RA. Chemical changes in rat leg muscle by phosphorus nuclear magnetic resonance. Am J Physiol - Cell Physiol. 1985 May 1;248(5):C542–9.

134. Adams GR, Foley JM, Meyer RA. Muscle buffer capacity estimated from pH changes during rest-to-work transitions. J Appl Physiol. 1990 Sep 1;69(3):968–72.

135. Jeneson JA, Wiseman RW, Kushmerick MJ. Non-invasive quantitative 31P MRS assay of mitochondrial function in skeletal muscle in situ. Mol Cell Biochem. 1997 Sep;174(1–2):17–22.

136. Harkema SJ, Meyer RA. Effect of acidosis on control of respiration in skeletal muscle. Am J Physiol - Cell Physiol. 1997 Feb 1;272(2):C491–500.

137. Lawson JW, Veech RL. Effects of pH and free Mg2+ on the Keq of the creatine kinase reaction and other phosphate hydrolyses and phosphate transfer reactions. J Biol Chem. 1979 Jul 25;254(14):6528–37.

138. Connet R, Sahlin K. Control of glycolysis and glycogen metabolism. Handbook of Physiology: Section 12: Regulation and Integration of Multiple Systems. Oxford University Press; 1996.

139. Sillau AH. Capillarity, oxidative capacity and fibre composition of the soleus and gastrocnemius muscles of rats in hypothyroidism. J Physiol. 1985 Apr;361:281–95.

140. Constable SH, Favier RJ, McLane JA, Fell RD, Chen M, Holloszy JO. Energy metabolism in contracting rat skeletal muscle: adaptation to exercise training. Am J Physiol. 1987 Aug;253(2 Pt 1):C316-322.

141. Green HJ, Jones S, Ball-Burnett M, Farrance B, Ranney D. Adaptations in muscle metabolism to prolonged voluntary exercise and training. J Appl Physiol Bethesda Md 1985. 1995 Jan;78(1):138–45.

142. Phillips SM, Green HJ, Tarnopolsky MA, Heigenhauser GJ, Grant SM. Progressive effect of endurance training on metabolic adaptations in working skeletal muscle. Am J Physiol. 1996 Feb;270(2 Pt 1):E265-272.

143. McAllister RM, Ogilvie RW, Terjung RL. Functional and metabolic consequences of skeletal muscle remodeling in hypothyroidism. Am J Physiol. 1991 Feb;260(2 Pt 1):E272-279.

144. Baldwin KM, Hooker AM, Herrick RE, Schrader LF. Respiratory capacity and glycogen depletion in thyroid-deficient muscle. J Appl Physiol. 1980 Jul;49(1):102–6.

145. Terjung RL, Koerner JE. Biochemical adaptations in skeletal muscle of trained thyroidectomized rats. Am J Physiol. 1976 May;230(5):1194–7.

146. Talanian JL, Holloway GP, Snook LA, Heigenhauser GJF, Bonen A, Spriet LL. Exercise training increases sarcolemmal and mitochondrial fatty acid transport proteins in human skeletal muscle. Am J Physiol Endocrinol Metab. 2010 Aug;299(2):E180-188.

147. Wu F, Jeneson JAL, Beard DA. Oxidative ATP synthesis in skeletal muscle is controlled by substrate feedback. Am J Physiol Cell Physiol. 2007 Jan;292(1):C115-124.

148. Balaban RS. The role of Ca(2+) signaling in the coordination of mitochondrial ATP production with cardiac work. Biochim Biophys Acta. 2009 Nov;1787(11):1334–41.

149. Brown GC. Control of respiration and ATP synthesis in mammalian mitochondria and cells. Biochem J. 1992 May 15;284(Pt 1):1–13.

150. Koretsky AP, Balaban RS. Changes in pyridine nucleotide levels alter oxygen consumption and extra-mitochondrial phosphates in isolated mitochondria: A 31P-NMR and NAD(P)H fluorescence study. Biochim Biophys Acta BBA - Bioenerg. 1987 Oct 7;893(3):398–408.

151. McCormack JG, Denton RM. Role of calcium ions in the regulation of intramitochondrial metabolism. Properties of the Ca2+-sensitive dehydrogenases within intact uncoupled mitochondria from the white and brown adipose tissue of the rat. Biochem J. 1980 Jul 15;190(1):95–105.

152. Harris RA, Bowker-Kinley MM, Huang B, Wu P. Regulation of the activity of the pyruvate dehydrogenase complex. Adv Enzyme Regul. 2002;42(0):249–59.

153. Patel MS, Korotchkina LG. Regulation of the pyruvate dehydrogenase complex. Biochem Soc Trans. 2006 Apr 1;34(2):217.

154. Hue L, Taegtmeyer H. The Randle cycle revisited: a new head for an old hat. Am J Physiol - Endocrinol Metab. 2009 Sep 1;297(3):E578–91.

155. Roberts PA, Loxham SJG, Poucher SM, Constantin-Teodosiu D, Greenhaff PL. The acetyl group deficit at the onset of contraction in ischaemic canine skeletal muscle. J Physiol. 2002 Oct 15;544(2):591–602.

156. Timmons JA, Gustafsson T, Sundberg CJ, Jansson E, Greenhaff PL. Muscle acetyl group availability is a major determinant of oxygen deficit in humans during submaximal exercise. Am J Physiol - Endocrinol Metab. 1998 Feb 1;274(2):E377–80.

157. Meyer RA, Brown TR, Kushmerick MJ. Phosphorus nuclear magnetic resonance of fast- and slow-twitch muscle. Am J Physiol - Cell Physiol. 1985 Mar 1;248(3):C279–87.

158. Peters SJ, St Amand TA, Howlett RA, Heigenhauser GJ, Spriet LL. Human skeletal muscle pyruvate dehydrogenase kinase activity increases after a low-carbohydrate diet. Am J Physiol. 1998 Dec;275(6 Pt 1):E980-986.

159. Balnave CD, Allen DG. Evidence for Na+/Ca2+ exchange in intact single skeletal muscle fibers from the mouse. Am J Physiol. 1998 Apr;274(4 Pt 1):C940-946.

160. Head SI. Membrane potential, resting calcium and calcium transients in isolated muscle fibres from normal and dystrophic mice. J Physiol. 1993 Sep 1;469(1):11–9.

161. Westerblad H, Allen DG. Changes of myoplasmic calcium concentration during fatigue in single mouse muscle fibers. J Gen Physiol. 1991 Sep;98(3):615–35.

162. Goodman MN, Ruderman NB, Aoki TT. Glucose and amino acid metabolism in perfused skeletal muscle. Effect of dichloroacetate. Diabetes. 1978 Nov;27(11):1065–74.

163. Phillips SK, Wiseman RW, Woledge RC, Kushmerick MJ. The effect of metabolic fuel on force production and resting inorganic phosphate levels in mouse skeletal muscle. J Physiol. 1993 Mar 1;462(1):135–46.

164. Bünger R, Mallet RT, Hartman DA. Pyruvate-enhanced phosphorylation potential and inotropism in normoxic and postischemic isolated working heart. Near-complete prevention of reperfusion contractile failure. Eur J Biochem. 1989 Mar 1;180(1):221–33.

165. Zweier JL, Jacobus WE. Substrate-induced alterations of high energy phosphate metabolism and contractile function in the perfused heart. J Biol Chem. 1987 Jun 15;262(17):8015–21.

166. Laughlin MR, Taylor J, Chesnick AS, DeGroot M, Balaban RS. Pyruvate and lactate metabolism in the in vivo dog heart. Am J Physiol. 1993 Jun;264(6 Pt 2):H2068-2079.

167. Greenhaff PL, Campbell-O'Sullivan SP, Constantin-Teodosiu D, Poucher SM, Roberts PA, Timmons JA. An acetyl group deficit limits mitochondrial ATP production at the onset of exercise. Biochem Soc Trans. 2002 Apr;30(2):275–80.

168. Timmons JA, Poucher SM, Constantin-Teodosiu D, Worrall V, Macdonald IA, Greenhaff PL. Increased acetyl group availability enhances contractile function of canine skeletal muscle during ischemia. J Clin Invest. 1996 Feb 1;97(3):879–83.

169. Evans MK, Savasi I, Heigenhauser GJ, Spriet LL. Effects of acetate infusion and hyperoxia on muscle substrate phosphorylation after onset of moderate exercise. Am J Physiol Endocrinol Metab. 2001 Dec;281(6):E1144-1150.

170. Watt MJ, Heigenhauser GJF, Stellingwerff T, Hargreaves M, Spriet LL. Carbohydrate ingestion reduces skeletal muscle acetylcarnitine availability but has no effect on substrate phosphorylation at the onset of exercise in man. J Physiol. 2002 Nov 1;544(Pt 3):949–56.

171. Kelley DE, Mandarino LJ. Fuel selection in human skeletal muscle in insulin resistance: a reexamination. Diabetes. 2000 May;49(5):677–83.

172. Zhang S, Hulver MW, McMillan RP, Cline MA, Gilbert ER. The pivotal role of pyruvate dehydrogenase kinases in metabolic flexibility. Nutr Metab. 2014 Feb 12;11(1):10.

173. Jeoung NH. Pyruvate Dehydrogenase Kinases: Therapeutic Targets for Diabetes and Cancers. Diabetes Metab J. 2015 Jun;39(3):188–97.

174. Kim YI, Lee FN, Choi WS, Lee S, Youn JH. Insulin regulation of skeletal muscle PDK4 mRNA expression is impaired in acute insulin-resistant states. Diabetes. 2006 Aug;55(8):2311–7.

175. Lee FN, Zhang L, Zheng D, Choi WS, Youn JH. Insulin suppresses PDK-4 expression in skeletal muscle independently of plasma FFA. Am J Physiol Endocrinol Metab. 2004 Jul;287(1):E69-74.

176. Jové M, Salla J, Planavila A, Cabrero A, Michalik L, Wahli W, et al. Impaired expression of NADH dehydrogenase subunit 1 and PPARgamma coactivator-1 in skeletal muscle of ZDF rats: restoration by troglitazone. J Lipid Res. 2004 Jan;45(1):113–23.

177. Knowler WC, Barrett-Connor E, Fowler SE, Hamman RF, Lachin JM, Walker EA, et al. Reduction in the incidence of type 2 diabetes with lifestyle intervention or metformin. N Engl J Med. 2002 Feb 7;346(6):393–403.

178. Nie J, DuBois DC, Jusko WJ, Almon RR. Mechanistic population modeling of diabetes disease progression in Goto-Kakizaki rat muscle. Biopharm Drug Dispos. 2011 Jan;32(1):50–63.

179. Matthews DR, Hosker JP, Rudenski AS, Naylor BA, Treacher DF, Turner RC. Homeostasis model assessment: insulin resistance and beta-cell function from fasting plasma glucose and insulin concentrations in man. Diabetologia. 1985 Jul;28(7):412–9.

180. Rueden CT, Schindelin J, Hiner MC, DeZonia BE, Walter AE, Arena ET, et al. ImageJ2: ImageJ for the next generation of scientific image data. BMC Bioinformatics. 2017 Nov 29;18(1):529.

181. Peters SJ, Harris RA, Heigenhauser GJ, Spriet LL. Muscle fiber type comparison of PDH kinase activity and isoform expression in fed and fasted rats. Am J Physiol Regul Integr Comp Physiol. 2001 Mar;280(3):R661-668.

182. Sugden MC, Lall HS, Harris RA, Holness MJ. Selective modification of the pyruvate dehydrogenase kinase isoform profile in skeletal muscle in hyperthyroidism: implications for the regulatory impact of glucose on fatty acid oxidation. J Endocrinol. 2000 Nov;167(2):339–45.

183. Jeoung NH, Rahimi Y, Wu P, Lee WNP, Harris RA. Fasting induces ketoacidosis and hypothermia in PDHK2/PDHK4-double-knockout mice. Biochem J. 2012 May 1;443(3):829–39.

184. Mandarino LJ, Consoli A, Jain A, Kelley DE. Interaction of carbohydrate and fat fuels in human skeletal muscle: impact of obesity and NIDDM. Am J Physiol. 1996 Mar;270(3 Pt 1):E463-470.

185. Coyle EF, Martin WH, Bloomfield SA, Lowry OH, Holloszy JO. Effects of detraining on responses to submaximal exercise. J Appl Physiol Bethesda Md 1985. 1985 Sep;59(3):853–9.